Interception and characterization of catalyst species in rhodium-bis(diazaphospholane)-catalyzed asymmetric hydroformylation

By

Eleanor Rolfe Nelsen

A dissertation submitted in partial fulfillment

of the requirements for the degree of

Doctor of Philosophy

(Chemistry)

at the

UNIVERSITY OF WISCONSIN – MADISON

2014

Date of final oral examination: 4/3/2014

This dissertation is approved by the following members of the Final Oral Committee:

Clark R. Landis, Professor, Chemistry
Shannon S. Stahl. Professor, Chemistry
Judith N. Burstyn. Professor, Chemistry
Tehshik P. Yoon, Professor, Chemistry
Ive Hermans, Associate Professor, Chemistry

Table of Contents

Chapter 1

Rhodium-Catalyzed Asymmetric Hydroformylation

1.1 Introduction

Discovered by Roelen in 1938, the hydroformylation of alkenes to give aldehydes today ranks among the most important industrial applications of homogeneous catalysis, responsible for the production of eighteen billion pounds of aldehydes per year worldwide. Using inexpensive and abundant starting materials – olefins and the CO/H_2 mixture known as syngas – this process introduces both chirality and functionality in a single step, with perfect atom economy: an efficient transformation which is both economically and environmentally attractive.[1]

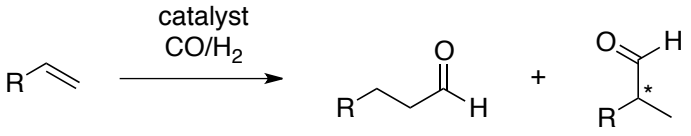

Scheme 1.1. The hydroformylation reaction.

Capitalizing on those advantages, however, requires addressing the major issue of selectivity. Because the double bond has two reactive positions, and reaction at one position introduces a chiral center, even the simplest cases – *i.e.* terminal alkenes not susceptible to isomerization – require discrimination among three possible products. Development of selective hydroformylation catalysts has therefore been an active area of study.

The earliest catalysts were unmodified cobalt carbonyl complexes, whose intrinsically low activity demanded harsh reaction conditions that tended to erode selectivity. Since Wilkinson's discovery in the 1960's that Vaska's rhodium-triphenylphosphine complex generated a highly active hydroformylation catalyst under

relatively mild conditions,[2] rhodium-phosphorus complexes have been the catalysts of choice for most applications. Over the last several decades a wide variety of phosphorus-based ligand systems have been explored in an effort to identify catalysts capable of combining high selectivity with reactivity suitable for a commodity-scale process.[1]

1.2 Catalysts for asymmetric hydroformylation

The development of hydroformylation catalysts has been largely devoted to maximizing selectivity for linear aldehydes, which are employed in downstream commodity-scale processes (mostly the synthesis of plasticizers and detergents). The comparatively underutilized asymmetric reaction, however, is an attractive source of chiral aldehydes branched aldehydes, however, are an attractive chiral feedstock for fine chemical and pharmaceutical synthesis (for example, the asymmetric hydroformylation of vinyl aromatics yield precursors for anti-inflammatory agents).[3] However, selectively generating the branched product is intrinsically more difficult, since it requires both regio- and enantiocontrol. Moreover, most branched-selective catalysts are plagued by low rates and narrow substrate scopes. These challenges have hindered the development of catalytic asymmetric hydroformylation, despite its potential in the synthesis of high-value products.

Platinum – chiral phosphine complexes were the first highly enantioselective hydroformylation catalysts (*ee* values between 70 and 80%), but the utility of these systems was limited by low rates, poor regioselectivity, and competing reduction of the starting material to the alkane.[4] Early attempts at asymmetric hydroformylation with both rhodium-phosphine[5] and –phosphite[6] systems failed to achieve high enantioselectivities

(see Figure 1 for examples of ligands used for asymmetric hydroformylation). A major exception was Takaya's 1997 report of the new phosphine-phosphite ligand BINAPHOS; in the hydroformylation of styrene and related substrates, this system achieved high conversion with branched-to-linear (b:l) ratios of 88:12, and 94 % *ee*.[7] However, a catalyst system that offered high rates and good selectivity for a broader range of substrates was elusive until, in 2004, Landis and coworkers introduced 3,4-bis(diazaphospholanes) (see Figure 1, bottom right). This new class of ligands for asymmetric hydroformylation showed unprecedented activity – greater than one turnover per second – and selectivity (see Table 1). For the benchmark substrates styrene, allyl cyanide, and vinyl acetate, these catalysts gave 89%, 90%, and 97% enantiomeric excess, and branched-to-linear ratios of 20:1, 60:1, and 50:1, respectively.[8]

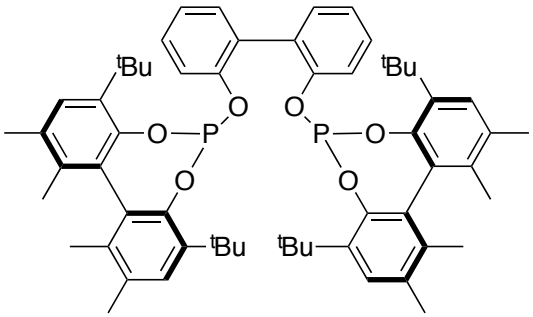

(*S,S*)-Kelliphite

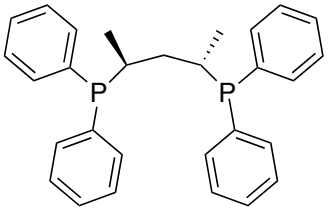

(*S,S*)-BDPP

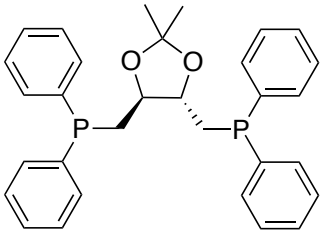

(*S,S*)-DIOP

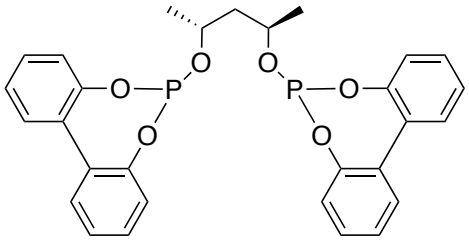

(*R,R*)-Chiraphite

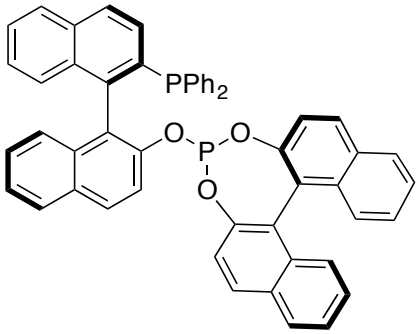

(*R,S*)-BINAPHOS

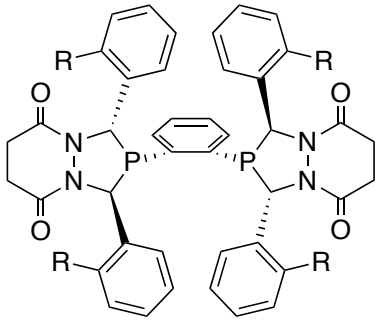

(S,S)-bis(3,4)-diazaphospholane

Figure 1.1. Chiral phosphine and phosphite ligands for asymmetric hydroformylation

Table 1.1. Conversion and selectivity in the hydroformylation of styrene, allyl cyanide, and vinyl acetate with chiral phosphorus ligands. Conditions: 80 °C, 150 psig 1:1 $CO:H_2$, ligand : Rh = 1.2, substrate : Rh = 5000, time = 3 h. Diazaphos = (*S*,*S*)-3,4-bis(diazaphospholane).

Ligand	**Styrene**			**Allyl cyanide**			**Vinyl acetate**		
	conv. (%)	*b:l*	*% ee*	*conv. (%)*	*b:l*	*% ee*	*conv. (%)*	*b:l*	*% ee*
Binaphos	96	4.5	82(*R*)	98	2.1	72(*R*)	72	8.2	48(*S*)
Kelliphite	78	8.9	2(*R*)	100	9.3	66(*S*)	78	61	73(*R*)
Chiraphite	90	9.0	49(*R*)	100	5.5	13(*R*)	75	190	50(*R*)
Diazaphos	**100**	**6.6**	**82(*S*)**	**100**	**4.1**	**87(*R*)**	**100**	**37**	**96(*S*)**

In the last decade, Rh(BDP)-catalyzed hydroformylation has been extended to new substrates,[9] carried out with immobilized, recyclable catalysts on a silica support,[10] and employed to significantly reduce the number of steps in the synthesis of natural products.[11] Meanwhile, the synthesis of new phosphine ligands by a variety of research groups has enabled remarkable progress in controlling the chemo-, regio- and enantioselectivity of rhodium-catalyzed hydroformylation.[12] Recent design motifs include scaffolding effects,[13,14] secondary coordination sphere hydrogen bonding,[15] and supramolecular constructions.[16]

1.3 Mechanistic studies of hydroformylation

Despite substantial progress in catalyst development, fundamental questions concerning the origins of regioselectivity and enantioselectivity in rhodium-catalyzed

hydroformylation remain unanswered. While a general mechanism for hydroformylation has been accepted for decades (see Scheme 1.2),[17] critical details regarding the control of stereo- and regioselectivity remain elusive.

The complexity of this reaction is one reason it has remained resistant to analysis. The mechanism comprises three distinct productive manifolds, one each for the linear and the two enantiomeric branched aldehydes. Catalysis is initiated by CO dissociation from a rhodium hydridodicarbonyl complex to generate the square-planar monocarbonyl complex. This coordinatively unsaturated species is the active catalyst, which binds the substrate to generate a five-coordinate alkene hydride. Because the face of the alkene bound to the metal and the regiochemistry of its insertion differentiate among each of the three reaction manifolds, the structure of this alkene complex (which has never been observed) and the nature of the insertion step have long been considered critically important.

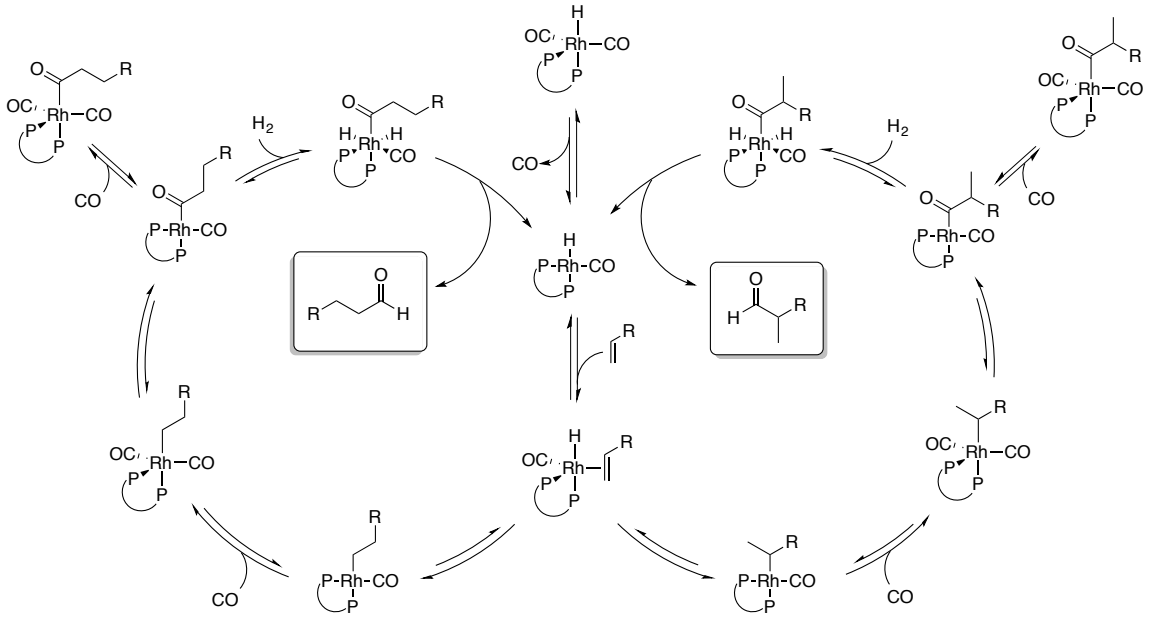

Scheme 1.2. Proposed mechanism for rhodium-bis(phosphine)-catalyzed hydroformylation.

Because many mechanistic studies have considered the structure of the alkene hydride complex predictive of selectivity, the way in which it might be influenced by ligand parameters has received considerable attention. (In these studies, the structure of the unobservable alkene hydride has been presumed analogous to that of the hydridodicarbonyl precatalyst). Casey's observation that diphosphine ligands that favored larger P-Rh-P angles ("bite angles") tended both to promote *n*-aldehyde formation and to prefer diequatorial coordination sites in a trigonal pyramid prompted an investigation of the relationship between ligand coordination mode and regioselectivity.[10] However, neither steric[11] or electronic[12] explanations for the influence of coordination mode proved satisfactory. Subsequent studies by van Leeuwen using the thixantphos ligand further discredited any influence of coordination geometry on selectivity, but

suggested that a wide bite angle might enhance activity by stabilizing the transition state for alkene coordination.[21] Two decades after the initial proposal of a "bite angle effect," no satisfactory explanation has been propounded; nevertheless, it continues to be invoked as an explanation for ligand performance.[22]

In any case, this preoccupation with the structure of the hydride assumes that selectivity is fixed at insertion. Alkene coordination and insertion fix selectivity only if these steps are irreversible. And several studies suggest that, at least for some catalyst systems under certain conditions, the situation is much more complicated.[19,23,24]

Mechanistic studies of Rh(BDP)-catalyzed hydroformylation of styrene reveal the potential influence of later steps in the cycle.[24] Because increased CO pressure inhibited the formation of the (*S*)-branched and linear aldehyde products, but had no effect on the formation of the (*R*)-branched product, both the branched-to-linear ratio and percent *ee* of the product for this system increased with increasing p_{CO}. Detailed analysis revealed a complicated kinetic scenario. Insertion of the alkene to give the (*R*)-branched alkyl, leading to the major product, is kinetically preferred but (unlike the other three insertion pathways) highly reversible, so that the rate of formation of the (*R*)-branched aldehyde depends both on the insertion to give the corresponding branched rhodium alkyl and the trapping of that alkyl by CO. Increased CO pressure enhances trapping, counterbalancing the normal CO inhibition and leading to an apparent independence of p_{CO}. At sufficiently high pressures, the insertion becomes irreversible; at this point, selectivity has reached its maximum value and product formation is again inhibited by CO.

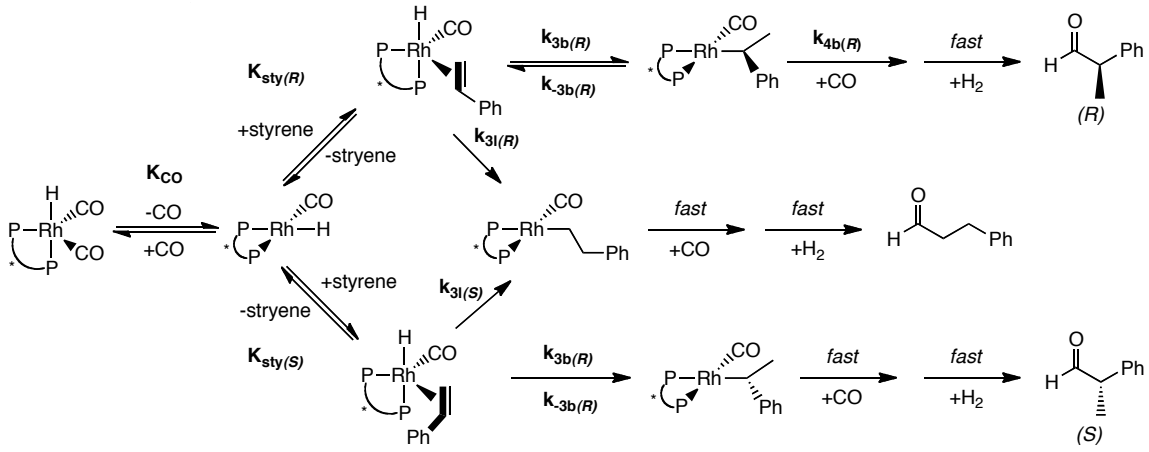

Scheme 1.3. Kinetic model for the hydroformylation of styrene by Rh(BDP) catalysts. The pathways leading to the linear and *S*-branched products (middle and bottom) are inhibited by CO, but reversible alkene insertion makes the pathway leading to the *R*-branched product (top) CO-neutral. As CO pressure increases, the *S* and linear pathways are suppressed, while the *R* pathway is unaffected, increasing regio- and enantioselectivity.

While this particular behavior appears specific to this system, this example does highlight the potential complexity of these reactions. The details of the mechanism are highly contingent on both the ligand and the reaction conditions: mechanistic studies on other ligand systems reveal a range of kinetic behavior such as, for example, the reaction order in substrate, CO, and H_2 (making it imperative that mechanistic studies be performed on catalyst systems of practical interest).[1,23,25,26d] Despite a surfeit of plausible hypotheses, no broad description of selectivity has emerged.

Understanding selectivity in hydroformylation has been significantly hampered by the inability to characterize key reaction intermediates structurally, kinetically, or thermodynamically. Observing and characterizing catalyst species (or their

independently-synthesized analogues) would be invaluable, allowing us to directly study the kinetics of individual steps and permitting a meaningful investigation into the relationship between structure and selectivity. These types of experiments have been informative in asymmetric hydrogenation, for example;[27] however, examples are rare in the hydroformylation literature. The hydridodicarbonyl precatalyst [Rh(H)$(CO)_2$(P^P)] has been thoroughly characterized for a number of ligand systems and repeatedly identified as the resting state of the catalyst.[7,26,28] Beyond this, however, the only other species ever observed are the five-coordinate acyl complexes (which actually lie off the catalytic cycle – see Scheme 2). Even for these, the few examples of detailed characterization are limited to catalyst systems of low activity and selectivity[29,30] or resort to replacing rhodium with iridium to stabilize these complexes.[31,32]

The best example remains Brown's studies of hydroformylation with rhodium-triphenylphosphine complexes in the nineteen-eighties.[29] Using a combination of ^{31}P, ^{1}H, and ^{13}C NMR spectroscopy, Brown and Kent identified five-coordinate acyl complexes formed from the reaction of [Rh(H)$(CO)_2(PPh_3)_2$] with styrene, 1-octene, and 1-decene. Only linear acyl complexes were observed for 1-octene and 1-decene, but both linear and branched isomers were observed for styrene (see Figure 1.2).

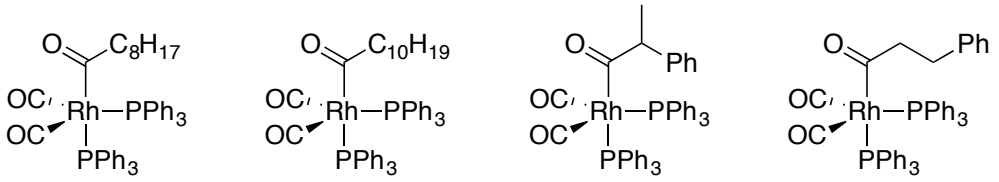

Figure 1.2. Rhodium-acyl complexes characterized by Brown and Kent. Of the three substrates investigated, only styrene gave both linear and branched acyl species.

This elegant study made effective use of ^{13}C labeling to complement ^{31}P and ^{1}H NMR data. Both the acyl and the terminal carbonyl signals in the ^{13}C NMR spectrum were well-characterized. The authors used phosphorus-carbon, rhodium-carbon, and carbon-carbon coupling constants, in addition to simulated NMR spectra, to establish the geometry and regiochemistry of these acyl complexes.

Their results demonstrate the power of the characterization of catalyst species to elucidate kinetic aspects of hydroformylation. In the case of styrene, the branched acyl complex was kinetically favored (consistent Landis' model of faster insertion at the styrene α-position with Rh(BDP) catalysts),[24] but isomerizes slowly ($t_{1/2}$ = 10 min at 298 K) to the linear acyl. The maximum l:b ratio of acyl complexes was approximately 4:1, dropping to 2:1 as aldehyde was formed by binuclear elimination. However, the authors point out that isomerization is unlikely to occur under catalytic conditions in the presence of H_2, and therefore assume that selectivity is set early in the cycle.

Since this study, however, no comparable analysis of catalyst species during hydroformylation has been produced. To address this gap in the literature, we have extended our mechanistic investigations of rhodium-bis(diazaphospholane)-catalyzed asymmetric hydroformylation to include direct observation and characterization of catalyst species. The high reactivity of hydroformylation catalysts, particularly bis(diazaphospholanes), do make the isolation of intermediates challenging. Fortunately, bis(diazaphospholanes) are relatively electron-poor phosphine ligands. Therefore, we might plausibly expect relatively facile CO dissociation and slow oxidative addition, a combination which could give us a kinetic window to observe alkyl and acyl complexes under the right set of temperature and gas conditions.

Our primary strategy will be monitoring the reaction of the rhodium hydride complex with olefins (for styrene, see Chapter 3; for other substrates, see Chapter 4) by multinuclear NMR spectroscopy. This approach provides both kinetic and structural information. The results, presented in subsequent chapters, have allowed us to identify and characterize five-coordinate acyl complexes and, for the first time, alkyl complexes formed during rhodium-catalyzed hydroformylation.

1.4 References

(1) For reviews of hydroformyation, see (a) Agbossou, F.; Carpentier, J.-F.; Mortreux, A. *Chem. Rev*. **1995**, *95*, 2485-2506. (b) Claver, C.; van Leeuwen, P. W. N. M. In *Rhodium Catalyzed Hydroformylation*; Claver, C., van Leeuwen, P. W. N. M., Eds.; Kluwer Academic Publishers: Dordrecht, The Netherlands, 2000. (c) Wiese, K.-D.; Obst, D. *Top. Organomet. Chem.* **2006**, *18*, 35-64.

(2) Evans, D.; Osborn, J.A.; Wilkinson, G. *J. Chem. Soc. A*. **1968**, 3133 – 3142.

(3) Botteghi, C.; Paganelli, S.; Schionato, A.; Marchetti, M. *Chirality* **1991**, *3*, 355-369.

(4) For examples, see (a) Consiglio, G.; Pino, P.; Flowers, L. I.; Pittman, C. U., Jr. *J. Chem. Soc.. Chem. Commun.* **1983**, 612. (b) Stille, J. K.; Su., H.; Brechot, P.; Parrinello, G.; Hegedus, L. S. *Organometallics* **1991**, *10*, 1183-1189. (c) Consiglio, G.; Nefkens, S. C. A.; Borer, A. *Organometallics* **1991**, *10*, 2046.

(5) (a) Gladiali, S; Pinna, L. *Tetrahedron: Asymm.* **1991**, *2*, 623. (b) Masdeu-Bulto, A. M.; Orejon, A.; Castellanos, A.; Castillon, S.; Claver, C. *Tetrahedron: Asymm.* **1996**, *7*, 1829.

(6) (a) Wink, J. D.; Kwok, T. J.; Yee, A. Inorg. Chem. **1990**, *29,* 5007. (b) Sakai, N.; Nozaki, K.; Mashima, K.; Takaya, H. *Tetrahedron Asymm.* **1992**, *3*, 583.

(7) (a) Nozaki, K.; Sakai, N.; Nanno, T.; Higashijima, T.; Mano, S.; Horiuchi, T.; Takaya, H. *J. Am. Chem. Soc.* **1997**, *119*, 4413-4423. (b) Cobley, C. J.; Gardner, K.; Klosin, J.; Praquin, C.; Hill, C.; Whiteker, G. T.; Zanotti-Gerosa, A.; Petersen, J. L.; Abboud, K. A. *J. Org. Chem.* **2004**, *69*, 4031-4040. (c) Cobley, C. J.; Klosin, J.; Qin, C.; Whiteker, G. *Org. Lett.* **2004**, *6*, 3277-3280. (d) Babin, J. E.; Whiteker, G. T. Patent WO 93/03830, 1992. (e) Whiteker, G. T.; Briggs, J. R.; Babin, J. E.; Barner, B. A. In *Catalysis of Organic Reactions*; Morrell, D. G., Ed.; Marcel Dekker: New York, 2003; p 359.

(8) (a) Clark, T. P.; Landis, C. R.; Freed, S. L.; Klosin, J.; Abboud, K. A. *J. Am. Chem. Soc.* **2005**, *127*, 5040-5042. (b) Klosin, J.; Landis, C. R. *Acc. Chem. Res*. **2007**, *40*, 1251-1259.

(9) (a) Watkins, A. L.; Hashiguchi, B. G.; Landis, C. R. *Org. Lett*. **2008**, *10*, 4553. (b) McDonald, R. I.; Wong, G. W.; Neupane, R. P.; Stahl, S. S.; Landis, C. R. *J. Am. Chem. Soc*. **2010**, *132*, 14027. (c) Watkins, A. L.; Landis, C. R. *Org. Lett.* **2011**, *13*, 164. (d) Adint, T. T.; Wong, G. W.; Landis, C. R. *J. Org. Chem*. **2013**, *78*, 4231-4238.

(10) Adint, T. T.; Landis, C. R. Manuscript submitted.

(11) (a) Risi, R. M.; Burke, S. D. *Org. Lett.* **2012**, *14*, 1180 – 1182. (b) Ho, S.; Bucher, C.; Leighton, J. L. *Angew. Chem. Int. Ed*. **2013**, *52*, 6757 – 6761.

(12) (a) Cobley, C. J.; Gardner, K.; Klosin, J.; Praquin, C.; Hill, C.; Whiteker, G. T.; Zanotti-Gerosa, A.; Petersen, J. L.; Abboud, K. A. *J. Org. Chem.* **2004**, *69*, 4031-4040. (b) Cobley, C. J.; Klosin, J.; Qin, C.; Whiteker, G. *Org. Lett.* **2004**, *6*, 3277-3280.

(c) Yan, Y. J.; Zhang, X. M. *J. Am. Chem. Soc.* **2006**, *128*, 7198-7202. (d) Axtell, A. T.; Klosin, J.; Abboud, K. A. *Organometallics* **2006**, *25*, 5003-5009. (e) Rubio, M.; Suárez, A.; Álvarez, E.; Bianchini, C.; Oberhauser, W.; Peruzzini, M.; Pizzano, A. *Organometallics* **2007**, *26*, 6428-6436. (f) Robert. T.; Abiri, Z.; Wassenaar, J.; Sandee, A. J.; Romanski, S.; Neudörfl, J.-M.; Schmalz, H.-G.; Reek, J. N. H. *Organometallics* **2010**, *29*, 478-483. (g) Wassenaar, J.; de Bruin, B.; Reek, J. N. H. *Organometallics* **2010**, *29*, 2767-2776. (h) Wang, X.; Buchwald, H. L. *J. Am. Chem. Soc.* **2011**, *133*, 19080-19083. (i) Chikkali, S. H.; Bellini, R.; de Bruin, B.; van der Vlugt, J. I.; Reek, J. N. H. *J. Am. Chem. Soc*. **2012**, *134*, 6607-6616.

(13) (a) Lightburn, T. E., Dombrowski, M. T., and Tan, K. L. *J. Am. Chem. Soc.* **2008**, 130, 9210-9211. (b) Worthy, A. D., Gagnon, M. M., Dombrowski, M. T., and Tan., K. L. *Org. Lett.* **2009**, 11, 2764– 2767. (c) Sun, X., Frimpong, K., and Tan, K. L. *J. Am. Chem. Soc.* **2010**, 132, 11841-11843. (d) Worthy, A. D.; Joe, C. L.; Lightburn, T. E.; Tan, K. L. *J. Am. Chem. Soc*. **2010**, *132*, 14757-14759.

(14) (a) Grünanger, C. U.; Breit, B. *Angew. Chem., Int. Ed.* **2008**, *47*, 7346-7349. (b) Grünanger, C. U.; Breit, B. *Angew. Chem., Int. Ed.* **2010**, *49*, 967-970. (c) Usui, I.; Nomura, K.; Breit, B. *Org. Lett*. **2011,** *13,* 612-615.

(15) (a) Šmejkal, T.; Breit, B. *Angew. Chem*. **2007**, *120*, 317-321. (b) Šmejkal, T.; Breit, B. *Angew. Chem*. **2008**, *120*, 4010-4013. (c) Šmejkal, T.; Gribkov, D.; Geier, J.; Keller, M.; Breit, B. *Chem. Eur. J.* **2010,** *16*, 2470-2478.

(16) (a) Kuil, M.; Soltner, T.; van Leeuwen, P. W. N. M.; Reek, J. N. H. *J. Am. Chem. Soc.* **2006,** *128,* 11344-11345. (b) Bellini, R.; Chikkali, S. H.; Berthon-Gelloz, G.;

Reek, J. N. H. *Angew. Chem. Int. Ed*. **2011**, *50*, 7342-7345. (c) Gadzikwa, T.; Bellini, R.; Dekker, H. L.; Reek, J. N. H. *J. Am. Chem. Soc.* **2012**, *134*, 2860-2863.

(17) Heck, R. F.; Breslow, D. S. *J. Am. Chem. Soc.* **1961**, *83*, 4023-4027.

(18) Casey, C. P.; Whiteker, G. T.; Melville, M. G.; Petrovich, L. M.; Gavney, J. A.; Powell, D. R. *J. Am. Chem. Soc.* **1992**, *114*, 5535-5542.

(19) Casey, C. P.; Petrovich, L. M. *J. Am. Chem. Soc.* **1995**, *117*, 6007-6014.

(20) Casey, C. P.; Paulsen, E. Beuttenmueller, E.; Proft, B.; Petrovich, L.; Matter, B.; Powell, D. *J. Am. Chem. Soc.* **1997**, *119*, 11817.

(21) van der Veen, L. A.; Boele, M. D. K.; Bregman, F. R.; Kamer, P. C. J.; van Leeuwen, P. W. N. M.; Goubitz, K.; Fraanje, J.; Schenk, H.; Bo, C. *J. Am. Chem. Soc.* **1998**, *120*, 11616-11626.

(22) Axtell, A. T.; Klosin, J.; Cobley, C. J.; Fox, M. E.; Whiteker, G. T.; Jackson, M. *Organometallics* **2009**, *28*, 2993-2999.

(23) Nozaki, K.; Matsuo, T.; Shibahara, F.; Hiyama, T. *Organometallics* **2003**, *22*, 594-600.

(24) Watkins, A. L.; Landis, C. R. *J. Am. Chem. Soc.* **2010**, *132*, 10306-10317.

(25) For example, see (a) Horiuchi, T.; Shirakawa, E.; Nozaki, K.; Takaya, H. *Organometallics* **1997**, *16*, 2981-2986.

(26) Pottier, Y.; Mortreux, A.; Petit, F. *J. Organomet. Chem.* **1989**, *370*, 333-342.

(27) (a) Brown, J. M.; Chaloner, P. A.; *J. Chem. Soc., Chem. Commun.* **1980**, 344. (b) Chan, A. S. C.; Halpern, J. A. *J. Am. Chem. Soc*. **1980**, *102*, 838.

(28) For example, see (a) Castellanos-Páez, A.; Castillón, S.; Claver, C.; van Leeuwen, P.; de Lange, W. *Organometallics* **1998**, *17*, 2543. (b) Molina, D.; Casey, C.;

Müller, I.; Nozaki, K.; Jäkel, C. *Organometallics* **2010**, *29*, 3362. (c) Doro, F.; Reek, J.; van Leeuwen, P. *Organometallics* **2010**, *29*, 4440. (d) Wassenaar, J.; de Bruin, B.; Reek, J. N. H. *Organometallics* **2010**, *29*, 2767-2776.

(29) (a) Brown, J. M.; Kent, A. G. *J. Chem. Soc., Chem. Commun.* **1982**, 723 – 725. (b) Brown, J.; Kent, A. *J. Chem. Soc. Perkin Trans*. *2* **1987**, 1597.

(30) van der Slot, S.; Kamer, P.; van Leeuwen, P.; Heaton, B.; Iggo, J. *Organometallics* **2001**, *20*, 430.

(31) Deutsch, P.; Eisenberg, R. *Organometallics* **1990**, *9*, 709.

(32) Chan, A.; Shieh, H. *Inorg. Chim. Acta* **1994**, *218*, 89.

Chapter 2

Synthesis and Characterization of Catalyst Precursors

2.1 Synthesis and characterization of Rh complexes with bis(diazaphospholane) ligands

2.1.1 Tetra(amide) bis(diazaphospholanes)

The first Rh bis(diazaphospholane) complex to be synthesized was the catalyst precursor $[Rh(H)(CO)_2(BDP)]$ (BDP = bis(diazaphospholane)). During catalytic hydroformylations, it is typically prepared *in situ* by pressurizing a solution of $[Rh(acac)(CO)_2]$ (acac = acetylacetonato) and the bis(diazaphospholane) ligand with syngas. However, this method is not well-suited to these studies, since analysis by ^{31}P NMR shows that it yields a mixture of products. However, the hydride complex can be cleanly prepared from [Rh(acac)(BDP)] (see Scheme 2.1b below).

The ligand and $Rh(acac)(CO)_2$ react easily in tetrahydrofuran or dichloromethane to generate [Rh(acac)(BDP] (see Scheme 2.1a). (It is necessary to vent the flask to allow the liberated CO to escape; if the reaction is performed in a sealed vessel, additional minor products – presumably CO complexes – appear).

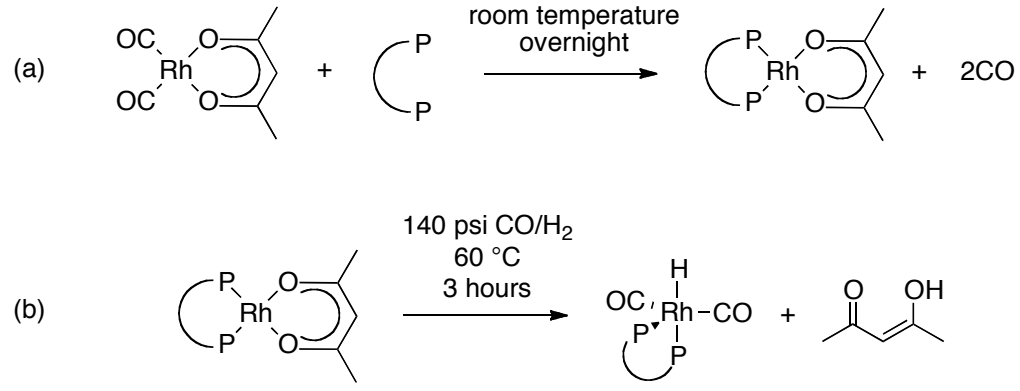

Scheme 2.1. Synthesis of [Rh(acac)(BDP)] and $[Rh(H)(CO)_2(BDP)]$. Solvent varies with ligand system.

Both complexes were initially prepared using a benzylamide-substituted bis(diazaphospholane), an achiral analogue of the catalytically-successful methylbenzylamide ligand.[1] However, the poor solubility of this ligand at the concentrations necessary for NMR experiments forced us to look for a more tractable substitute.

Suspecting that a long aliphatic substituent might confer greater solubility, we synthesized an octylamide bis(diazaphospholane) (R = $C(=O)NHC_8H_{17}$). Like the majority of the bis(diazaphospholanes) made in our group, this ligand was prepared via a straightforward PyBOP coupling of octylamine to the tetra(carboxylic acid).[2]

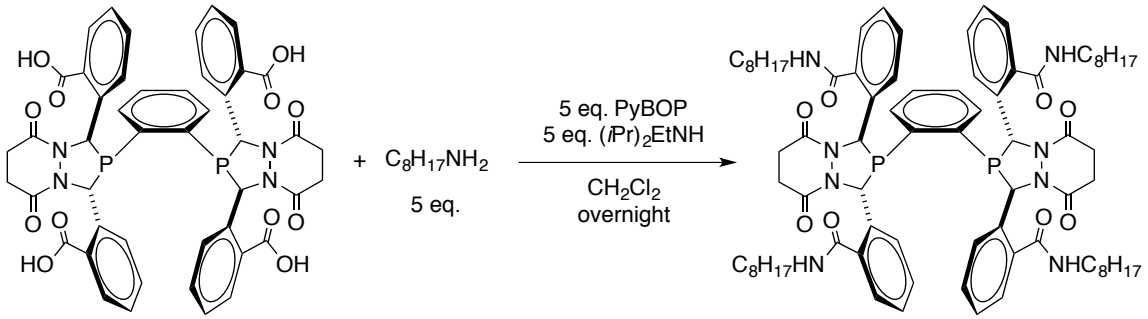

Scheme 2.2. Synthesis of octylamide bis(diazaphospholane) via peptide coupling of octylamine with the tetra(carboxylic acid)bis(diazaphospholane). PyBOP = (benzotriazol-1-yl-oxytripyrrolidinophosphonium hexafluorophosphate)

A new addition to our group's library, this ligand was thoroughly characterized by one- and two-dimensional ^1H and ^{13}C NMR spectroscopy. This ligand and the metal complexes derived from it were highly soluble in polar solvents (acetone, ethyl acetate,

THF, etc.), and it was successfully used to synthesize both the acac and hydride complexes.

The octylamide substituents are sufficiently bulky to prevent rapid exchange between axial and equatorial phosphorus atoms in the trigonal bipyramidal hydride complex; as a result, the $^{31}P\{^{1}H\}$ NMR spectrum shows two distinct phosphorus resonances (δ 101.2 ppm, dd, $J_{P\text{-}Rh}$ = 110 Hz, $J_{P\text{-}P}$ = 27 Hz; δ 91.4 ppm, dd, $J_{P\text{-}Rh}$ = 150 Hz, $J_{P\text{-}P}$ = 27 Hz); the proton NMR spectrum shows a single hydride signal at δ -9.1 ppm (dt, $J_{H\text{-}P}$ = 130 Hz, $J_{H\text{-}Rh}$ = 12 Hz) (see Supporting Information). Some fluxionality persists, however, as indicated by the relatively broad phosphorus signals. When, in an effort to generate other species on the catalytic cycle, we added styrene to the rhodium hydride, the resulting peaks were too poorly-defined to deduce any useful structural information. Moreover, variable-temperature NMR experiments on a solution of the rhodium hydride showed unusual dynamic behavior which made us less certain of its structure.

2.1.2 Tetraphenyl bis(diazaphospholane)

The tetraphenyl bis(diazaphospholane), which has no amide substituent in the *ortho* position, offered an attractive alternative. The variant with the phthaloyl (vs. succinyl)-protected diazaphospholane ring is highly soluble in CH_2Cl_2, and its NMR spectra are more straightforward. Furthermore, the absence of any aliphatic protons facilitates characterization of intermediates.

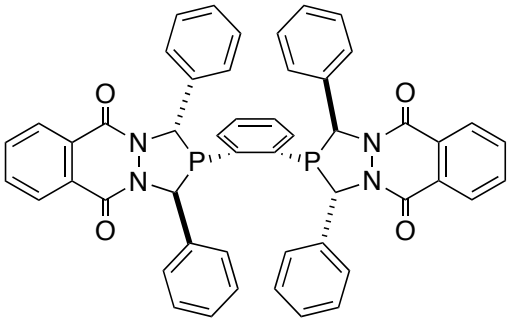

Figure 2.1. Tetraphenyl bis(diazaphospholane).

Because this ligand system is being modeled by Dow in computational studies of hydroformylation (see Chapter 6), its use here offers us a direct comparison between empirical and computational mechanistic studies. It is also worth nothing that because this ligand synthesis does not involve a PyBOP coupling, we avoid the use of PF_6^- salts, which we were not able to remove from the amide ligands without destroying reactivity.

From this point forward, the abbreviation "BDP" will refer to the racemic tetraphenyl bis(diazaphospholane) pictured above unless otherwise noted.

Both Rh(acac)(BDP) and $Rh(H)(CO)_2$(BDP) (**1**) are easily synthesized as described above for the tetra(amide) ligands. The ^{31}P NMR spectrum of Rh(acac)(BDP) shows a doublet at δ 85.9 ppm ($^1J_{PRh}$ = 208 Hz), which is consistent with a square-planar Rh(I) complex.[3] The proton-coupled ^{31}P NMR spectrum of **1** shows a doublet of doublets at 83.7 ppm ($^1J_{PRh}$ = 136.6 Hz; $^2J_{PH}$ = 75.6 Hz); these values are consistent with those reported for other Rh(I) bis(phosphine) hydrides.[4] Because the phosphorus atoms of the hydridodicarbonyl exchange rapidly (probably via a turnstile mechanism rather than Berry pseudo-rotation,[5] they appear as a single peak in the ^{31}P NMR spectrum (see Figure 2.2), and the observed $^1J_{PRh}$ is an average of the values for P_{ax} and P_{eq}. In the proton NMR spectrum, the hydride signal appears at δ -9.8 ppm as a triplet of doublets; the

triplet splitting (75.6 Hz) arises from the two magnetically equivalent phosphorus nuclei, and the smaller (9 Hz) splitting is $^{1}J_{HRh}$. These values, too, are consistent with those reported for similar complexes.

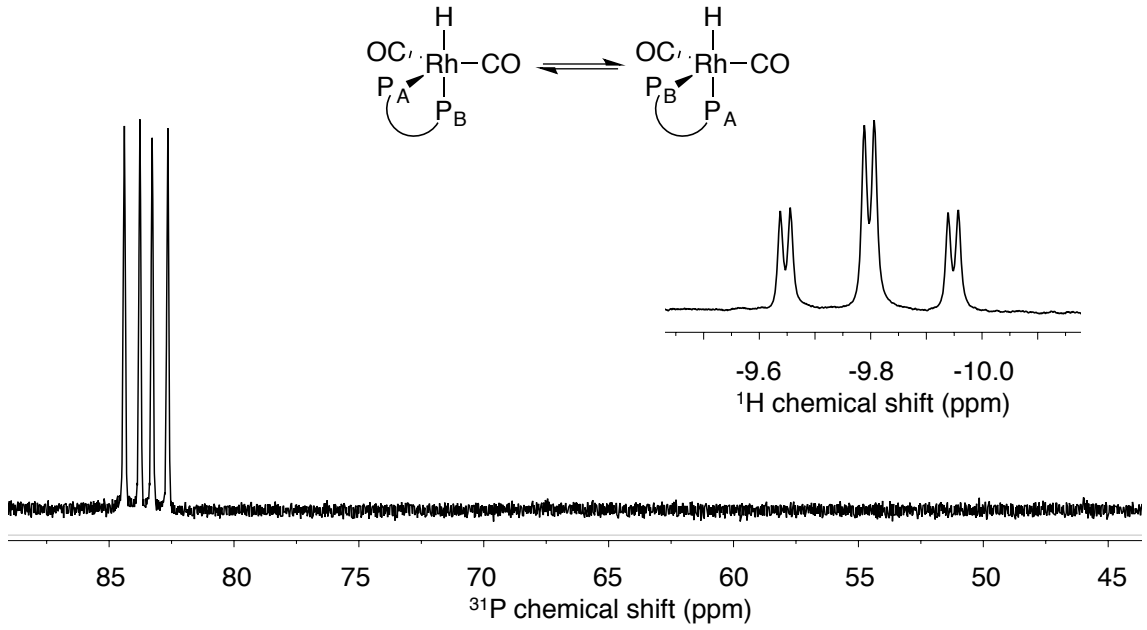

Figure 2.2. ^{31}P spectrum and hydride resonance (inset) of [Rh(H)(CO)$_2$(BDP)]; (BDP) = tetraphenyl bis(diazaphospholane). The two phosphorus atoms of the ligand are in rapid exchange, and appear equivalent.

Although hydroformylation using this ligand is less regio- and enantioselective than that performed using the tetra(amide) bis(diazaphospholanes), the R-branched products are still preferred for the three "benchmark" AHF substrates styrene, vinyl acetate, and allyl cynanide .* We are hopeful that the tetraphenyl ligand will therefore be an adequate model for our NMR studies of Rh(BDP)-catalyzed hydroformylation.

* Jerzy Klosin; unpublished results.

2.1.3 Synthesis of an anionic rhodium precursor

The motivation for clean synthesis of the rhodium hydrides was the potential interception of hydroformylation intermediates via reaction of this hydride with stoichiometric amounts of substrate at low temperatures and pressures – essentially replicating hydroformylation under conditions more amenable to the characterization of intermediates. Another approach to these intermediates is their independent synthesis from rhodium precursors and organic fragments. One plausible method is the reaction of a nucleophilic rhodium anion with an organic electrophile such as an acid chloride. For the synthesis of anionic rhodium species we turned to work published by Chan, who was able to generate complexes of the type $[Rh(CO)_xL_y]^-$ (L = phosphine ligand) by reducing the corresponding chlorocarbonylbis(phosphine) species with sodium- or potassium-mercury amalgam under a CO atmosphere.[6]

We wondered if we might be able to achieve the same result by simply deprotonating the hydridodicarbonyl species with a strong base. We found that, by adding an excess of potassium hydride to a THF solution of the rhodium hydride, we could cleanly generate the anionic rhodium species $[Rh(CO)_2(BDP)]K$ (see Scheme **xxx**).

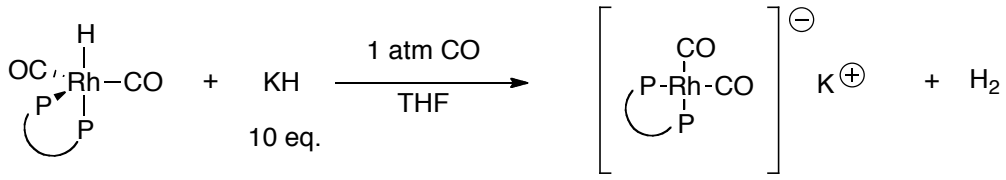

Scheme 2.3. Deprotonation of the rhodium hydride to give an anionic rhodium dicarbonylbis(phosphine) species.

The ^{31}P NMR spectrum of this reaction mixture shows a single species at δ 77.0 ppm (d, $^{1}J_{PRh}$ = 191 Hz; see Supporting Information) . Obvious gas evolution, the absence of a hydride signal in the proton spectrum, and the identical appearance of the proton-coupled and -decoupled phosphorus spectra confirm deprotonation. Moreover, this complex reacts (albeit slowly) with water to regenerate the rhodium hydride. For reaction of this species with organic electrophiles, see Chapter 4.

2.2 Experimental

2.2.1 General considerations

All manipulations were carried out under nitrogen using standard Schlenk, high vacuum, and glovebox techniques. All solvents and liquid reagents were degassed by at least three freeze-pump-thaw cycles unless otherwise noted. Dichloromethane and CD_2Cl_2 were distilled from P_2O_5 and degassed. Tetrahydrofuran was distilled from sodium benzophenone ketyl and degassed. Ethanol and $CDCl_3$ were used as received. All solvents used in column chromatography were used as received. Benzaldehyde, 2-carboxy benzaldehyde, phenylenebis(phosphine), hydrazine, diisopropylethylamine, benzylamine, and octylamine (all from Sigma) were used as received. PyBOP (benzotriazol-1-yloxytripyrrolidino-phosphonium hexafluorophosphate) was purchased from EMD Biosciences and used as received. [Rh(acac)$(CO)_2$] was used as received from Dow and stored in the glovebox. Potassium hydride was washed with hexanes and stored in the glovebox.

Routine ^{1}H and ^{31}P NMR spectra were recorded on a Bruker AC-300 MHz spectrometer; ^{13}C, ^{2}H, and all reaction monitoring and two-dimensional experiments were

performed using Varian Inova-500 MHz or Unity-500 MHz spectrometers. Proton spectra were referenced to residual protio solvent; an xref macro was used to reference ^{2}H, ^{13}C, and ^{31}P spectra to accompanying proton spectra.

Syntheses of rhodium complexes are essentially identical for all ligands used; synthetic details (masses, solvents , etc.) and spectroscopic data apply to the tetraphenyl ligand system unless otherwise noted. All pressures given are gauge pressures unless otherwise noted.

2.2.2 Synthesis of ligands and Rh complexes

Benzylamide bis(diazaphospholane): The tera(carboxylic acid) bis(diazaphospholane) was synthesized as described in ref. 2. This white solid (380 mg, 0.42 mmol) and 891 mg (1.71 mmol) PyBOP were suspended in 25 mL CH_2Cl_2 under a nitrogen atmosphere. Diisopropylethylamine (0.3 mL, 1.72 mmol) and benzylamine (0.18 mL, 1.5 mmol) were added via syringes, solubilizing the solids to generate pale yellow solution, and the mixture was allowed to stir at room temperature overnight. The reaction mixture was washed with 1M HCl , saturated $NaHCO_3$, and saturated NaCl, and dried over $MgSO_4$. The product was purified by column chromatography (2:1 ethyl acetate:dichloromethane). Yield: 195 mg (0.16 mmol, 37%). ^{1}H NMR (300 MHz, $CDCl_3$): δ 8.68 (br s, 2H), 7.17 (t, J = 5 Hz, 2H) 7.5 – 6.9 (overlapping multiplets, 38H), 6.81 (t, 7.5 Hz, 1H), 6.64 (t, 7.4 Hz, 1H), 6.21 (s, 2H), 6.17 (d, $J_{H\text{-}P}$ = 7.5 Hz, 2H), 4.64 (d, J = 6 Hz, 2H), 4.26 (dd, J = 14.7, 6.3 Hz, 1H), 3.58 (dd, J = 15, 4.8 Hz, 1H), 2.50 (m, 8 H). $^{31}P\{^{1}H\}$ NMR (121.4 MHz, $CDCl_3$): δ 7.0 (s, 2P), -143.7 (septet, $J_{P\text{-}F}$ = 712 Hz, PF_6^-).

Octylamide bis(diazaphospholane): The procedure is analogous to that for the synthesis of the benzylamide bis(diazaphospholane). ^{1}H NMR (500 MHz, acetone-d_6): δ 8.67 (t, J = 5.5 Hz, 2H), 7.74 (t, J = 5.0 Hz, 2H), 7.64 – 7.56 (m, 6H), 7.49 (t, J = 7.5 Hz, 2H), 7.28 – 7.20 (m, 6H), 7.15 (d, J = 7.5 Hz, 2H), 6.98 (t, J = 7.5 Hz, 2H), 6.74 (t, J = 8.0 Hz, 2H), 6.55 (d, J = 7.5 Hz, 2H), 6.14 (s, 2H), 3.49 (m, 5H), 3.22 (m, 3H), 2.95 (m, 4H), 2.40 (m, 4H), 1.70 (m, 4H), 1.58 (m, 4H), 1.49 – 1.18 (m, 40H), 0.92 (m, 12H). ^{13}C{^{1}H} NMR (125.7 MHz, acetone-d_6): δ 168.84, 167.53, 167.16, 140.11, 136.63, 136.26, 135.62, 132.53, 131.06, 130.94, 130.23, 128.99, 128.81, 128.26, 128.07, 127.44, 126.43, 126.17, 58.57 (vt, $J_{C\text{-}P}$ = 18.5 Hz), 56.26 (vt, $J_{C\text{-}P}$ = 5.5 Hz), 39.84, 38.75, 31.78, 29.68, 29.58, 29.51, 29.40, 29.32, 29.32, 29.24, 29.19, 29.09, 28.93, 28.78, 28.62, 28.47, 27.07, 26.96, 22.48, 13.53. ^{31}P{^{1}H} NMR (121.4 MHz, acetone-d_6) : δ 3.8 (br s, 2P), -142.6 (septet, $J_{P\text{-}F}$ = 709 Hz)

Phenyl azine: Benzaldehyde (30 mL, 296 mmol) acid was dissolved in 150 mL ethanol in an Erlenmeyer flask; to this was added, dropwise, a solution of 7.2 mL (148 mmol) hydrazine monohydrate in 60 mL ethanol. This gave a yellow solution; after stirring for two minutes, a yellow precipate formed. The flask was placed in an ice bath and the reaction mixture was allowed to cool to 0 °C. The mixture was filtered, and the product, a yellow solid, washed with cold ethanol and dried under vacuum overnight. Isolated yield: 20.88 g (103 mmol, 70%). ^{1}H NMR (300 MHz, $CDCl_3$): δ 8.69 (s, 2H, N=C*H*), 7.87 (m, 4H), 7.46 (m, 6H).

Tetraphenyl bis(diazaphospholane): Phenyl azine (1.09 g, 5.4 mmol) was dissolved in 10 mL THF in a Schlenk flask. Phthaloyl dichloride (1.1 mL, 7.7 mmol) and1,2-bis(phosphino)benzene (0.32 mL, 2.5 mmol) were added via syringe. A white solid precipitated immediately, but redissolved within one minute of stirring. After thirty minutes, another solid was formed. The reaction mixture was allowed to stir under nitrogen overnight. The product, a white solid, was filtered by suction and washed sequentially with THF and diethyl ether; it was purified by flash column chromatography (9:1 CH_2Cl_2:EtOAc). Yield: 427 mg (0.58 mmol, 23%). ^{1}H NMR (300 MHz, $CDCl_3$, 24 °C): δ 8.41 (dd, *J* = 8.1, 1.8 Hz, 2H), 8.25 (dd, *J* = 7.2, 1.5 Hz, 2H), 7.84 (m, 4H), 7.3 - 7.5 (overlapping multiplets, 8H), 7.22 (t, *J* = 7.5 Hz, 2H), 7.14 (d, *J* = 7.5 Hz, 4H), 7.01 (br t, *J* = 7 Hz, 4H), 6.64 (br s, 2H), 6.23 (s, 2H), 6.17 (d, *J* = 10.2 Hz, 2H). ^{31}P{^{1}H} NMR (121 MHz, $CDCl_3$, 24 °C): δ -14.72 (s, 2P).

Rh(acac)(BDP): In the glovebox, 500 mg (0.61 mmol) tetraphenyl ligand and 158 mg (0.61 mmol) Rh(acac)$(CO)_2$ were combined in a Schlenk flask. The flask was placed under nitrogen on a Schlenk line and vented to an external oil bubbler. Upon addition of 50 mL of dichloromethane via a cannula, the solids dissolved, giving a yellow solution; copious bubbling indicated liberation of CO. The reaction mixture was allowed to stir at room temperature for two hours, after which the vent was removed and stirring continued overnight. The solvent was removed under vacuum, and the product, a yellow powder, was collected in the glovebox. Conversion: 100% (NMR). ^{1}H NMR (300 MHz, CD_2Cl_2, 24 °C): δ 8.36 (m, 4H), 7.92 (m, 4H), 7.50 (m, 2H), 7.1 – 7.4 (overlapping

multiplets, 26H), 6.56 (s, 2H), 5.76 (t, J = 3 Hz, 2H), 5.05 (s, 1H), 1.50 (s, 6H). $^{31}P\{^{1}H\}$ NMR (121 MHz, CD_2Cl_2, 24 °C): δ 206.1 (d, J = 206 Hz, 2P).

Rh(H)(CO)$_2$(BDP): In the glovebox, 60 mg (59 μmol) of Rh(acac)(P^P) was dissolved in 1 mL CH_2Cl_2 in a 15-mL pressure bottle. The pressure bottle was attached to a reactor head, removed from the glovebox, and connected to a tank of 1:1 CO/H_2 (syngas) using QuickConnect adapter. The reactor was purged with syngas for approximately one minute and then pressurized to 140 psig. The solution was allowed to stir in a 60 °C oil bath for at least three hours, by which time the color has changed to red-brown. Conversion: 97 % (NMR; other products are phosphine mono- and dioxides.) ^{1}H NMR (300 MHz, CD_2Cl_2, 24 °C): δ 8.30 (m, 4H), 7.87 (m, 4H), 7.59 (m, 2H), 7.0 – 7.5 (overlapping multiplets, 22H), 6.90 (d, J = 6.9 Hz, 4H), 6.15 (s, 2H), 5.86 (t, J = 3.3 Hz), -9.73 (td; $J_{H\text{-}P}$ = 75.6 Hz, $J_{H\text{-}Rh}$ = 9.0 Hz; 1H; hydride). Acetylacetone: δ 15.65 (br s, 1H, enol O*H*), 5.53 (s, 1H, enol =C*H*), 2.04 (s, enol C*H*$_3$); 3.57 (s, 2H, keto C*H*$_2$), 2.20 (s, 6H, keto C*H*$_3$). Keto:enol = 1:4. ^{31}P NMR (121 MHz, CD_2Cl_2, 24 °C): δ 83.5 (dd; $J_{P\text{-}Rh}$ = 137, $J_{P\text{-}H}$ = 76 Hz; 2P).

Addition of styrene to Rh(H)(CO)$_2$(octylamide-BDP): A pressure reactor containing a 60 μM solution of Rh(H)(CO)$_2$(octylamide-BDP) in acetone-d_6 was depressurized and refilled with 20 psi CO. It was connected via a cannula to an oven-dried septum-capped NMR tube equipped with a vent, and the pressure reactor/NMR tube system was purged with CO for several minutes. The cannula was then used to transfer the solution to the NMR tube, and the tube was sealed with Parafilm. Initial

NMR spectra were taken, after which the sample was ejected from the spectrometer, and 20 μL (0.2 mmol) styrene was added via a gastight syringe; the tube was inverted three times and quickly returned to the spectrometer.

[Rh(CO)$_2$(BDP)]K: [Rh(H)(CO)$_2$(BDP)] was generated as described above, but in tetrahydrofuran instead of dichloromethane. The reactor was vented and pressurized with CO; using a cannula, it was connected to a Schlenk flask containing 30 mg (0.75 mmol) KH. The reactor/Schlenk flask system was purged with CO for several minutes, and then the solution was transferred from the pressure reactor to the Schlenk flask via the cannula. Gas was evolved from the reaction mixture, which darkened to a deep brown. The mixture was allowed to stir at room temperature for one hour. The flask was placed under positive nitrogen pressure, and the solution was transferred away from the excess potassium hydride into an NMR tube via a filter cannula. Conversion (NMR): 100 %. ^{31}P NMR (121 MHz, THF, 24 °C): δ 77.0 (d, $J_{P\text{-}Rh}$ = 190 Hz, 2P).

2.3 References

(1) Clark, T. P.; Landis, C. R.; Freed, S. L.; Klosin, J.; Abboud, K. A. *J. Am. Chem. Soc.* **2005**, *127*, 5040-5042.

(2) Clark, T. P.; Landis, C. R. *J. Am. Chem. Soc*. **2003**, *125*, 11792 – 11793.

(3) Fennis, P. J.; Budzelaar, P. H. M.; Frijns, J. H. G.; Orpen, A. G. *J. Organomet. Chem*. **1990**, *393*, 287 – 298.

(4) (a) Brown, J.; Kent, A. *J. Chem. Soc. Perkin Trans*. *2* **1987**, 1597. (b) Casey, C. P.; Whiteker, G. T.; Melville, M. G.; Petrovich, L. M.; Gavney, J. A.; Powell, D. R. *J.*

Am. Chem. Soc. **1992**, *114*, 5535 – 5543. (c) Makado, G.; Morimoto, T.; Sugimoto, Y.; Tsutsumi, K.; Kagawa, N.; Kakiuchi, K. *Adv. Synth. Catal*. **2010**, *352*, 299 – 304.

(5) Claver, C.; van Leeuwen, P. W. N. M. In *Rhodium Catalyzed Hydroformylation*; Claver, C., van Leeuwen, P. W. N. M., Eds.; Kluwer Academic Publishers: Dordrecht, The Netherlands, 2000.

(6) Chan, A. S. C.; Shieh, H.-S.; Hill, J. R. *J. Organomet. Chem.* **1985**, *279*, 171-179.

Chapter 3

Interception and characterization of catalyst species: styrene

Portions of this chapter were published as Nelsen, R. R.; Landis, C. R. *J. Am. Chem. Soc.* **2013**, *135*, 9636 – 9639.

3.1 Introduction

Rhodium-catalyzed hydroformylation of alkenes has long been important to the production of commodity chemicals and increasingly shows promise for fine, and even enantiopure, chemical production.[1] A general mechanism was first presented by Breslow and Heck for cobalt-catalyzed hydroformylation some fifty years ago (See Scheme 3.1).[2] However, fundamental questions concerning the origins of regioselectivity and enantioselectivity in rhodium-catalyzed hydroformylation remain unanswered because key reaction intermediates have not been characterized structurally, kinetically, or thermodynamically. Herein we report the first interception of linear and branched rhodium alkyl intermediates along a hydroformylation pathway, characterization of their structures by multinuclear NMR spectroscopy, and estimation of their relative thermodynamic stabilities. Furthermore we demonstrate that the thermodynamic preference for linear vs. branched isomers inverts upon conversion of the rhodium alkyls to the rhodium acyls.

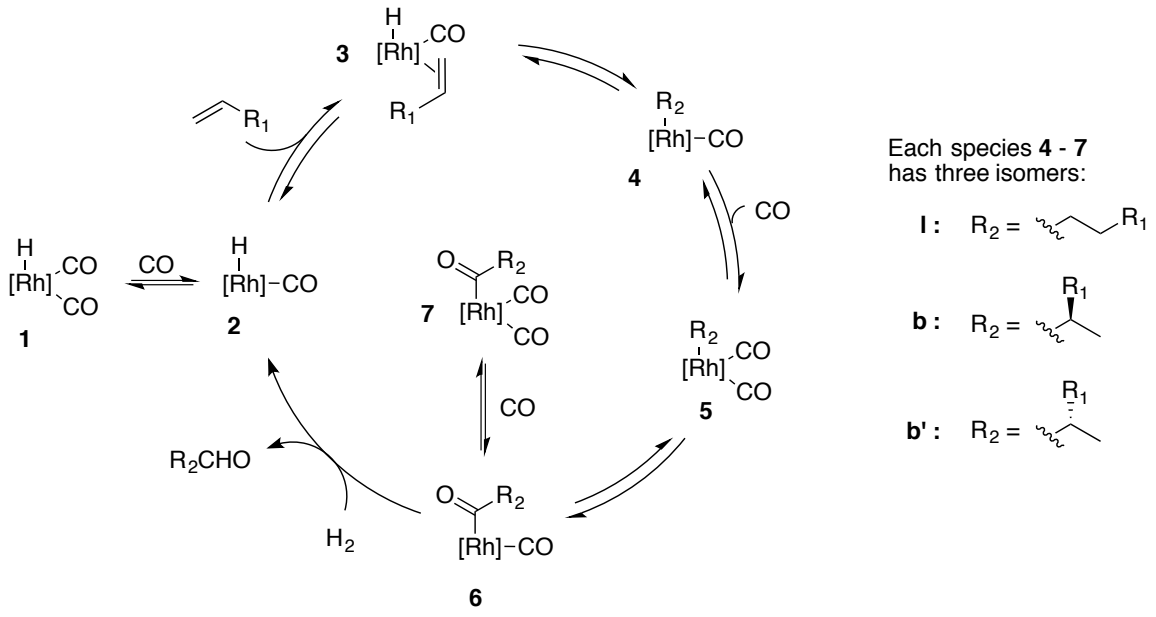

Scheme 3.1. Proposed mechanism for hydroformylation.

The 3,4-bis(diazaphospholane) (BDP) class of ligands introduced in 2004 combine high activity – greater than one turnover per second – and useful selectivities for the enantioselective hydroformylation of various alkene substrates.[3]

Previous work from this group on the Rh(BDP)-catalyzed hydroformylation of styrene demonstrated that both the branched-to-linear ratio and percent *ee* of the product increases with increasing partial pressure of CO (P_{CO}). These observations, along with the results of isotopic labeling experiments and *in situ* IR monitoring, are consistent with a kinetic model in which CO dissociation from the resting state **1** is required to initiate the cycle. For the kinetically favored (*R)*-branched alkyl species **4**, β-hydride elimination is competitive with trapping by CO to give product. Thus, CO promotes formation of (*R*)-branched product but inhibits entry of catalyst from the resting state, leading to an overall

independence of the rate with respect to [CO]. Production of linear and (*S*)-branched aldehydes show inhibition, only, by CO. [4]

However, the data supporting this kinetic model are indirect; direct observation of critical intermediates could provide additional insight into the fundamental thermodynamics and kinetics that control selectivity. To date the most detailed characterization of species along the hydroformylation pathway comes from Brown and Kent's NMR studies of the reaction of styrene with $[Rh(H)(CO)(PPh_3)_3]$ in the absence of H_2.[5] These studies revealed formation of branched and linear acyls of the formula $Rh(acyl)(PPh_3)_2(CO)_2$, with the branched acyl formed first and followed by equilibration to the more stable linear acyl. Since that time, however, the few examples of related intermediates have been limited to slow and/or unselective catalysts or synthesis of analogous iridium complexes.[6] Because Rh(BDP) catalysts exhibit such high hydroformylation activities, we speculated that reaction of styrene with $RhH(BDP)(CO)_2$ at low temperatures and in the absence of H_2 would proceed to alkyl or acyl intermediates at rates convenient for characterization by NMR.

3.2 Reaction of rhodium hydride with styrene and identification of acyl complexes

The hydrido dicarbonyl complex **1** cleanly forms upon exposure of [Rh(acac)(BDP)] to 140 psi 1:1 CO/H_2 overnight at 60 °C in dichloromethane. The ^1H and ^{31}P NMR spectra of **1** are consistent with a fluxional trigonal bipyramidal species with axial-equatorial coordination of the bisphosphine, as has been seen for other small-bite-angle ligands.[7]

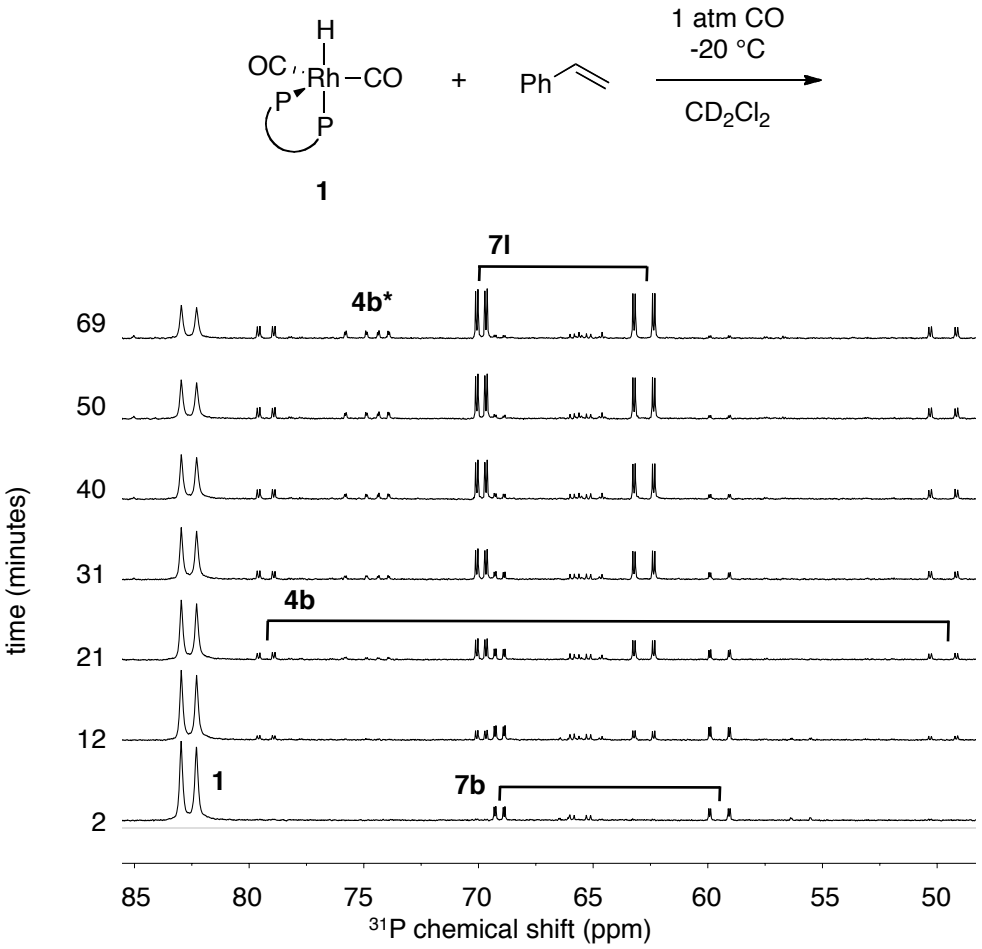

Figure 3.1. $^{31}P\{^{1}H\}$ NMR spectra (202.5 MHz) monitoring the reaction of [Rh(H)(CO)$_2$(BDP)] (**1**; δ 83 ppm; 60 mM) with styrene under a CO atmosphere at −20 °C in CH_2Cl_2. Spectra show acyl complexes **7b$_{sty}$**, **7l$_{sty}$** and alkyl complexes **4b$_{sty}$**, **4b*$_{sty}$** growing in over time. Conversion to aldehydes <1%.

Under a narrow range of conditions (ca. 1 atm. CO, 0 to -30 °C), the reaction of this rhodium hydride with five equivalents of styrene can be monitored directly by ^{1}H and ^{31}P NMR spectroscopy. A representative set of $^{31}P\{^{1}H\}$ spectra, showing the course of the reaction at -20 °C under a CO atmosphere, is presented in Figure 3.1. The phosphorus signal of the hydride complex **1** (δ 83 ppm) disappears in a roughly first-order fashion,

with a half-life of about thirty minutes. It is replaced by several new ligand-containing species. The two major species are the five-coordinate linear and branched acyl complexes **7l$_{sty}$** and **7b$_{sty}$** (see Figure 3.2), each of which have two distinct phosphorus resonances at δ 69.1 & 59.3 ppm and δ 69.8 & 62.4 ppm, respectively. Each peak is a doublet of doublets; the larger coupling is $^{1}J_{PRh}$, and the smaller is $^{2}J_{PP}$.

7b$_{sty}$ **7l$_{sty}$**

Figure 3.2. Five-coordinate acyl complexes formed by the reaction of **1** with styrene. Chiral centers are denoted by (*).

The branched (**7b$_{sty}$**) and linear (**7l$_{sty}$**) regioisomers are distinguished by ^{31}P-^{1}H multiple-bond correlation experiments. These data show through-bond coupling from the ligand phosphorus atoms of **7b$_{sty}$** to a methine quartet and methyl doublet at δ 3.47 and 0.79 ppm respectively, and from those of **7l$_{sty}$** to diastereotopic methylene protons at δ 2.92 and 1.95 ppm (α-methylene) and δ 2.53 and 2.23 ppm (β-methylene) (See Figure 3.3). Acyl carbonyl signals, characterized by their far-downfield chemical shifts, confirm the assignment as acyl rather than alkyl complexes (see Figure 3.4). Each of these signals is a doublet of doublets, with $^{2}J_{CP}$ = 86 Hz and $^{1}J_{CRh}$ = 21 Hz (**7b$_{sty}$**), and $^{2}J_{CP}$ = 83 Hz

and $^{1}J_{CRh}$ = 19 Hz (**7l$_{sty}$**). The chemical shifts and coupling constants are consistent with those reported by Brown for the five-coordinate acyl complexes of triphenylphosphine.[5]

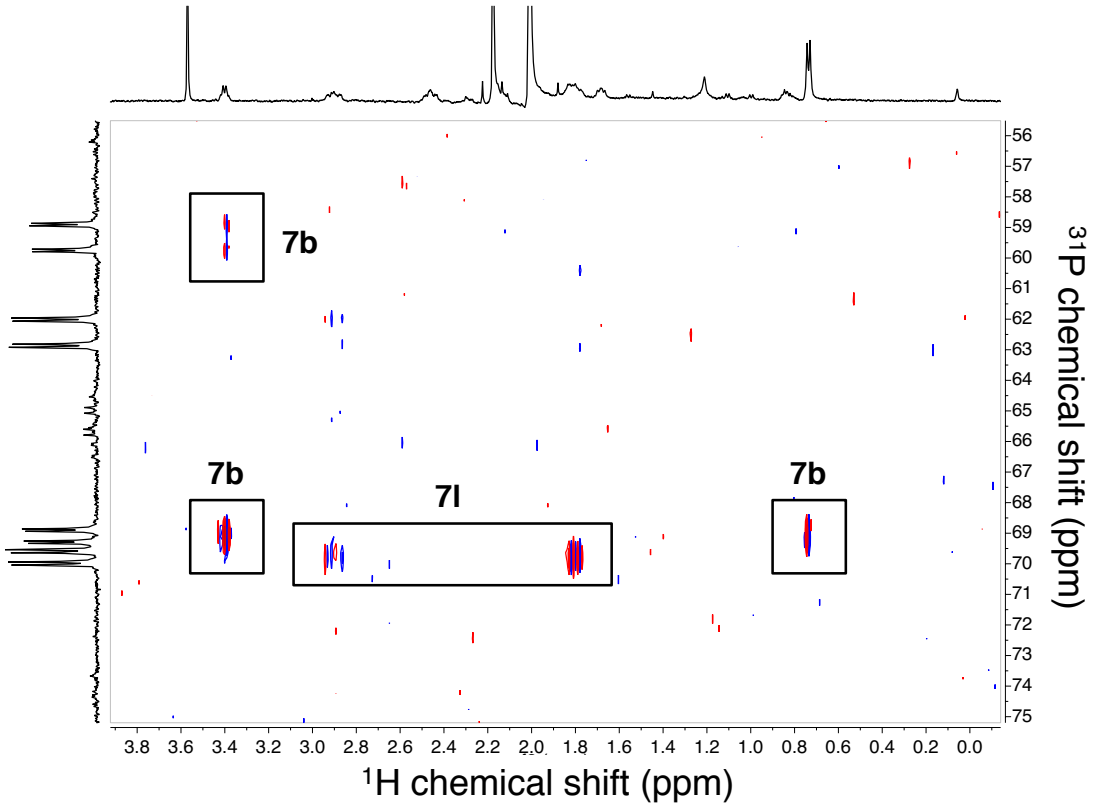

Figure 3.3. ^{1}H-^{31}P gHMBC taken during the reaction of **1** with styrene ((f1,f2) = (500, 202.5 MHz), CH_2Cl_2, -40 °C; nt = 4, ni = 256, jnxh = 3 Hz).

While both four- and five-coordinate acyl complexes are possible under these conditions, the coupling pattern of the acyl complexes generated using ^{13}CO rules out four-coordinate species. Figure **xxx** shows that P_A is coupled to three ^{13}C nuclei; it is coupled strongly ($^{2}J_{PC}$ = 82 Hz) to the acyl group, and more weakly ($^{2}J_{PC}$ = 17 Hz) to the two terminal CO ligands. (Although this multiplet is correctly interpreted as a *dddt*, it appears as a triplet of quartets because the large $^{2}J_{PC}$ is coincidentally equal to $^{1}J_{PRh}$, and the two smaller $^{2}J_{PC}$ to $^{2}J_{PP}$.) These data demonstrate that species **7b,l$_{sty}$** are five-

coordinate trigonal bipyramidal species with two terminal CO ligands, where the acyl group is in the axial position *trans* to one of the ligand phosphorus atoms.

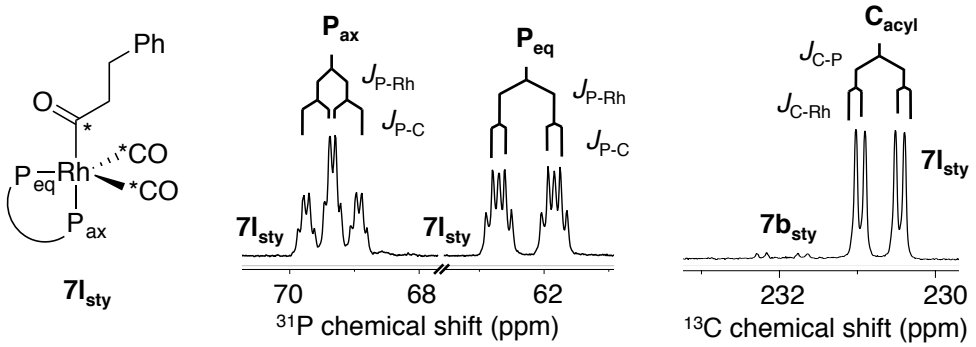

Figure 3.4. Using ^{13}C labeling to determine the coordination number of **7b$_{sty}$**, **7l$_{sty}$**. An * denotes a ^{13}C nucleus. This experiment also permitted observation of the acyl carbonyl signals, shown at right.

Although this result was somewhat disappointing – because the five-coordinate acyl complexes are not on the catalytic cycle but reversibly linked to it via CO binding to four-coordinate acyl complexes **6$_{sty}$** (see Scheme 3.1) – it is not unexpected. Square-planar complexes typically have larger J_{PRh} values than observed for these species, and five-coordinate complexes are known to be preferred for d^8 transition-metal complexes.[8] Computational studies of hydroformylation have consistently cited these acyl dicarbonyls as energetic minima.[13]

The other diastereomer of the branched acyl complex, **7b'$_{sty}$**, cannot be distinguished in the relatively crowded ^{31}P NMR spectrum; however, the ^{13}C NMR spectrum shows a doublet-of-doublets 1 ppm upfield from the methine resonance of **7b** which is consistent with **7b'$_{sty}$** (for both multiplets, $^3J_{CP}$ = 33 Hz and $^2J_{CRh}$ = ~2 Hz; the

smaller coupling is not well-resolved). If this assignment is correct, **7b$_{sty}$** : **7b'$_{sty}$** ≈ 18 : 1 – much higher than the observed enantioselectivity with this catalyst.

3.3. Identification of alkyl complexes

Under conditions of low [CO], three species with ^{31}P resonances at δ 50 & 79 ppm, δ 73.7 & 74.4 ppm, and 57 & 78 ppm become more prominent. We have characterized these as the branched rhodium-alkyl monocarbonyl complex **4b$_{sty}$**, the η ^{3}-benzyl complex **4b*$_{sty}$** resulting from CO dissociation from **4b$_{sty}$**, and the linear alkyl-rhodium dicarbonyl complex **5l$_{sty}$**, respectively (see Figure 3.5).

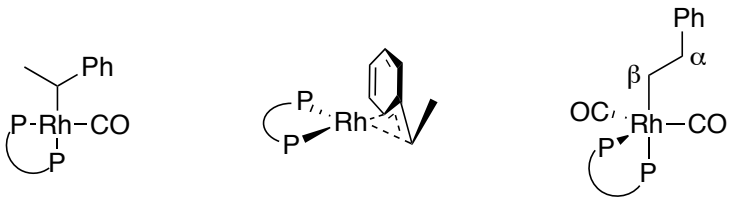

4b$_{sty}$ **4b*$_{sty}$** **5l$_{sty}$**

Figure 3.5. Rh-alkyl complexes characterized following the reaction of **1** with styrene.

3.3.1 4b$_{sty}$

The large ^{1}JPRh coupling constants observed for **4b$_{sty}$** (134 and 232 Hz for the peaks at 78 and 48 ppm, respectively) are consistent with a four-coordinate square-planar species. An alkyl or acyl monocarbonyl complex could be consistent with this geometry; however, because these complexes differ in number of carbonyl groups, ^{31}P-^{13}C coupling data allows us to distinguish between them. When **4b$_{sty}$** is generated using ^{13}CO, the downfield resonance for shows one 13-Hz ^{31}P-^{13}C coupling (consistent with a *cis*

arrangement); the upfield peak shows one 68-Hz ^{31}P-^{13}C coupling (consistent with a *trans* arrangement)[9] (see Figure 3.6). These observations are consistent with a complex with only one carbonyl group, ruling out a four-coordinate acyl species.

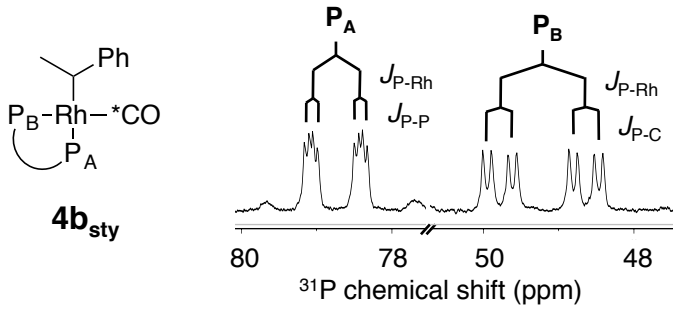

Figure 3.6. Labeling with ^{13}CO demonstrates that 4bsty is a four-coordinate alkyl monocarbonyl complex. Only one peak (P_B) shows a J_{PC} consistent with a *trans* carbonyl or acyl group. Istotopic label denoted by (*).

To definitively characterize **4b$_{sty}$** as the four-coordinate branched (rather than the linear) alkyl, α- and β-^{13}C-labeled styrene were synthesized and used to generate 4b. After the reaction of **1** with β-^{13}C-styrene, ^{31}P-^{13}C gHMBC revealed a correlation between the downfield ^{31}P resonance of **4b$_{sty}$** (δ 79.3 ppm) and a narrow doublet ($^3J_{CP}$ = 2.6 Hz) in the ^{13}C NMR spectrum at δ 20.3 ppm, which could plausibly be assigned to either a methyl carbon or a methylene carbon shifted upfield by coordination to the metal (although the absence of strong coupling argued against the latter interpretation). ^{13}C-^{13}C COSY showed a correlation between this peak and a second ^{13}C resonance at δ 37.7 ppm. Direct analysis of this resonance was only possible after the reaction of **1** with α-^{13}C-styrene, which revealed that this signal is a doublet of doublets ($^2J_{CP}$ = 45.7 Hz, $^1J_{CRh}$

= 9.8 Hz; coupling constants assigned by comparison with the corresponding ^{31}P NMR spectrum), consistent with a carbon atom α to rhodium and *trans* to a phosphine ligand. DEPT experiments confirmed that the two signals at δ 20.3 and 37.7 ppm are a methyl/methine pair, finalizing the assignment of **4b$_{sty}$** as a four-coordinate branched alkyl monocarbonyl complex.

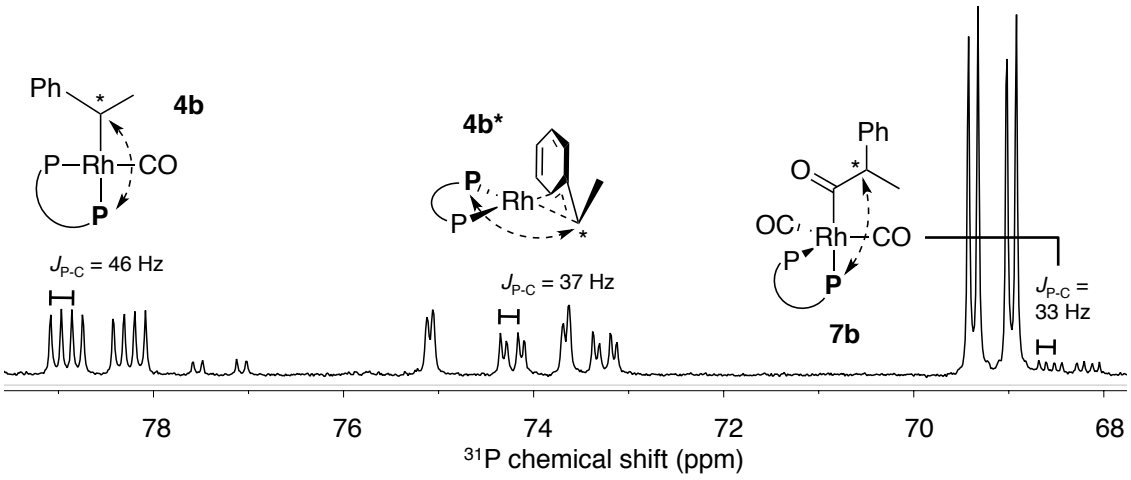

Figure 3.7. Upon reaction of **1** with α-^{13}C-styrene, new J_{PC} appear in the signals for **4b$_{sty}$** (left), **4b*$_{sty}$** (center), and **7b$_{sty}$** (far right), demonstrating that each of these species is the branched regioisomer. ^{13}C nuclei are denoted by (*).

^{1}H-^{31}P gHMBC showed through-bond coupling from the ^{31}P signals of **4b$_{sty}$** to a doublet-of-doublets at δ 1.7 ppm and a broad multiplet at 2.4 ppm, which can be assigned as the methyl and methine signals, respectively.

3.3.2 4b$_{sty}$*

The identity of **4b*$_{sty}$** was initially confusing, because the very small (< 1 ppm) difference in chemical shift between its two phosphorus atoms was inconsistent with the

alkyl and acyl complexes already characterized. However, nearly-identical ^{31}P chemical shifts of the two ligand phosphorus atoms are seen in rhodium allyl bis(phosphine) complexes,[10] suggesting that **4b*$_{sty}$** could be an η^3-benzyl species. The characterization of **4b*$_{sty}$** as an η^3-benzyl species is supported by the observation of strong (37 Hz) ^{31}P-^{13}C coupling when α-^{13}C- labeled styrene is used (see Figure 3.7). The methine carbon (δ 52.5 ppm) shows a measurable (5 Hz) carbon-rhodium coupling in addition to carbon-phosphorus coupling. Because no additional splitting appears in the ^{31}P NMR spectrum when ^{13}CO is used, we assume that **4b*$_{sty}$** has no terminal carbonyl ligands, and is a formally three-coordinate species as drawn in Figure 3.5. We assume that it is in equilibrium with **4b$_{sty}$** via CO dissociation/binding (see Scheme 3.2).

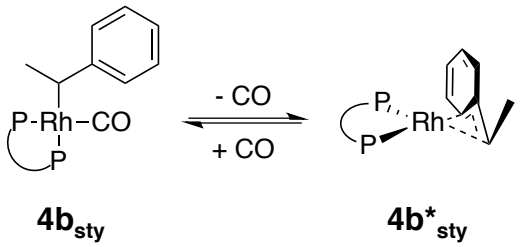

4b$_{sty}$ **4b*$_{sty}$**

Scheme 3.2. Formation of **4b*$_{sty}$** via reversible CO dissociation from **4b$_{sty}$**.

In addition to the unusually-close ^{31}P signals, other NMR features of **4b***sty were originally puzzling. Superficial examination of the 1-D ^{31}P NMR spectrum is misleading: while it is clear that the four peaks corresponding to **4b*$_{sty}$** belong to two doublets-of-doublets, the peaks' leaning suggests the *opposite* of the correct pairing. In fact, the two doublets-of-doublets overlap, and the deceptive leaning is a second-order effect. The correct assignment for P_A (δ 74.4 ppm; *dd*; $^1J_{PRh}$ = 290 Hz, $^2J_{PP}$ = 12 Hz) and P_B (δ 73.7

ppm; *dd*; $^{1}J_{PRh}$ = 196 Hz, $^{2}J_{PP}$ = 12 Hz) was enabled by the use of α-^{13}C-styrene and careful interpretation of the ^{31}P-^{31}P COSY spectrum (see Figure 3.8). Simulation of signals with these parameters using WinDNMR produced a pattern consistent with the one observed in the NMR spectrum of **4b*$_{sty}$**. (This simulation also clarified why the ^{31}P NMR signals collapse to an apparent doublet-of-doublets and singlet at room temperature (see Figure 3.8): the chemical shift of P_B is more temperature-sensitive than P_A, and as the temperature increases $\Delta(\delta P_A - \delta P_B)$ shrinks. This magnifies the AB-character of the ^{31}P NMR spectrum.

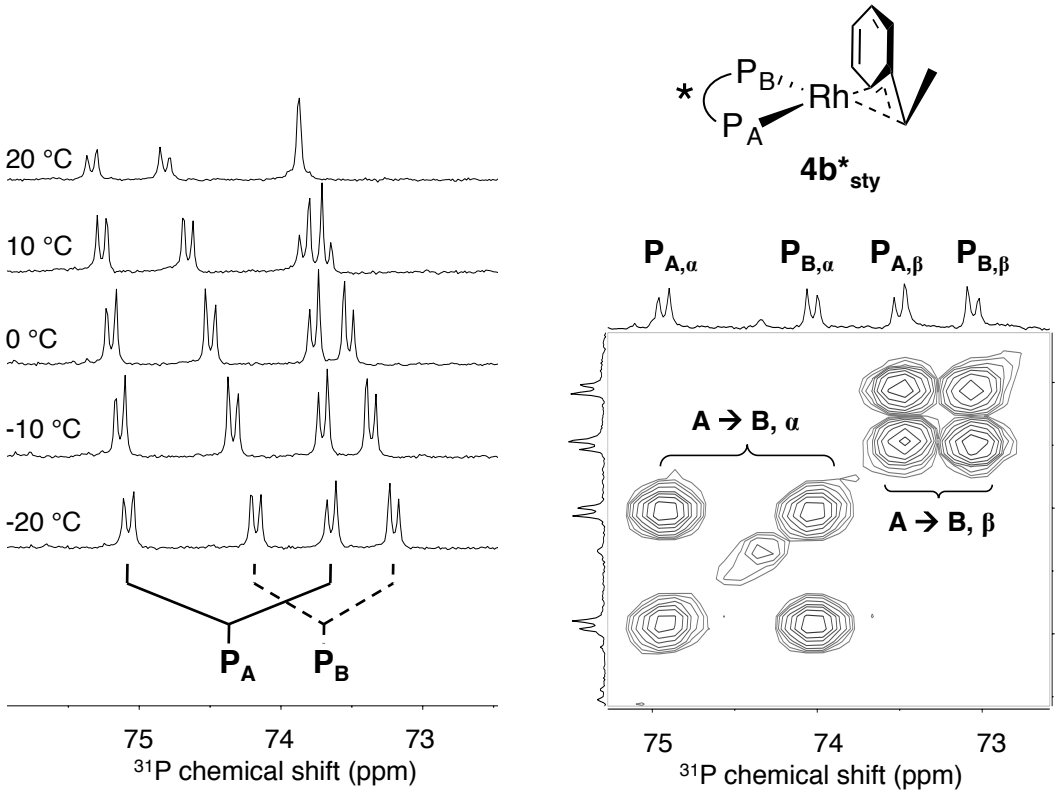

Figure 3.8. Variable-temperature ^{31}P NMR spectra (left) and ^{31}P-^{31}P COSY spectrum (right) of **4b*$_{sty}$**.

3.3.3 ***5l$_{sty}$***

When **5l$_{sty}$** is generated using [Rh(H)(^{13}CO)$_2$(BDP)], each of its phosphorus signals shows two new ^{31}P-^{13}C couplings, indicating that there are two carbonyl groups on this complex; however, none of these coupling constants has a magnitude larger than 41 Hz, making it unlikely that either of the two carbonyl groups is *trans* to a ligand phosphorus atom. (Moreover, the $^1J_{PRh}$ values – 93 and 162 Hz for the downfield and upfield peaks, respectively – are consistent with a 5-coordinate trigonal bipyramidal complex.) The most plausible structure consistent with these constraints is a 5-coordinate dicarbonyl alkyl complex.

As for **4b$_{sty}$**, the use of ^{13}C-labeled styrenes was crucial in determining the regiochemistry of this complex. When **5l$_{sty}$** is generated using β-^{13}C-styrene, the ^{31}P signal at δ 78.1 ppm shows a 60-Hz coupling consistent with a two-bond coupling between *trans* ^{13}C and ^{31}P nuclei (see Figure 3.9), suggesting that **5l$_{sty}$** is the linear regioisomer (when α-^{13}C styrene was used, no new coupling appeared in either peak for **5l$_{sty}$**). In the ^{13}C NMR spectrum, the signal for the methylene carbon α to rhodium and *trans* to the phosphorus atom (multiplicity confirmed by DEPT-135) is upfield-shifted to δ 10.3 ppm, and shows distinct *J*-coupling to phosphorus (60.4 Hz) and to rhodium (13.8 Hz).

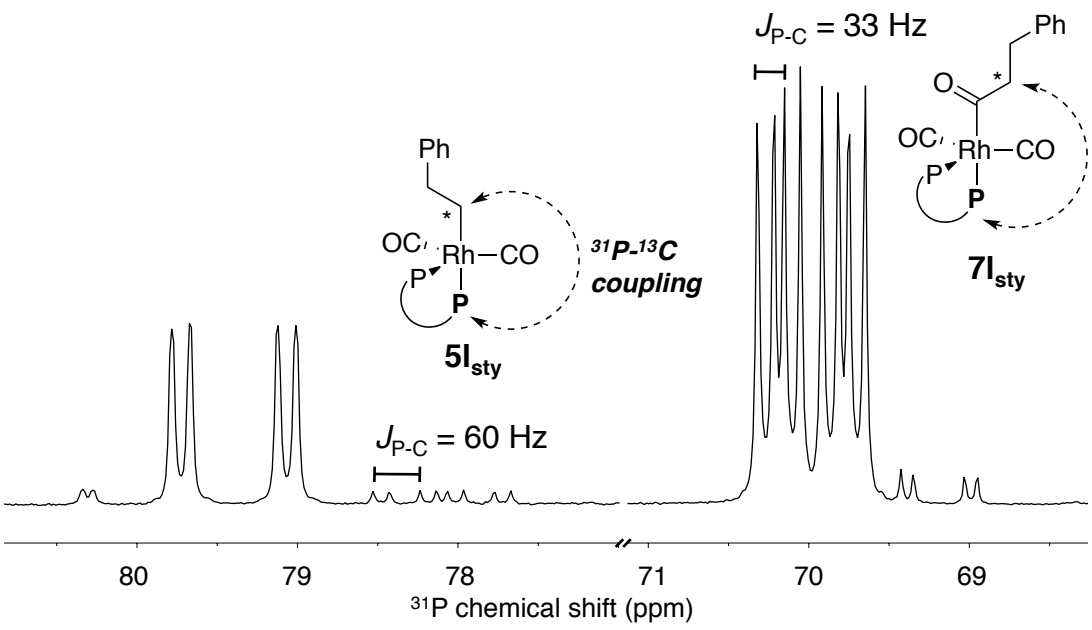

Figure 3.9. Following the reaction of **1** with β-^{13}C-styrene, new J_{PC} appear in the signals of **5l$_{sty}$** (left) and **7l$_{sty}$** (right), demonstrating that these are the linear regioisomers. ^{13}C nuclei are denoted by (*).

To the best of our knowledge, the data reported above constitute the first direct observation of alkyl intermediates for any rhodium hydroformylation catalyst.[11] See Table 3.1 for selected spectroscopic data for **7b$_{sty}$**, **7l$_{sty}$**, **4b$_{sty}$**, **4b*$_{sty}$** and **5l$_{sty}$**.

3.4 Isomerization of acyl complexes

The isomerization of **7b$_{sty}$** to **7l$_{sty}$** must involve β-hydride elimination to give an olefin hydride complex (**3** in Scheme 3.1). Does isomerization proceed with styrene dissociation, as suggested by earlier catalytic studies from this group,[4] or is it intramolecular? To address this question, we added *p*-CF_3-styrene to an equilibrated mixture of **7b$_{sty}$** and **7l$_{sty}$** (see Figure 3.10), having already verified that the rates of

reaction of **1** with styrene and *p*-CF_3-styrene are similar. The rate of formation of the CF_3-containing linear acyl complex (which requires olefin dissociation, followed by branched acyl formation and subsequent isomerization) is comparable to the rate of isomerization of $\mathbf{7b_{sty}}$ to $\mathbf{7l_{sty}}$. If the rate of $\mathbf{7b_{sty}}$/$\mathbf{7l_{sty}}$ isomerization had been substantially faster, that would have suggested that olefin dissociation might not occur during isomerization. The results shown in Figure 3.10 are consistent with a pathway for $\mathbf{7b_{sty}}$-to-$\mathbf{7l_{sty}}$ isomerization that proceeds with olefin dissociation – that is, through rhodium hydrido carbonyl species **2**.

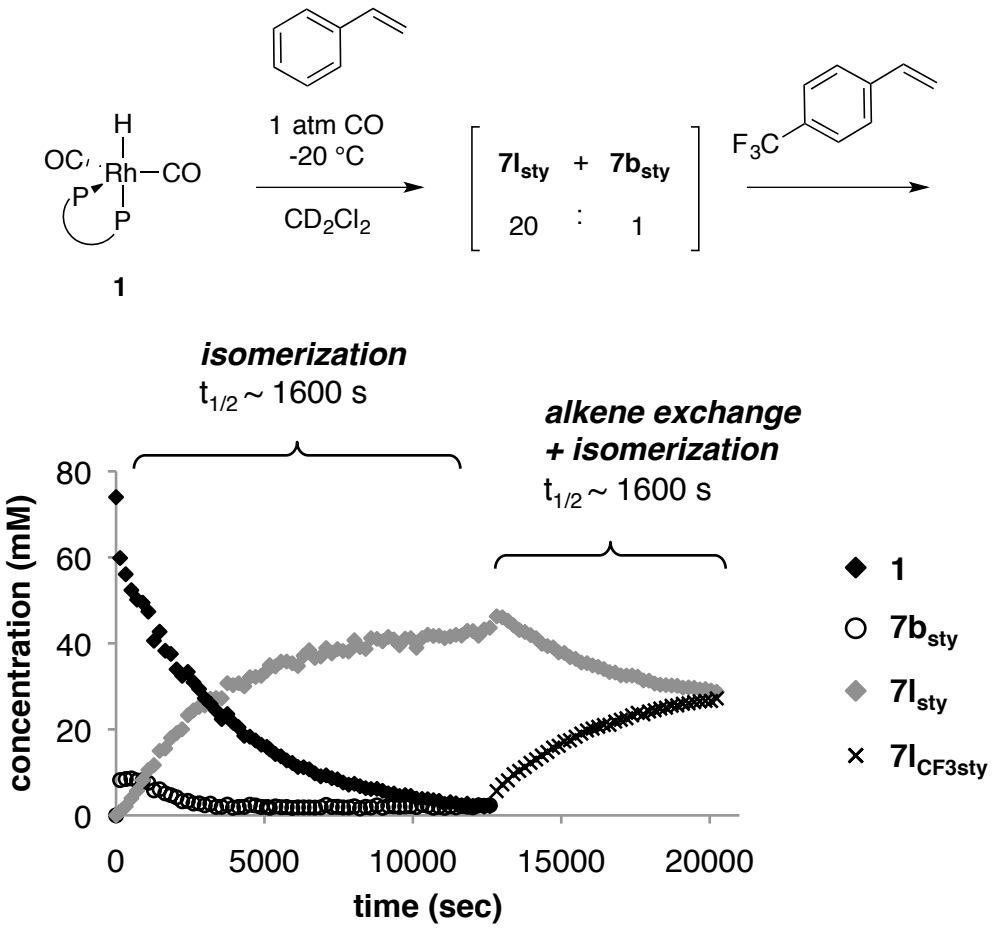

Figure 3.10. Reaction of **1** with styrene in CD_2Cl_2, followed by reaction (time = 12 500 s) of the equilibrated mixture of **7b,l$_{sty}$** with *p*-CF_3-styrene. Concentrations calculated from $^{31}P\{^1H\}$ NMR spectra. These data are consistent with a model in which regioisomerization between acyl complexes occurs with alkene dissociation.

However, it is important to note that this analysis assumes that the concentration of **2** is roughly equivalent throughout the reaction, and therefore has no effect on the relative rates of formation of the unsubstituted and CF_3-labeled acyls. It is impossible to confirm this assumption with our current protocol, which doesn't permit observation of this species.

3.5 Reaction order in styrene

The inability to regulate the CO concentration in solution under the conditions used for these experiments makes it impossible to perform accurate kinetic experiments. However, in an attempt to measure the effect of the styrene concentration on the rate of formation of the acyl complexes, we attempted to approximate reproducible conditions by transferring 1-mL aliquots of a solution of **1**, using the same flow rate of CO, to each of three septum-capped NMR tubes. By adding a different amount of styrene to each, over a range of concentrations spanning an order of magnitude, we can obtain a rough estimate of the reaction order in styrene.

The results are shown in Figure 3.11. Initial rates were obtained by measuring the drop in concentration of **1** from its initial value to its value (calculated relative to a PPh_3 internal standard) when the first spectrum was taken, typically at approximately 100 seconds. The data suggest that the rate becomes saturated in styrene over this concentration range.

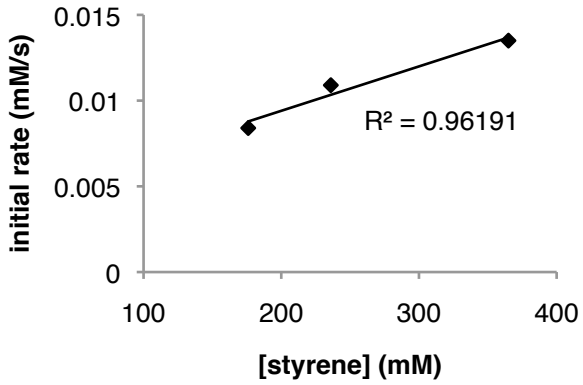

Figure 3.11. Rate dependence on [styrene] of the reaction of **1** with styrene.

3.6 Monitoring the reaction of acyl complexes with syngas by NMR spectroscopy

The acyl complexes **7b,l$_{sty}$** can be generated, and persist as the major species, under an atmosphere of syngas (and even after purging the solution with H_2). Because we know that equilibration between acyl complexes is occurring, the four-coordinate acyl complexes **6b,l$_{sty}$** is present in solution (at a concentration below the limit of detection by NMR spectroscopy). Even in the presence of H_2, however, under these conditions CO binding to **6b,l$_{sty}$** to give **7b,l$_{sty}$** clearly outcompetes hydrogenolysis, which would yield **1** and an equivalent of aldehyde.

However, by continuously purging a solution of **7b,l$_{sty}$** with syngas over a period of one hour, it is possible to force some conversion to aldehyde. Inspection of NMR spectra taken throughout this reaction reveal an interesting phenomenon: although **7b$_{sty}$** : **7l$_{sty}$** = 1 : 2.5 (the higher CO pressure during this reaction inhibits isomerization), 2-phenylpropional : 3-phenylpropional = 2.5 : 1 (see Figure 3.12). That implies that the branched acyl complex **7b$_{sty}$** must go on to give aldehyde nearly an order of magnitude faster than the linear complex **7l$_{sty}$** under these conditions. It is important to note that the five-coordinate acyl complexes **7$_{sty}$** must lose an equivalent of CO prior to reaction with hydrogen, and this experiment cannot distinguish whether the faster rate observed for **7b$_{sty}$** is a result of faster CO dissocation, faster reaction of H_2 with **6b$_{sty}$**, or some combination of the two. However, the results do suggest a stronger role for hydrogenolysis in determining selectivity in AHF than previously thought.

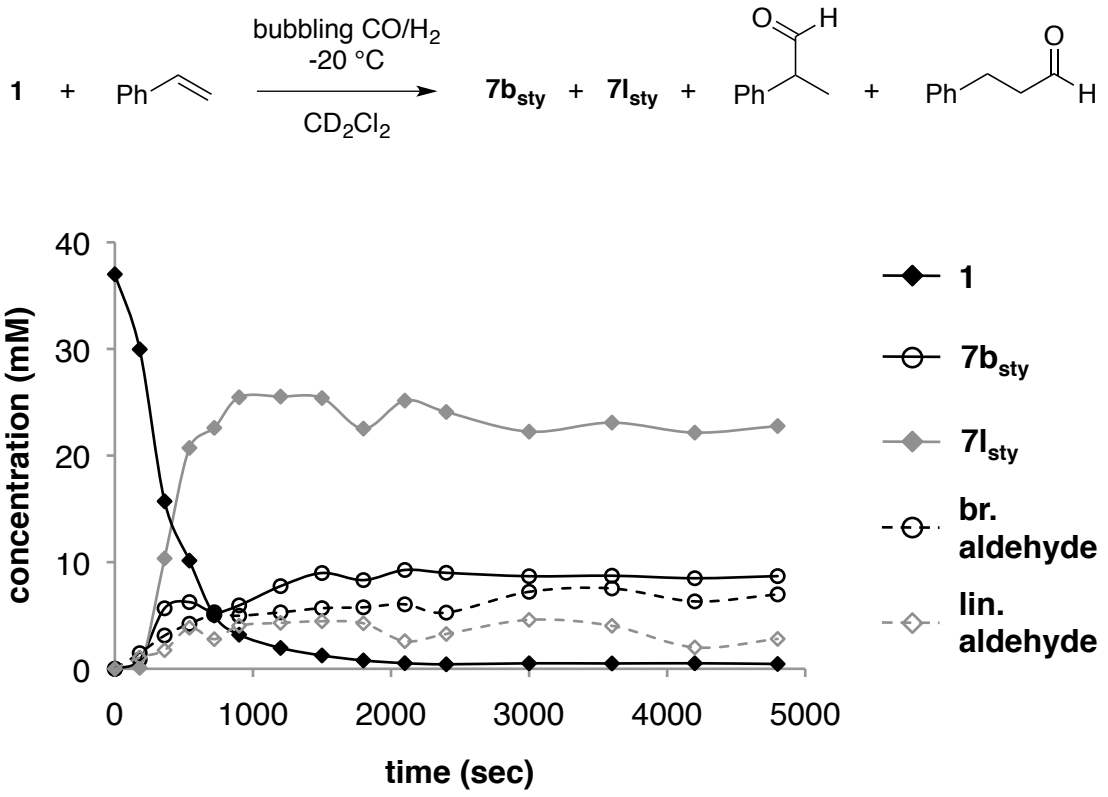

Figure 3.12. Reaction of **1** with styrene while bubbling with syngas. Because $b:l_{acyl} < b:l_{CHO}$, the conversion of the branched acyl to aldehyde must be faster than conversion of the linear acyl.

For a different strategy for studying relative rates of hydrogenolysis, see Chapter 5.

3.7 Discussion and conclusions

The characterization of linear and branched acyl and alkyl complexes provides unique insights into kinetic and thermodynamic influences in hydroformylation. *The branched acyl complex is kinetically favored* (consistent with the conclusion of earlier

studies that insertion to form a branched alkyl is fastest*), but isomerizes to the thermodynamically favored linear acyl complex* ([**7l**$_{sty}$]:[**7b**$_{sty}$] ≈ 35:1). Moreover, **7b**$_{sty}$ appears to be favored over its diastereomer **7b'**$_{sty}$ by a ratio of 18:1. Equilibration between the acyls **7b**$_{sty}$ and **7l**$_{sty}$ must occur via the alkyls **4b**$_{sty}$ and **5l**$_{sty}$. Thus, **4b**$_{sty}$ and **5l**$_{sty}$ must also be equilibrated under conditions where the acyls are in equilibrium; they appear in a ratio of [**4b**$_{sty}$]:[**5l**$_{sty}$] ≈ 9:1. Although monocarbonyl **4b**$_{sty}$ and dicarbonyl **5l**$_{sty}$ differ in the number of terminal CO ligands, *these data demonstrate a thermodynamic preference for the branched alkyl regioisomer* (and facile coordination of CO to the minor species **4l**$_{sty}$) (see Scheme 3.3).

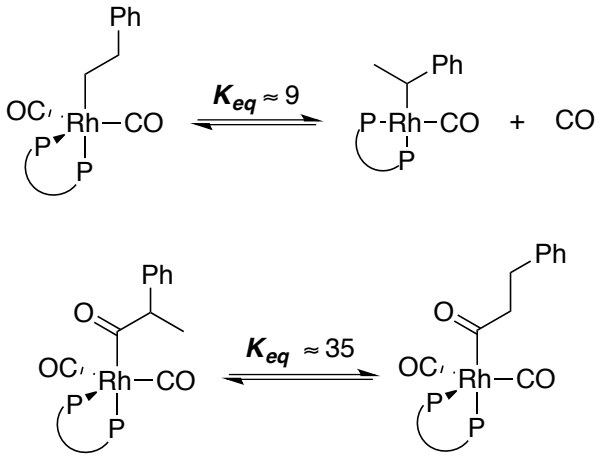

Scheme 3.3. While the branched regioisomer is thermodynamically favoried at the alkyl stage, the preference is reversed at the acyl stage.

The apparent thermodynamic preference for the branched alkyl is consistent with recent work by the Jones group,[12] whose analysis of metal-carbon and carbon-hydrogen bond strengths suggested that branched regiochemistry is often favored for electron-

deficient substrates (like styrene) because the strength of the primary C-H bond formed in the branched species exceeds that of the primary C-M bond formed in the linear species. However, we cannot currently offer an electronic argument for the dominance of the linear isomer at the acyl stage; we assume that steric interactions drive this preference.

In conclusion, we have characterized five-coordinate rhodium acyl and four- and five-coordinate alkyl complexes of Rh(BDP) catalysts. To the best of our knowledge, this is the first example of characterization of an alkyl intermediate for any rhodium hydroformylation catalyst and the first example of detailed characterization of an acyl complex for an enantioselective hydroformylation catalyst. All data point to a strong kinetic preference for formation of the branched alkyl and acyl species. In contrast, thermodynamics appear to favor the linear isomer at the acyl stage but the branched isomer at the alkyl stage. These observations indicate that a delicate balance of rates and thermodynamics leads to the common observation of strong dependence of regioselectivity upon reaction conditions for styrene hydroformylation.

3.8 Catalytic experiments

The conditions used for the NMR experiments described in the preceding sections – low temperature and pressure and high catalyst concentration – differ substantially from catalytic conditions. We were interested in whether the results we obtained in NMR studies would be relevant to the catalytic reaction (Rh(BDP)-catalyzed hydroformylation is especially sensitive to CO pressure, and obviously the selectivity of many catalytic – *i.e.* kinetically-controlled – reactions depends heavily on temperature).

A natural approach to this question was to perform a series of catalytic experiments at more realistic pressures and catalyst loadings, at a range of temperatures bridging our NMR conditions and more usual catalytic conditions. The results, shown in Figure 3.13, suggest that these conditions cover two regimes.

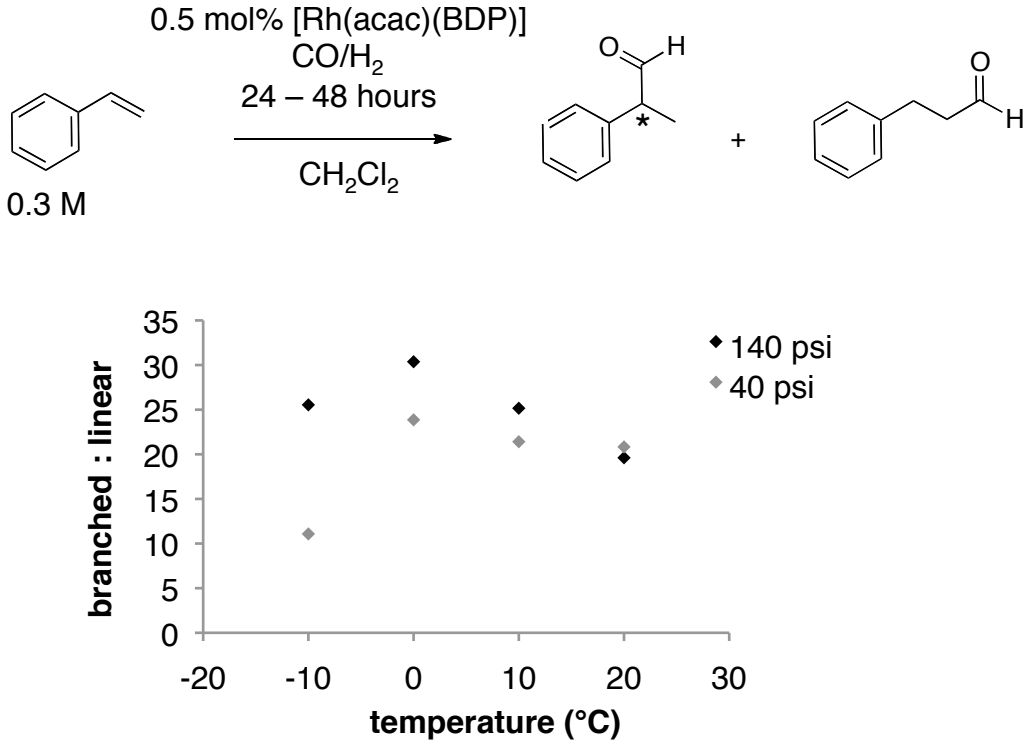

Figure 3.13. Regioselectivity versus temperatures in the Rh(BDP)-catalyzed hydroformylation of styrene. B:l ratio (determined by GC) average of two runs.

Above 0 °C, selectivity is apparently controlled by the kinetic preference for formation of the branched alkyl (suggested by previous work[4] and supported by the early formation of **7b**$_{sty}$). As the temperature drops, selectivity increases as the kinetic preference is magnified by the decrease in available energy; this effect is more dramatic,

as shown, at higher pressures where trapping by CO is more efficient. The thermodynamic preference for the linear acyl $\mathbf{7l_{sty}}$ appears irrelevant.

Below 0 °C, selectivity decreases. Presumably, hydrogenolysis becomes turnover-limiting, allowing equilibration of acyls. High CO pressure, which inhibits isomerization, blunts this effect. (These experiments were performed with resolved ligand; the trend in enantioselectivity matches the trend in regioselectivity, but is less dramatic.)

These results suggest that, while the thermodynamic stability of either the five-coordinate acyl complexes or the alkyl complexes is unlikely to be a relevant factor in the selectivity of catalytic hydroformylation, the *kinetic* preference for one acyl over the other does seem to reflect catalytic selectivity. In short, even though the well-characterized five-coordinate acyls are not strictly on-cycle, they do (so far) seem to be reasonable *kinetic* models for catalytically relevant species.

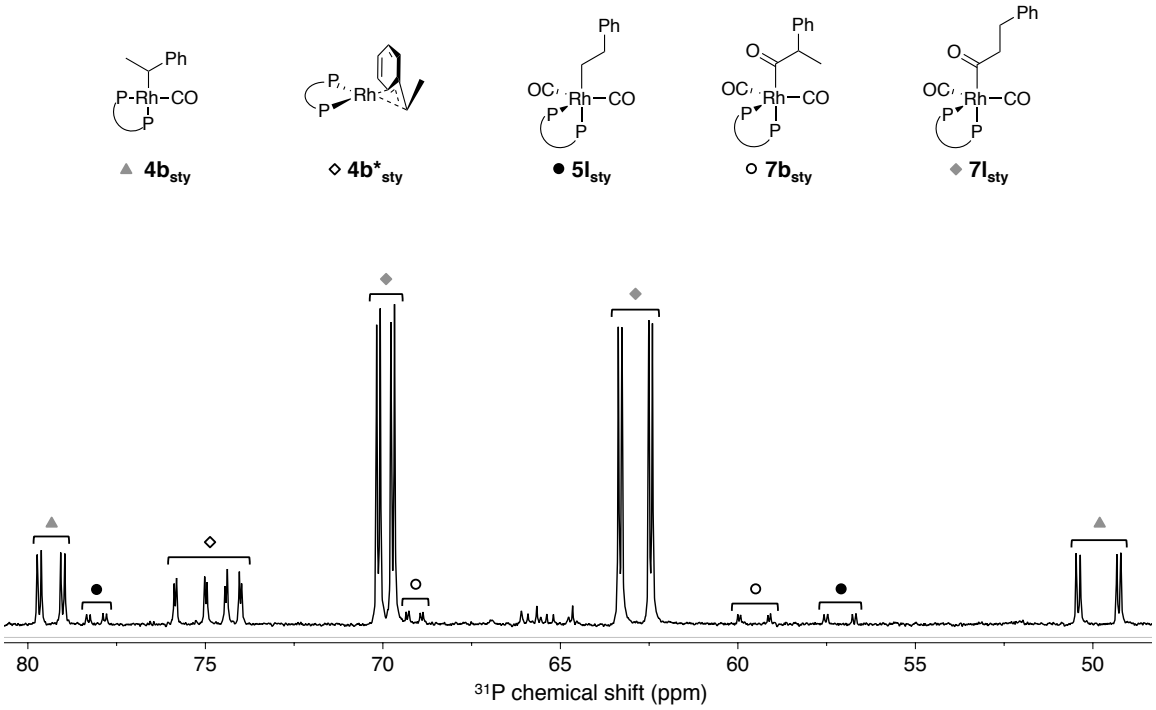

Figure 3.14. 31P{1H} NMR spectrum taken after the reaction of **1** with styrene (202.5 MHz, -15 °C, CD_2Cl_2).

Table 3.1. ^{13}C (125.79 MHz), ^{31}P (202.50 MHz), and ^{1}H (500.21 MHz) NMR data for alkyl and acyl complexes formed following the reaction of **1** with styrene. Data taken at -20 °C in CH_2Cl_2 or CD_2Cl_2.

^{13}C		δ (ppm)	J_{CRh} (Hz)	J_{CP} (Hz)
7b	acyl C=O	232.0	20.8	86.4
	methine	74.0	< 2	32.7
7l	acyl C=O	230.3	18.9	83.3
	α-methylene	67.5	-	33.2
	β-methylene	31.0	-	-
4b	methine	37.7	9.8	45.7
	methyl	20.3	-	2.6
4b*	methine	52.5	5	38
5l	α-methylene	10.3	60.4	13.8
^{31}P		δ (ppm)	J_{PRh} (Hz)	J_{PP} (Hz)
7b	P_{ax}	69.1	80	16
	P_{eq}	59.3	171	16

7l	P_{ax}	69.8	81	21
	P_{eq}	62.4	173	21
4b	P_{trans}	79.3	123	23
	P_{cis}	49.7	232	23
4b*	P_A	74.4	290	12
	P_B	73.7	196	12
5l	P_{ax}	78.1	93	21
	P_{eq}	57.2	162	21
^{1}H		δ (ppm)	mult.	*J* (Hz)
7b	methine	3.47	q	6.5
	methyl	0.79	d	6.5
7l	α-methylene	2.92	ddd	18, 10.5, 4.5
		1.95	ddd	18, 11, 5
	β-methylene	2.53	ddd	14, 10.5, 5
		2.23	ddd	14, (11, 4.5)

3.9 Experimental

3.9.1 General considerations

All manipulations were carried out under nitrogen using standard Schlenk, high vacuum, and glovebox techniques. All solvents and liquid reagents were degassed by at least three freeze-pump-thaw cycles unless otherwise noted. Dichloromethane and CD_2Cl_2 were distilled from P_2O_5 and degassed. Styrene was dried over $MgSO_4$, vacuum-transferred, and degassed. *p*-CF_3-styrene was degassed. Benzaldehyde, potassium *tert*-butoxide, triphenylphosphine, and methyl iodide (all from Sigma), were used as received. ^{13}CO and α-^{13}C-benzaldehyde were purchased from Cambridge Isotope Laboratories and used as received. 1:1 CO:H_2, CO, and H_2 were purchased from Airgas. [Rh(acac)$(CO)_2$] was used as received from Dow and stored in the glovebox.

Rh(acac)(BDP) (BDP = tetraphenyl bis(diazaphospholane) was synthesized as described in Chapter 2 and stored in the glovebox. Rh(H)$(CO)_2$(BDP) was synthesized as needed as described in Chapter 2 and used immediately.

Routine ^{1}H and ^{31}P NMR spectra were recorded on a Bruker AC-300 MHz spectrometer; ^{13}C, ^{19}F, and all reaction-monitoring and two-dimensional experiments were performed using Varian Inova-500 MHz or Unity-500 MHz spectrometers, or Bruker Avance-500 spectrometers. Proton spectra were referenced to residual protio solvent; an xref macro was used to reference ^{13}C and ^{31}P spectra to accompanying proton spectra.

All pressures given are gauge pressures unless otherwise noted.

3.9.2 Syntheses of rhodium complexes and substrates

Rh(H)(^{13}CO)$_2$(BDP): In the glovebox, 51 mg (50 μmol) of Rh(acac)(P^P) was dissolved in 0.8 mL CH_2Cl_2 in a 5-mL pressure bottle. The pressure bottle was attached to a reactor head, removed from the glovebox, and connected to the Schlenk line and to a lecture bottle of ^{13}CO. The solution was frozen and the reactor evacuated. The solution was allowed to warm to room temperature; the valve to the gas tank was opened, and the reactor was pressurized to 20 psi (the maximum delivery pressure of the lecture bottle). The valve to the gas tank was closed and the pressure bottle cooled with liquid nitrogen until the gauge pressure dropped below 10 psi. The valve to the gas tank was opened and quickly closed, and the solution and headspace were allowed to warm to room temperature. This allowed the ^{13}CO pressure in the lecture bottle to reach 40 psi. The reactor was then pressurized with 40 psi H_2 and allowed to stir in a 60 °C oil bath overnight. Conversion: 80% (NMR; other products are the phosphine mono- and dioxides and a complex we believe to be [Rh(acac)(BDP)(CO)]). $^{31}P\{^{1}H\}$ NMR (204.5 MHz, CH_2Cl_2): δ 82.2 (appears as broad dd, J = 140, 70 Hz). $^{13}C\{^{1}H\}$ NMR (125.7 MHz, CH_2Cl_2): δ 193.5 (dt; $J_{C\text{-}Rh}$ = 69 Hz, $J_{C\text{-}P}$ = ±14 Hz, terminal *C*=O).

β-^{13}C-styrene: β-^{13}C-styrene was synthesized as described in Keliher, E. J.; Burrell, R. C.; Chobanian, H. R.; Conkrite, K. L.; Shukla, R.; Baldwin, J. E. *Org. Biomol. Chem*. **2006**, *4*, 2777-2784. For synthesis of $^{13}CH_3PPh_3I$, see Nozaki, K.; Sato, N.; Tonomura, Y.; Yasutomi, M.; Takaya, H.; Hiyama, T.; Matsubara, T.; Koga, N. *J. Am. Chem. Soc.* **1997**, *119*, 12779-12795.

α-^{13}C-styrene: α-^{13}C-styrene was synthesized via an analogous procedure from α-^{13}C-benzaldehyde and CH_3PPh_3I.

3.9.3 General procedure for NMR experiments

A pressure reactor containing a 60 μM solution of $Rh(H)(CO)_2(BDP)$ was depressurized and refilled with 20 psi CO. It was connected via a cannula to an oven-dried septum-capped NMR tube equipped with a vent, and the pressure reactor/NMR tube system was purged with the desired gas (generally CO) for several minutes. The cannula was then used to transfer the solution to the NMR tube, and the tube was sealed with Parafilm. The NMR spectrometer was cooled to -20 °C (actual temperature determined using a methanol standard), and initial spectra were taken. The sample was ejected from the spectrometer, and styrene was added via a gastight syringe; the tube was inverted three times and quickly returned to the spectrometer. For kinetic experiments, the time elapsed between mixing and taking the first spectrum was recorded (typically less than one minute).

3.9.4 General procedure for catalytic experiments

To a pressure bottle was added 50 μL of a 30 mM solution of [Rh(acac)(BDP)] (1.5 μmoles) in CH_2Cl_2, 50 μL (0.3 mmol) diphenylmethane (as an internal standard), and 866 μL additional CH_2Cl_2. The pressure bottle was attached to a reactor head, sealed, and removed from the glovebox. The reactor was pressurized with 140 psi 1:1 H_2/CO and allowed to stir in a 60 °C oil bath for three hours. The reactor was removed from the oil bath and vented, and 34 μL (0.3 mmol) styrene was injected into the pressure bottle via a gastight syringe. The reactor was pressurized an vented three times, then finally pressurized with either 40 or 140 psi 1:1 CO/H_2 and allowed to stir for 24 hours (48 hours for reactions at -10 °C) in an isopropyl alcohol bath cooled by a recirculating chiller set to the desired temperature. The reactor removed from the oil bath (if applicable) and vented; the reaction mixture was concentrated and analyzed by ^{1}H NMR spectroscopy (conversion) and gas chromatography (regio- and enantioselectivity).

3.10 References

(1) For reviews of hydroformylation, see: (a) Agbossou, F.; Carpentier, J.-F.; Mortreux, A. Chem. Rev. 1995, 95, 2485−2506. (b) Claver, C.; van Leeuwen, P. W. N. M. In *Rhodium Catalyzed Hydroformylation*; Claver, C., van Leeuwen, P. W. N. M., Eds.; Kluwer Academic Publishers: Dordrecht, The Netherlands, 2000. (c) Wiese, K.-D.; Obst, D. *Top. Organomet. Chem.* **2006**, *18*, 35−64. (d) Franke, R.; Selent, D.; Börner, A. *Chem. Rev*. **2012**, 112, 5675−5732.

(2) Heck, R. F.; Breslow, D. F. *J. Am. Chem. Soc*. **1961**, *83*, 4023− 4027.

(3) (a) Clark, T. P.; Landis, C. R.; Freed, S. L.; Klosin, J.; Abboud, K. A. *J. Am. Chem. Soc.* **2005**, *127*, 5040−5042. (b) Klosin, J.; Landis, C. R. *Acc. Chem. Res.* **2007**, *40*, 1251−1259. (c) Watkins, A. L.; Hashiguchi, B. G.; Landis, C. R. *Org. Lett.* **2008**, *10*, 4553. (d) McDonald, R. I.; Wong, G. W.; Neupane, R. P.; Stahl, S. S.; Landis, C. R. *J. Am. Chem. Soc.* **2010**, *132*, 14027. (e) Watkins, A. L.; Landis, C. R. *Org. Lett.* **2011**, *13*, 164. (f) Adint, T. T.; Wong, G. W.; Landis, C. R. *J. Org. Chem*. **2013**, *78*, 4231−4238.

(4) Watkins, A. L.; Landis, C. R. *J. Am. Chem. Soc*. **2010**, *132*, 10306−10317.

(5) (a) Brown, J.; Kent, A. J. Chem. Soc., *Chem. Commun*. **1982**, 723−725. (b) Brown, J.; Kent, A. *J. Chem. Soc., Perkin Trans. 2* **1987**, 1597−1607.

(6) (a) Deutsch, P.; Eisenberg, R. *Organometallics* **1990**, *9*, 709− 718. (b) Chan, A.; Shieh, H. *Inorg. Chim. Acta* **1994**, *218*, 89. (c) van der Slot, S.; Kamer, P.; van Leeuwen, P.; Heaton, B.; Iggo, J. *Organometallics* **2001**, *20*, 430−441. (d) Gellrich, U.; Seiche, W.; Keller, M.; Breit, B. *Angew. Chem., Int. Ed*. **2012**, *51*, 11033−11038.

(7) For example, see: (a) Pottier, Y.; Mortreux, A.; Petit, F. *J. Organomet. Chem*. **1989**, *370*, 333−342. (b) Nozaki, K.; Sakai, N.; Nanno, T.; Higashijima, T.; Mano, S.; Horiuchi, T.; Takaya, H. *J. Am. Chem. Soc.* **1997**, *119*, 4413−4423. (c) Casey, C. P.; Paulsen, E. L.; Beuttenmueller, E. W.; Proft, B. R.; Petrovich, L. M.; Matter, B. A.; Powell, D. R. *J. Am. Chem. Soc.* **1997**, *119*, 11817−11825. (d) Castellanos-Paéz, A.; Castilloń, S.; Claver, C.; van Leeuwen, P.; de Lange, W. *Organometallics* **1998**, *17*, 2543−2552. (e) Wassenaar, J.; de Bruin, B.; Reek, J. N. H. *Organometallics* **2010**, *29*, 2767−2776.

(8) Collman, J. P.; Roper, W. R. *Adv. Organomet. Chem.* **1968**, *7*, 57.

(9) (a) Brown, J. M.; Chaloner, P. A.; *J. Chem. Soc., Chem. Commun.* **1980**, 344. (b) Chan, A. S. C.; Halpern, J. A. *J. Am. Chem. Soc*. **1980**, *102*, 838.

(10) Fryzuk, M. D. *Inorg. Chem*. **1982**, *21*, 2134−2139.

(11) Wilkinson and co-workers characterized $[Rh(C_2F_4H)(CO)(PPh_3)_2]$ and $[Rh(C_2F_4H)(CO)_2(PPh_3)_2]$ by ^1H and ^{19}F NMR and IR spectroscopy in 1970; however, these species did not go on to produce aldehyde in the presence of syngas. See: Yagupsky, G.; Brown, C. K.; Wilkinson, G. J. *Chem. Soc. (A)* **1970**, 1392−1401.

(12) Jiao, Y.; Evans, M. E.; Morris, J.; Brennessel, W. W.; Jones, W. D. *J. Am. Chem. Soc.* **2013**, *135*, 6994−7004.

(13) Sparta, M.; Børve, K. J.; Jensen, V. R. *J. Am. Chem. Soc.* **2007**, *129*, 8487 – 8499.

Chapter 4

Interception and characterization of alkyl and acyl complexes: other substrates

4.1 Introduction

The styrene system explored in Chapter 3 was particularly well-suited for detailed study because it gives clean and easily-interpreted NMR spectra, and the synthesis of labeled substrates to aid characterization is straightforward. However, in an effort to acquire a broader understanding of hydroformylation with Rh(BDP) catalysts, it is necessary to expand these studies to other substrates.

This chapter will describe the application of the techniques described in Chapter 3 to vinyl acetate, allyl cyanide, and 1-octene. While all these are terminal olefins, they span a modest range of electronic parameters, with vinyl acetate being the most strongly electron-withdrawing (in the σ sense) and 1-octene obviously the most electron-rich.

Styrene, vinyl acetate, and allyl cyanide are considered "benchmark" substrates for asymmetric hydroformylation because they seem to be intrinsically selective for the branched product. For the tetraphenyl BDP catalyst, AHF of vinyl acetate at 75 °C and 150 psig gives 14% *ee* and b:l = 13.l; AHF of allyl cyanide gives 65.8% *ee* and b:l = 4.9 under the same conditions; for styrene, 52.2% *ee*, b:l = 6.0.[†]

Terminal alkyl olefins like 1-octene, on the other hand, typically give the linear product. For example, for 1-octene hydroformylation with the (*S,S,S*)-methylbenzylamide BDP catalyst, b : l = 0.36 , while styrene hydroformylation under similar conditions gives b : l = 30 .

In fact, rhodium bis(phosphine)-catalyzed hydroformylation of most substrates gives predominantly linear aldehyde, a preference commonly attributed to steric crowding in the branched insertion product.[1] The high branched selectivity for electron-

[†] Jerzy Klosin; unpublished results.

deficient olefins, on the other hand, is typically explained by invoking the ability of the electron-withdrawing group to stabilize branched alkyl complexes **4**. In these species, the methine carbon, metal center, and *trans* phosphorus atom comprise a three-center, four-electron bond in which the phosphorus atom pushes electron density onto the alkyl carbon (see Figure **4.1**). For substrates like styrene, the EWG mitigates charge buildup on that carbon, stabilizing the branched alkyl species. The alkyl chain of 1-octene has the opposite effect, destabilizing $\mathbf{4b_{oct}}$ relative to $\mathbf{4l_{oct}}$ and reinforcing the steric preference for linear insertion.

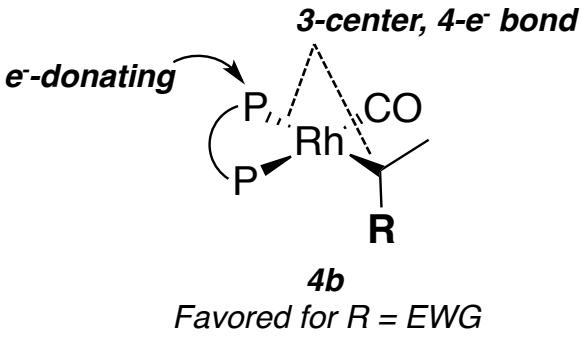

Figure 4.1. Electron-withdrawing substituents R mitigate charge buildup on the carbon *trans* to the phosphine ligand, stabilizing the branched alkyl species.

While the identification of alkyl and acyl complexes with vinyl acetate, allyl cyanide, and 1-octene is not as straightforward as for styrene, the results nevertheless permit us to draw some general conclusions about the interaction of our Rh(BDP) catalyst with these substrates.

4.2 Vinyl acetate

4.2.1 Identification of acyl complexes $7b_{va}$, $7b'_{va}$, $7l_{va}$

When vinyl acetate is added to the rhodium hydride **1** at -10 °C under a CO atmosphere, the reaction can be easily monitored by ^{1}H and ^{31}P NMR spectroscopy. As for styrene, **1** disappears in a roughly first-order fashion, with a half-life of about ten minutes, and the major species which replace it are the five-coordinate acyl dicarbonyl species. The diastereomeric branched acyl species $\mathbf{7b_{va}}$ and $\mathbf{7b'_{va}}$ appear as eight-line patterns at δ 69.5, 60.4 ppm and δ 68.5, 57.8 ppm, respectively (because the ligand used in these experiments is racemic, diastereomers are expected). The linear acyl species $\mathbf{7l_{va}}$ is responsible for the eight-line patterns at δ 70.1, 62.4 ppm (see Table 4.2 for complete NMR data), and increases in concentration over time (see Figure 4.2).

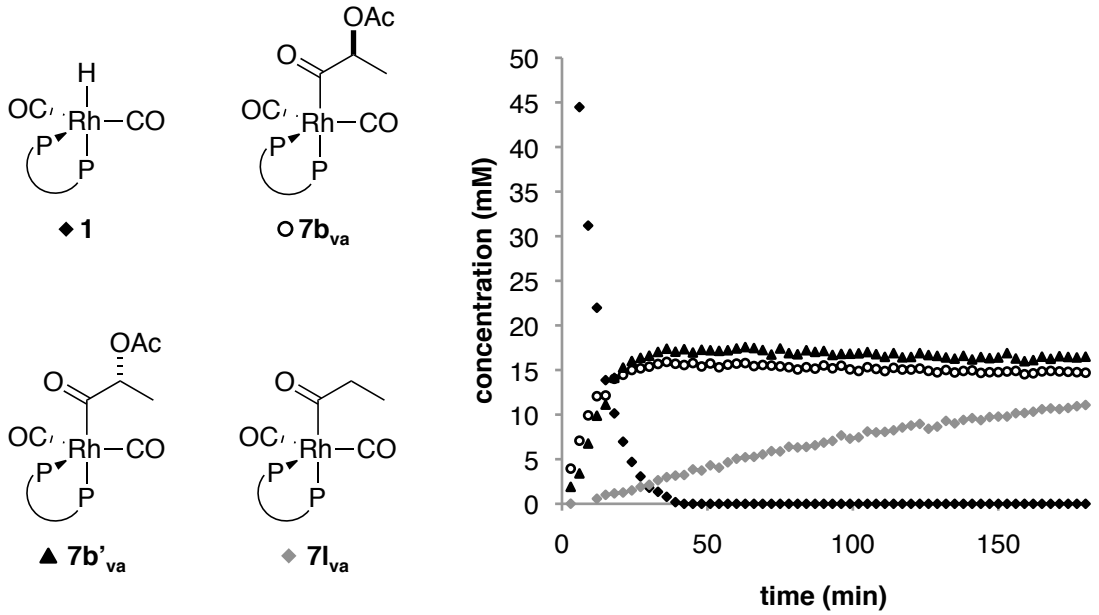

Figure 4.2. Catalyst speciation following the reaction of **1** with vinyl acetate

^{31}P-^{1}H HMBC experiments show through-bond coupling from each set of ligand phosphorus atoms of **7b$_{va}$** and **7b'$_{va}$** to methine quartets and methyl doublets in the ^{1}H NMR spectrum. This experiment also revealed that, notably, the linear acyl complex **7l$_{va}$** is not β-acetoxypropionyl complex that was expected, but the unsubstituted propionyl species (see Figure 4.2). The HMBC spectrum shows correlations to two diastereotopic methylene protons at δ 2.62 and 1.67 ppm, as expected, but a COSY spectrum shows that these protons, rather than being correlated to an adjacent methylene group, are vicinal instead to a methyl group, which appears as a triplet at δ 0.5 ppm (^{1}H-^{13}C HSQC shows that these protons are attached to a carbon atom with a signal at 10 ppm, also consistent with a methyl group).

A variety of other one- and two-dimensional NMR experiments, including ^{31}P-^{31}P COSY and ^{13}C-^{1}H HSQC, corroborate these assignments. The methine carbons of **7b$_{va}$** and **7b'$_{va}$** are visible at δ 86.2 and 83.9 ppm, respectively. The enhanced ^{13}C sensitivity of a cryoprobe available nearby at NMRFAM allows us to observe even the acyl (as well as the terminal) carbonyl carbons of these complexes; as for complexes **7$_{sty}$**, the chemical shifts and coupling constants are consistent with those reported by Brown.

Because the ^{31}P NMR signals for complexes **7$_{va}$** are so close in chemical shift, the spectrum obtained after labeling these complexes with ^{13}CO is too crowded to extract useful coupling information. Therefore, the coordination number of complexes **7$_{va}$** was determined by comparison to the results for styrene (*vide supra*), allyl cyanide, and 1-octene (*vide infra*), all of which can be definitively identified as dicarbonyl acyl complexes. The $J_{P\text{-}Rh}$ values for these complexes – 81 and 152 Hz for **7b$_{va}$** and 80 and

167 Hz for **7b'$_{va}$** – are more consistent with five-coordinate, trigonal bipyramidal species than with a square planar complex.

Like **7b,l$_{sty}$**, these complexes are formed even in the presence of H_2, and persist under an atmosphere of syngas: evidently the oxidative addition of H_2 (and subsequent reductive elimination of the product) is not competitive with CO association under these conditions.

Some isomerization to linear acyl **7l$_{va}$** occurs over the course of the reaction; however, the branched isomers are favored at equilibrium by a ratio of 2.6 : 1. This is in contrast to the styrene system, where a thermodynamic preference for the branched regioisomer at the alkyl stage was reversed at the acyl stage.

For vinyl acetate, the ratio of the diastereomeric acyl complexes reveals a slight kinetic preference (1.2:1) for **7b$_{va}$** which is eventually overtaken by a slight thermodynamic preference (1.1:1) for **7b'$_{va}$**. These small countervailing preferences are consistent with the low enantioselectivity of this system. This equilibration between acyl complexes, along with continuing isomerization to the linear isomer, indicates that all steps leading to the formation of the acyl complexes are reversible under these conditions. As for styrene, even though complexes **7$_{va}$** do not lie directly on the catalytic cycle, *in situ* observation of catalyst speciation and reactivity nevertheless offers empirically substantiated data that cannot be obtained by more indirect methods.

4.2.2 Proposal for formation of 7l$_{va}$

Propionyl complex **7l$_{va}$** could plausibly be formed by the reaction of hydride **1** (or monocarbonyl hydride **2**, not observed) with ethylene. We propose that ethylene is generated by β-acetoxy elimination from alkyl complex 4lva; ethylene dissociates and

goes on to react with another rhodium hydride to generate 7lva (see Scheme 4.1)). (Even after dicarbonyl hydride 1 has been consumed, the equilibration of alkyl and acyl complexes implies that **2** persists in solution, albeit below the limit of detection, as discussed in Chapter 3). β-acetoxy elimination is often cited in transition-metal mediated reactions, although most commonly for Group 10 metals;[2] however, it has been specifically invoked to explain the reaction of rhodium hydrides with vinyl acetate to generate ethylene.[3]

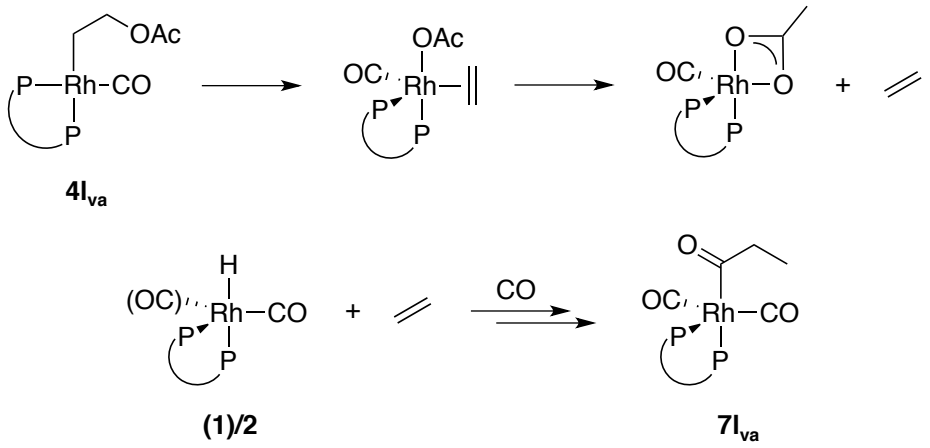

Scheme 4.1. Propionyl species **7l$_{va}$** could be generated by hydride exchange with **2**.

We do not see any evidence for a rhodium acetate species which would, along with propionyl species **7l$_{va}$**, be a product of this series of reactions. However, we propose that it undergoes fast exchange with the acetylacetone in solution to regenerate [Rh(acac)(BDP)]; see Figure 4.3.

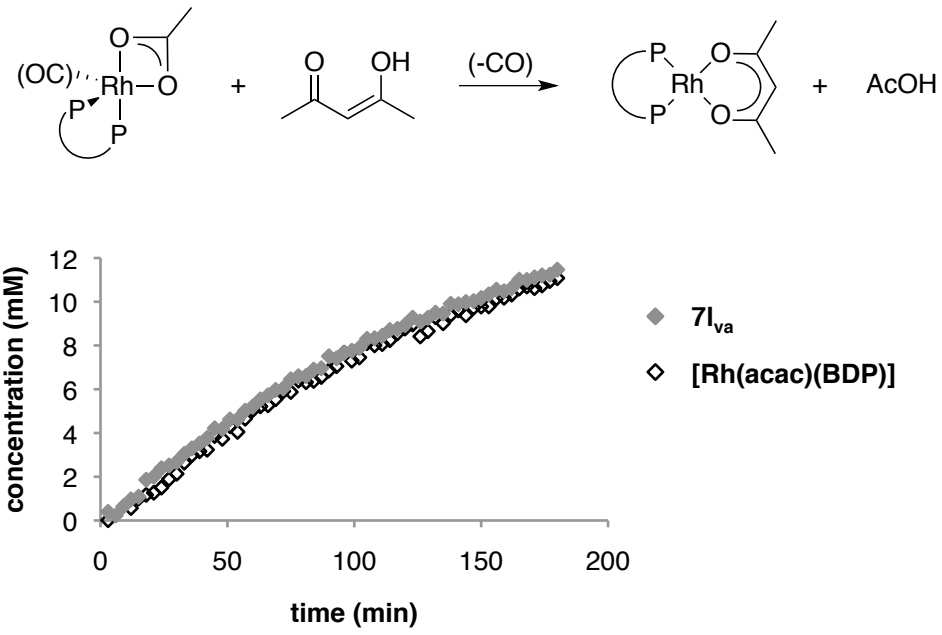

Figure 4.3. The acetate ligand of the complex formed by hydride exchange between **2** and an acyl specie readily exchanges with acetylacetone to regenerate [Rh(acac)(BDP)]. Therefore, **7l$_{va}$** and [Rh(acac)(BDP)] are formed at the same rate.

As shown in Figure **4.3**, [Rh(acac)(BDP] and **7l$_{va}$** are generated at exactly the same rate, lending support to this hypothesis. We do not directly observe acetic acid in the ^{1}H NMR spectrum; however, the acid resonance could easily be broadened into the baseline.

4.2.3 Characterization of alkyl complexes

The ^{31}P{^{1}H} NMR spectrum in Figure 4.6 shows at least five additional species, in addition to [Rh(acac)(BDP)] (which is regenerated over the course of the reaction) and the rhodium dimer. Three of these can be tentatively identified as alkyl complexes, as

indicated by the absence of any additional signals in the acyl region of the ^{13}C NMR spectrum.

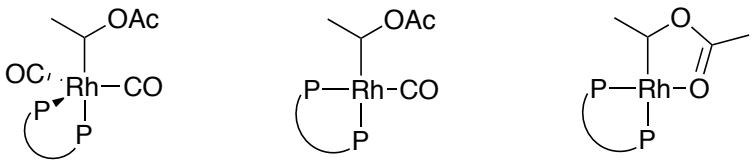

$5b_{va}$ **$4b_{va}$** **$4b^*_{va}$**

Figure 4.4. Alkyl complexes characterized following the reaction of **1** with vinyl acetate.

The species we have assigned as **$4b_{va}$** has phosphorus signals at δ 82.6 and 39.2 ppm, and shows one new 89-Hz ^{31}P-^{13}C splitting (in the upfield peak) following the reaction of vinyl acetate with [Rh(H)($^{13}CO)_2$(BDP)]; along with its large $^1J_{PRh}$ (101 and 213 Hz), this suggests it is as four-coordinate alkyl complex. (Note: this designation should not be taken to imply that **$4b_{va}$** and **$7b_{va}$** have the same absolute stereochemistry; we do not currently have a method to determine the configuration of any of these species.) ^1H-^{31}P HMBC shows that this species is correlated to an apparent triplet at 1.58 in the ^1H NMR spectrum, which shows through-bond coupling to a multiplet at 4.69 ppm. We propose that the upfield signal is actually a doublet of doublets belonging to a methyl group; the second 6.5-Hz coupling is created by the *trans* ligand phosphorus atom. While a triplet might seem to be more consistent with the methyl group of an ethyl fragment, the COSY correlation to a single downfield signal belies this simple assignment: methylene protons would almost certainly be further upfield. Moreover, in all other linear [Rh(BDP)] complexes characterized thus far, the diastereotopic methylene protons have had a substantial (ca. 1-ppm) difference in chemical shift. Therefore, we ascribe these

signals to branched alkyl **4b$_{va}$**. The signal from the methine proton is not observed directly; however, because this signal would be at least a doublet of quartets (and possibly a ddq) in a crowded region of the spectrum, this is not surprising.

Five-coordinate branched alkyl complex **5b$_{va}$** was identified by its moderate (δ 83- and 159-Hz) phosphorus-rhodium coupling constants, the presence of 2 CO ligands (both *cis* to the ligand's phosphorus atoms, as established by labeling with ^{13}CO), and through-bond coupling to, as above, an apparent triplet at δ 1.4 ppm in the ^{1}H NMR spectrum showing through-bond coupling to a downfield (δ 4.7 ppm) signal. In the ^{31}P NMR spectrum (see Figure 4.6), another small set of doublets-of-doublets appears just upfield of each ^{31}P signal for **5b$_{va}$**; the signals are too small to provide any useful characterization information, but because of the similarity of their spectral features to those of 5bva, they could very well belong to the other diastereomer, **5b'$_{va}$**. If that is the case, the diastereomeric ratio for these alkyl complexes is 3.9:1 – much greater than that observed at the acyl stage.

The final alkyl species does not appear to have any CO ligands; this observation, along with its large (256- and 129-Hz) $^{1}J_{PRh}$ and apparent correlation to a broad quartet in the ^{1}H NMR spectrum leads us to assign it as **4b*$_{va}$**, in which the acetate group occupies the fourth coordination site.

There is a fourth unidentified species, with broad phosphorus signals at δ 78.5 and 54.6 ppm. Its large (107 and 221-Hz) phosphorus-rhodium coupling constants suggest that it is a four-coordinate species (although the peaks are too broad following labeling with ^{13}CO to provide any more-conclusive information). Through-bond coupling to a quartet and doublet in the ^{1}H NMR spectrum are consistent with a branched species.

These peaks could belong to four-coordinate branched acyl $\mathbf{6_{va}}$; however, there is no definitive evidence for this assignment.

While we are reasonably confident in assigning the coordination number and general geometry of the alkyl complexes described above, the evidence for their regiochemistry is less compelling. Our ability to thoroughly characterize the styrenyl alkyl and acyl species was based on access to ^{13}C NMR data for isotopically-labeled complexes. Unfortunately, the straightforward Wittig route used to generate the ^{13}C-labeled styrenes is not applicable to the synthesis of labeled vinyl acetate, and commercially available ^{13}C-vinyl acetate is prohibitively expensive. Therefore, any conclusions about their regiochemistry must be largely drawn from the crowded ^{1}H NMR spectrum. These practical challenges prevent the definitive characterization of the complexes described above.

For NMR data for alkyl and acyl complexes generated from the reaction of **1** with vinyl acetate, see Table 4.2.

Attempted synthesis of alkyl and acyl complexes from [Rh(CO)$_2$(BDP)]K

The alkyl and acyl complexes formed during the hydroformylation of vinyl acetate could, in theory, be prepared from the reaction of the rhodium anion described in Chapter 2 with 2-bromoethylacetate and acetoxypropionyl chloride (see Scheme **4.2**).

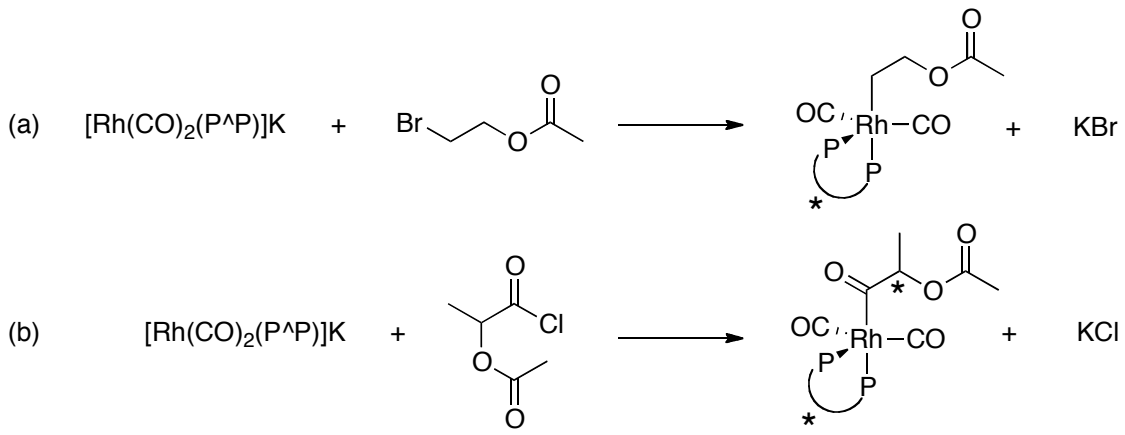

Scheme 4.2. Proposed reaction sequences to generate rhodium alkyl (a) and acyl (b) complexes formed during the hydroformylation of vinyl acetate.

The reaction of the rhodium anion with bromoethylacetate yielded a species whose ^{31}P NMR spectrum showed equivalent phosphorus atoms (δ 87 ppm, d, $J_{P\text{-}Rh}$ = 207 Hz). This is obviously inconsistent with the desired species, whose phosphorus atoms would be inequivalent (it is consistent with a square-planar species; a dimeric complex with bridging bromine atoms is one possibility).

The reaction with acid chloride was slightly more successful; when *S*-acetoxypropionyl chloride (5 equivalents) was added to a solution of the rhodium anion, a white precipitate (presumably KCl) formed immediately. Filtration of the supernatant away from this solid gave a reddish solution; the ^{31}P NMR spectrum showed two doublets-of doublets (δ 90 ppm, J_{PRh} = 175 Hz, $J_{P\text{-}P}$ = 40 Hz; δ 68 ppm, J_{PRh} = 145 Hz, J_{PP} = 40 Hz; see Supporting Information). These data do not match those for complexes **7b$_{va}$**, which would be the most obvious product. The NMR data are not inconsistent with a four-coordinate monocarbonyl acyl complex (which would have two J_{PRh} > 100 Hz). Because the experiment was performed under an N_2 atmosphere, CO loss is not

implausible (although no gas evolution was observed). However, because the ligand is racemic, any rhodium acyl complex (barring acetoxy elimination) we should give two diastereomers (*i.e. two* eight-line patterns), and only one set of signals is observed. (The possibility that the reaction is simply highly enantioselective is ruled out by the absence of unreacted rhodium anion.)

Monitoring the reaction by NMR might yield more insight; however, the inevitable generation of large amounts of salt makes that approach impractical. It is possible that alternative strategies such as the use of specialized glassware or more soluble counterions might mitigate these difficulties, but we have not yet pursued this further. The strategy described above and in the preceding chapter, of reacting **1** with substrate under NMR conditions, is both a more fruitful and operationally simpler route to the characterization of catalyst species.

4.2.3 Rate dependence on CO, vinyl acetate

While the rate of appearance of the acyl complexes can provide us with limiting values for the rates of the preceding steps in the cycle, any additional detail about these steps must be derived from other methods.

Because catalysis is initiated by CO dissociation from the rhodium hydride, it is conceivable that the reaction might be inhibited by CO pressure (and, indeed, earlier work in this group on the rhodium-bis(diazaphospholane)-catalyzed hydroformylation of styrene found that this is the case. Quantitatively investigating CO dependence under these conditions is problematic, since there is no convenient way to measure or regulate the gas pressure in a standard NMR tube. However, by simply purging the solution and headspace with N_2, we can qualitatively create a low-CO-pressure environment. Under

these conditions, the half-life for the disappearance of the rhodium hydride drops from ca. 600 seconds to ca. 100 seconds (see Table 3, entries 1 and 2), indicating significant CO inhibition under these conditions.

Table 4.1. Kinetics of the conversion of the rhodium hydride to acyl complexes $\mathbf{7_{va}}$ under various conditions. Conditions: 60 mM 1, CD_2Cl_2, -10 °C.

Entry	Conditions	Eq. vinyl acetate	Half-life (s)
1	1 atm CO	5	600
2	Purged with N2	5	100
3	1 atm CO	50	100

We were also interested in the rate dependence on vinyl acetate. The shape of the hydride's decay profile suggested an approximately first-order reaction; to verify this supposition, we increased the amount of vinyl acetate from five to fifty equivalents. This also decreased the reaction's half-life to approximately 100 seconds (see Table **4.1**, entries 1 and 3). The scale of this change implies that these conditions approach the onset of saturation behavior in substrate. Together, the results in Table **xxx** suggest that these experiments cover a range where trapping of the monocarbonyl with vinyl acetate is initially competitive with CO coordination to regenerate **1**. However, as substrate concentration increases, eventually every monocarbonyl hydride generated is immediately trapped by alkene, and the rate of reaction becomes limited by slow (and reversible) CO dissociation from the precatalyst **1**.

4.2.4 Deuterium-labeling experiments: vinyl acetate insertion is reversible

Because the selectivity and reversibility of the alkene insertion step is critical to the selectivity of the overall reaction, it is important to address its key features. For example, is alkene insertion reversible under these conditions? Is deinsertion via β-hydride elimination fast or slow relative to acyl complex formation? Deuterium-labeling, a classic tool for probing the reversibility of olefin insertions, is applied here by following the reaction of vinyl acetate with the rhodium deuteride.

There are two limiting cases: first, if insertion is irreversible, all the deuterium will be incorporated into the methyl groups of the acyl complexes; if, on the other hand, β-hydride elimination from the alkyl complex is fast relative to acyl complex formation, so that insertion/deinsertion occurs many times before the acyl complexes form, then most of the deuterium will be incorporated into the unreacted vinyl acetate (see Scheme 4.3).

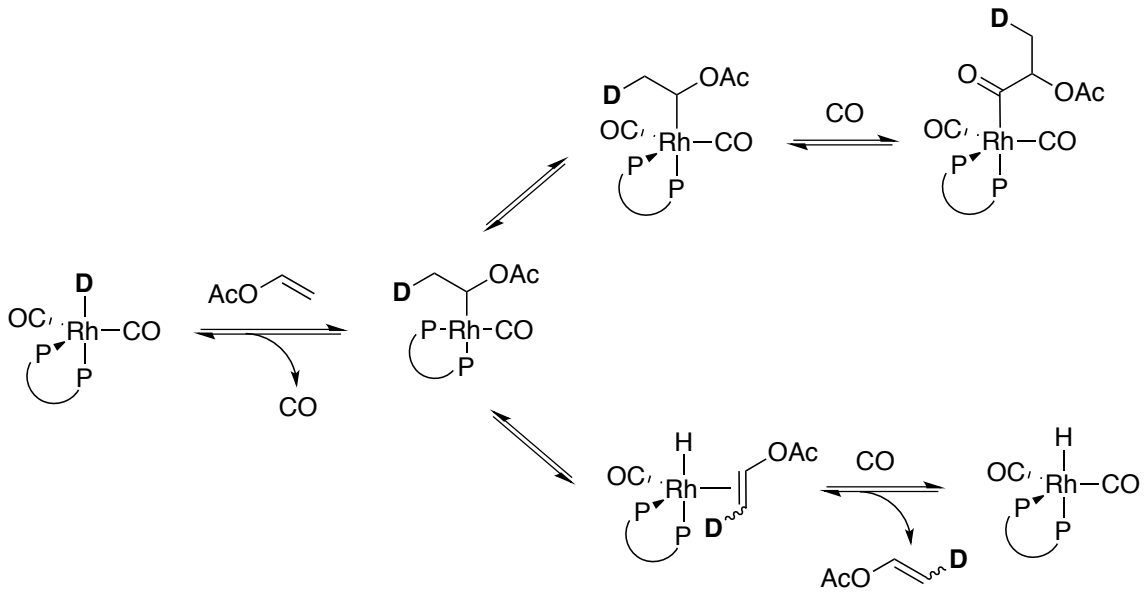

Scheme 4.3. Reaction of the rhodium deuteride with vinyl acetate. The deuterium label will be incorporated either into the acyl methyl groups (upper pathway) or the terminal positions of vinyl acetate (lower pathway).

We make several simplifying assumptions: that there is no kinetic isotope effect, that elimination of each of the three hydrides/deuterides is equally likely (that is, deuterium is equally likely to end up in the *cis* and *trans* positions of the olefin), and that deuterium incorporation at the 2-position (from formation of the linear alkyl) is negligible. Under those circumstances, and considering five equivalents of vinyl acetate relative to the rhodium hydride, the second case would give approximately nine percent deuterium at each position; twenty percent of the each acyl methyl group would be deuterated.

The rhodium deuteride can be generated by reacting [Rh(acac)(BDP)] with 1:1 D_2/CO (although there is always some amount of rhodium hydride, increasing at longer reaction times, as a result of reversible coordination and insertion of acetylacetone).

When vinyl acetate is allowed to react with this complex under our typical NMR conditions, ^{1}H, ^{2}H, and ^{13}C NMR spectra all show deuterium incorporation into both the acyl methyl groups and unreacted vinyl acetate (see Figure **4.5**). The ratio of deuterium in vinyl acetate to that in the acyl complexes is 2:1, less than the 4:1 that we would expect if the insertion/β-hydride elimination sequence were very fast relative to acyl complex formation. The actual kinetic scenario, then, lies between the two limiting cases: vinyl acetate insertion is reversible under these conditions, but trapping of the alkyl complexes by CO, and subsequent alkyl migration, is competitive with β-hydride elimination and alkene dissociation.

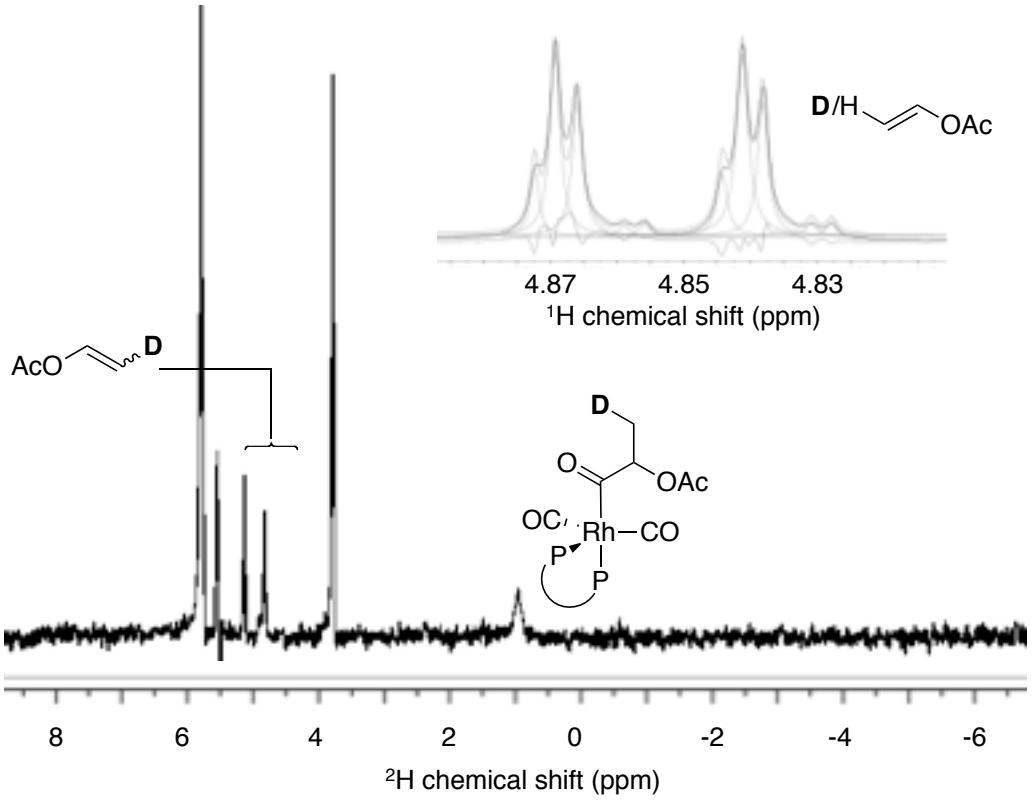

Figure 4.5. ^{2}H NMR spectrum, and ^{1}H signal for *trans* vinyl proton of vinyl acetate (inset), after the reaction of $[Rh(D)(CO)_2(BDP)]$ with vinyl acetate, showing deuterium

incorporation into the methyl groups of the acyl complexes and free vinyl acetate. The other peaks in the ^{2}H NMR spectrum are assigned to deuterated acetylacetone (δ 5.8, 3.8 ppm) and residual deuterated solvent (δ 5.3 ppm).

We hoped that we might be able to quantitatively approach the forward and reverse rate constants for alkene insertion by monitoring the reaction of the rhodium deuteride with vinyl acetate by alternating $^{1}H/^{31}P$ NMR spectra. Unfortunately, however, because the shims vary during the course of the reaction, and the peaks for the deuterated alkene are small and overlap the peaks for the perprotio species, it was not possible to accurately track H/D exchange. EXSY experiments to monitor exchange between the hydride and vinyl acetate ^{1}H signals were also unsuccessful.

Monitoring the incorporation of protons into deuterated vinyl acetate would be simpler spectroscopically. We envisioned a route to vinyl acetate from tetrahydrofuran,[4] the deuterated form of which is commercially available as an NMR solvent, via the reaction of the lithium enolate of acetaldehyde with acetyl chloride (see Scheme 4.4).[5]

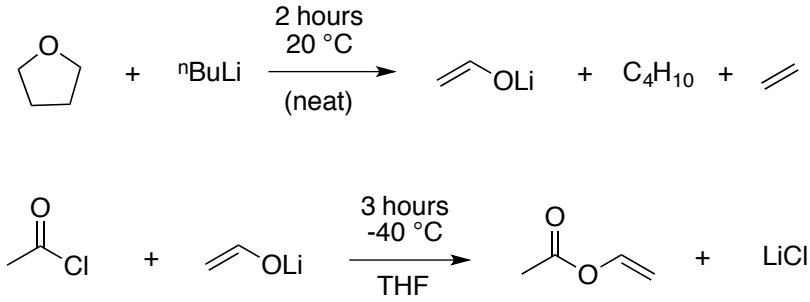

Scheme 4.4. Synthesis of vinyl acetate from tetrahydrofuran, intended as a route to vinyl acetate-d_3.

While this route does give vinyl acetate, isolation of the product proved challenging. Synthesis of the higher-boiling analogue vinyl benzoate through an analogous route is complicated by the formation of the undesired C-alkylation product (see Scheme **4.5**).

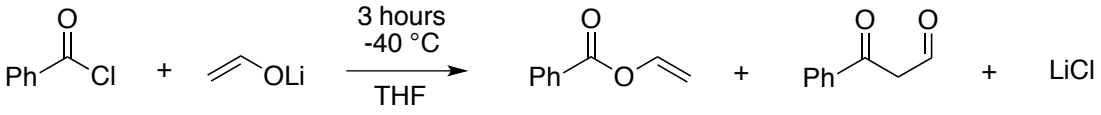

Scheme 4.5. Synthesis of vinyl benzoate using the lithium enolate of acetaldehyde.

4.2.5 Conclusions

The high selectivity for the branched product in catalytic hydroformylations of vinyl acetate seems to be reflected in the strong preference (apparently both kinetic and thermodynamic) for branched alkyl and acyl complexes versus their linear counterparts. In fact, the only linear species observed is propionyl acyl complex $\mathbf{7l_{va}}$, and this species is presumably formed from addition of ethylene to **1**, for which the products formed by reaction at either end of the olefin are degenerate.

The work described in this chapter also demonstrates that, as with styrene, insertion of vinyl acetate into the rhodium-hydride bond is reversible. Determining the rate of the insertion/β-hydride elimination sequence is theoretically possible by tracking the incorporation of protons into vinyl acetate-d_3; however, difficulty synthesizing that substrate has so far prevented such an analysis.

More synthetic difficulties, this time in the reaction of organic electrophiles with an anionic rhodium species to produce alkyl and/or acyl species, underscored the utility

of reaction monitoring by NMR as a route to characterization of catalyst species – as well as the fortuitous identification of reaction conditions that make this analysis possible.

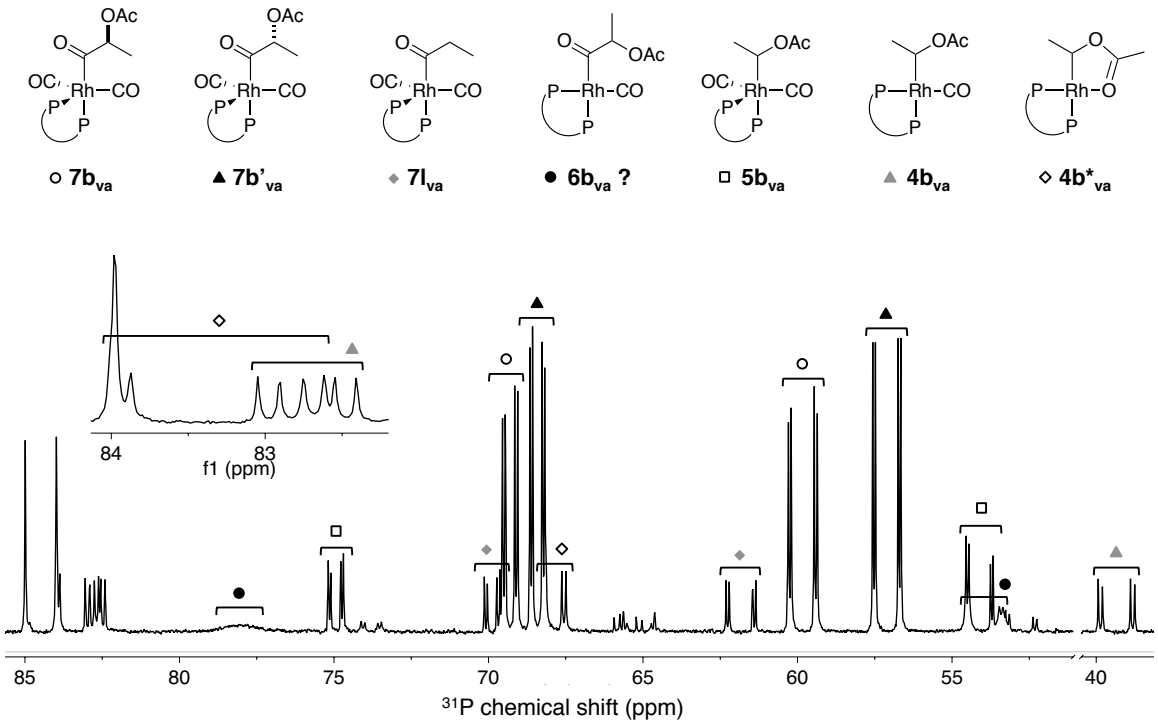

Figure 4.6. $^{31}P\{^{1}H\}$ NMR spectrum taken following the reaction of **1** with vinyl acetate.

4.3 Allyl cyanide

4.3.1 Characterization of acyl complexes

Addition of allyl cyanide to a solution of **1** at -10 °C under an atmosphere of CO gives the five-coordinate linear acyl complex **7l$_{ac}$** as the major product. While the higher enantioselectivity observed for allyl cyanide in catalytic hydroformylation initially led us to assume that this acyl complex was simply the preferred diastereomer of the branched species, ^{1}H-^{31}P HMBC experiments confirmed that it was, in fact, the linear regioisomer.

The half-life for the disappearance of **1** is comparable to that measured with vinyl acetate (approximately ten minutes).

As for styrene, the coordination number was determined by generating **7l$_{ac}$** from **1** labeled with ^{13}CO, giving the ^{13}C-labeled acyl complexes. If these complexes were four-coordinate, we would expect to see two large (> ca. 60 Hz) couplings for *each* phosphorus atom, since one would be *trans* to the acyl carbonyl and the other would be *trans* to the carbonyl ligand. This arrangement would give each atom a large ^{31}P-^{13}C coupling in addition to the phosphorus-rhodium coupling already present.

While one phosphorus atom (P_{ax}) has an 80-Hz coupling to the acyl carbon (making the gross structure a pseudo triplet, since the coupling to rhodium is also approximately 80 Hz) and smaller (ca. 15 Hz) couplings to the carbonyl ligands, however, the other (P_{eq}) has only moderate phosphorus-carbon coupling constants of 38 and 20 Hz, both to the carbons of the carbonyl ligands in the equatorial plane (the coupling to the acyl carbon is not resolved). Therefore, we can conclude that this species is the *five*-coordinate acyl complex.

At first glance, it is somewhat surprising that the coupling constants between P_{eq} and the two carbonyl ligands have such different values; however, examination of the calculated structure for the (presumably analogous) five-coordinate *alkyl* complex reveals that while the angles between P_{ax} and the two carbonyl ligands vary only by about three degrees, the two P_{eq}-Rh-CO angles differ by about fifteen degrees – conceivably enough to promote appreciably stronger electronic interactions with one than with the other.

While there are several species in the ^{31}P NMR spectrum which are candidates for the branched acyl **7b$_{ac}$** based on their chemical shifts and coupling constants, they are

present at concentrations too low for characterization. The other species in the spectrum are similarly resistant to analysis: either they are insufficiently concentrated to show correlations in the ^{1}H-^{31}P HMBC spectrum – the most useful first-line tool for characterization – or their crosspeaks occur in non-diagnostic regions of the 1H NMR spectrum and correspond to protons with poorly-defined multiplicity (if they are visible at all). The inability to characterize these species is unfortunate because at least two display potentially interesting dynamic behavior (see Figure 4.7). One species (**b**) increases at first and then decreases over time (δ 78.8 ppm, $^{1}J_{PRh}$ = 94 Hz, $^{2}J_{PP}$ = 22 Hz; δ 57.6 ppm, $^{1}J_{PRh}$ = 162 Hz, $^{2}J_{PP}$ = 22 Hz). Another (**a**) is already disappearing when the first spectrum is taken (δ 68.6 ppm, $^{1}J_{PRh}$ = 80 Hz, $^{2}J_{PP}$ = 17 Hz; δ 59.7 ppm, $^{1}J_{PRh}$ = 169 Hz, $^{2}J_{PP}$ = 17 Hz); this is the most promising candidate for branched acyl **7b$_{ac}$**.

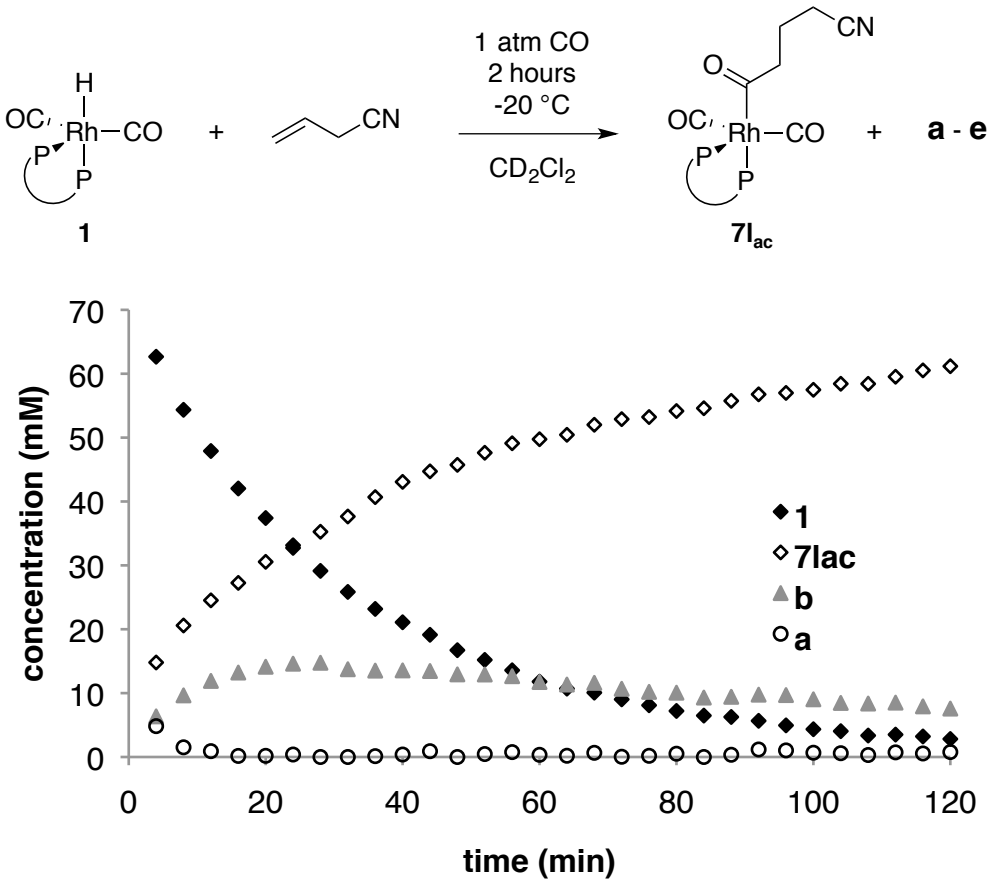

Figure 4.7. Catalyst speciation following the reaction of **1** with allyl cyanide.

As with vinyl acetate, the absence of a simple synthesis of ^{13}C-labeled material is a major obstacle to further characterization.

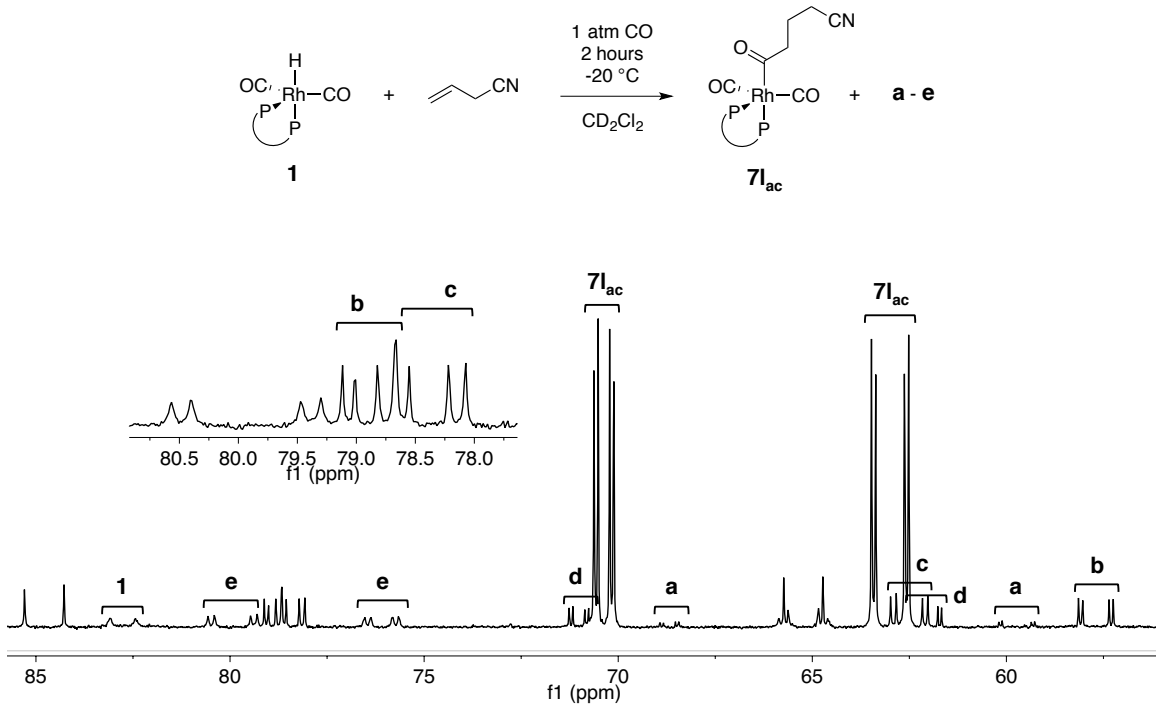

Figure 4.7. $^{31}P\{^{1}H\}$ NMR spectrum taken after the reaction of **1** with allyl cyanide (202.5 MHz, -40 °C, CH_2Cl_2).

4.4 1-octene

4.4.1. Characterization of acyl and alkyl complexes

Because 1-octene behaves differently in AHF, stoichiometric NMR studies of this substrate should provide an instructive counterpoint to the results obtained with styrene and other electron-deficient substrates.

It is also important to point out that, unlike styrene, 1-octene can isomerize under hydroformylation conditions to give internal alkenes, primarily 2-octene (in hydroformylation with the methylbenzylamide BDP ligand, at 50 °C and 150 psig

H_2/CO, 32 % of the starting material had isomerized to 2-octene after 24 hours).[‡] Therefore, alkyl and acyl complexes derived from the reaction of **1** with internal alkenes should be considered as possible products.

As with the other substrates, the major product of the reaction of 1-octene with **1** is a five-coordinate dicarbonyl acyl complex. In this case (as for styrene and allyl cyanide), the linear acyl $\mathbf{7l_{oct}}$ dominates, as seen in the ^{31}P NMR spectrum (Figure **xxx**). The branched acyl $\mathbf{7b_{oct}}$ could only be observed when the reaction temperature was lowered to -30 °C to monitor speciation very early in the reaction. Again, the regiochemistry of $\mathbf{7l_{oct}}$ was determined by ^{1}H-^{31}P HMBC (see Supporting Information). The concentration of $\mathbf{7b_{oct}}$ was too low to give a crosspeak in the 2-D spectrum; however, the observation of a doublet in the ^{1}H NMR spectrum early in the reaction at δ 0.37 ppm, and comparison of the chemical shifts and coupling constants in the ^{31}P NMR spectrum corroborate this assignment.

The minor species were more difficult to characterize. Most were not well-resolved until the temperature was lowered to -40 or -80 °C. The two most prominent minor species have eight-line patterns at δ 70.8 and 67.4 ppm and δ 63.2 and 57.6 ppm. We have tentatively characterized these as $\mathbf{5b_{oct}}$ and $\mathbf{4b_{oct}}$, respectively (see Figure **xxx**). Generating these species with 1-^{13}C-octene (see Figure **4.9**) demonstrates that neither is a linear isomer (insertion at the 1-position of the alkene would result in measurable ^{31}P-^{13}C coupling for both alkyl and acyl species). However, it is important to point out that while these species have been drawn with methyl branches, the data from this ^{13}C-labeling experiment are also consistent with complexes formed by the insertion of internal

[‡] Tyler Adint, unpublished results.

octenes, formed by isomerization, into the R-H bond of **1**. We do not currently have any data that would rule out species of this type. Indeed, the presence in the ^{1}H and ^{13}C NMR spectra of at least two distinct types of ^{13}C-labeled methyl groups shows that isomerization is occurring under these conditions. (Of course, isomerization must also occur during the reaction of **1** with *un*labeled substrate; however, the crowded alkyl and vinyl region of these spectra make detection of isomerization virtually impossible without isotopic enrichment.)

After addition of 1-octene to [Rh(H)($^{13}CO)_2$(BDP)], $\mathbf{5b_{oct}}$ shows two new poorly-resolved ^{31}P-^{13}C couplings, consistent with an alkyl dicarbonyl, where the phosphorus atom (P_{eq}) showing the new coupling shares the equatorial plane with the two labeled carbon atoms. On the other hand, on the upfield phosphorus signal (P_{ax}) of $\mathbf{4b_{oct}}$ shows one new 34-Hz phosphorus-carbon splitting, while the downfield peak (P_{eq}) shows a larger 81-Hz coupling; this is consistent with an alkyl monocarbonyl where the large coupling belongs to the phosphorus atom *trans* to the labeled carbonyl group. Curiously, for the other alkyl complexes identified the phosphorus atom *trans* to the organic fragment is responsible for the downfield signal: if this assignment of $\mathbf{4b_{oct}}$ is correct, the downfield signal belongs instead to the phosphorus atom *trans* to the carbonyl ligand. We do not currently have any explanation for the discrepancy; however, the difference in magnitude of the phosphorus-carbon coupling constants would make a different assignment of the coordination geometry implausible.

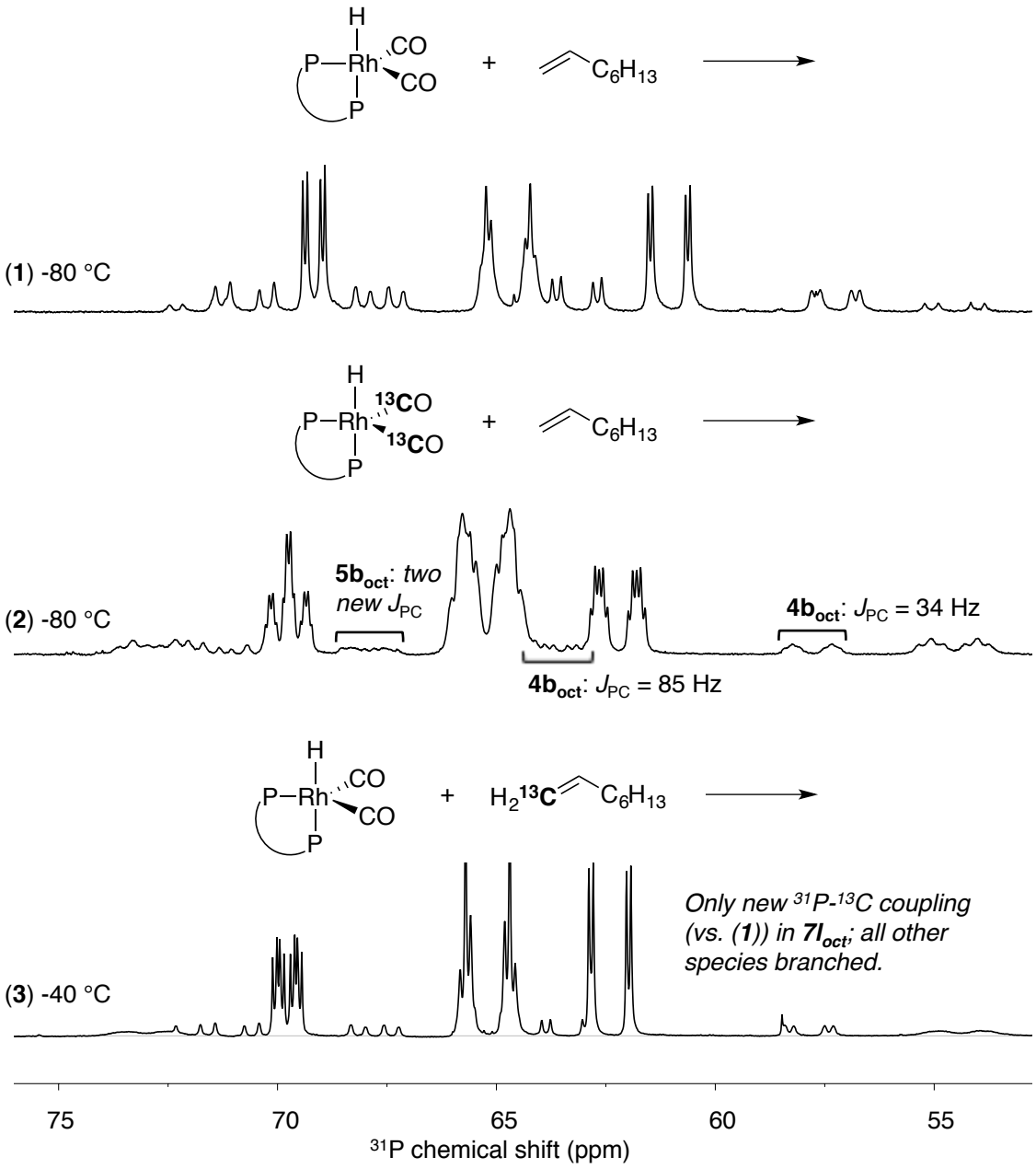

Figure 4.9. Using ^{13}C labeling to determine coordination number and regiochemistry for the species formed from the reaction of 1 with 1-octene.

Unfortunately, the absence of strong correlations in the ^{1}H-^{31}P HMBC spectrum prevents the use of ^{1}H NMR data to further substantiate these assignments. The ^{13}C NMR

spectra of the material generated using either ^{13}CO or 1-^{13}C-octene are similarly unhelpful, beyond the observation that the acyl region of the former seems to have at least two minor acyl signals in the baseline (in addition to the major peak for **7l$_{oct}$**), suggesting that at least one of the unresolved species in the baseline may be another acyl complex. See Table 4.2 for NMR data for **7b$_{oct}$**, **7l$_{oct}$**, **4b$_{oct}$**, and **5b$_{oct}$**.

4.4.3 Comparison with styrene

At equilibrium, catalyst speciation in the reaction of **1** with 1-octene resembles, in general terms, that seen with styrene: the five-coordinate linear acyl dominates, accounting for more than 50 percent of the total ^{31}P integration. However, the data early in the reaction, under conditions where **7b$_{oct}$** is observable, reveal an important distinction. Whereas for styrene there was a clear kinetic preference for the branched acyl **7b$_{sty}$** (presumably reflecting a preference for the branched intermediate **4b$_{sty}$**), 1-octene displays no such preference (see Figure 4.10). The two species grow in at roughly the same rate; if anything, there appears to be a slight kinetic preference for the *linear* acyl (although the low concentrations of both species at short reaction times lead to relatively low signal-to-noise, making overinterpretation of these data inadvisable).

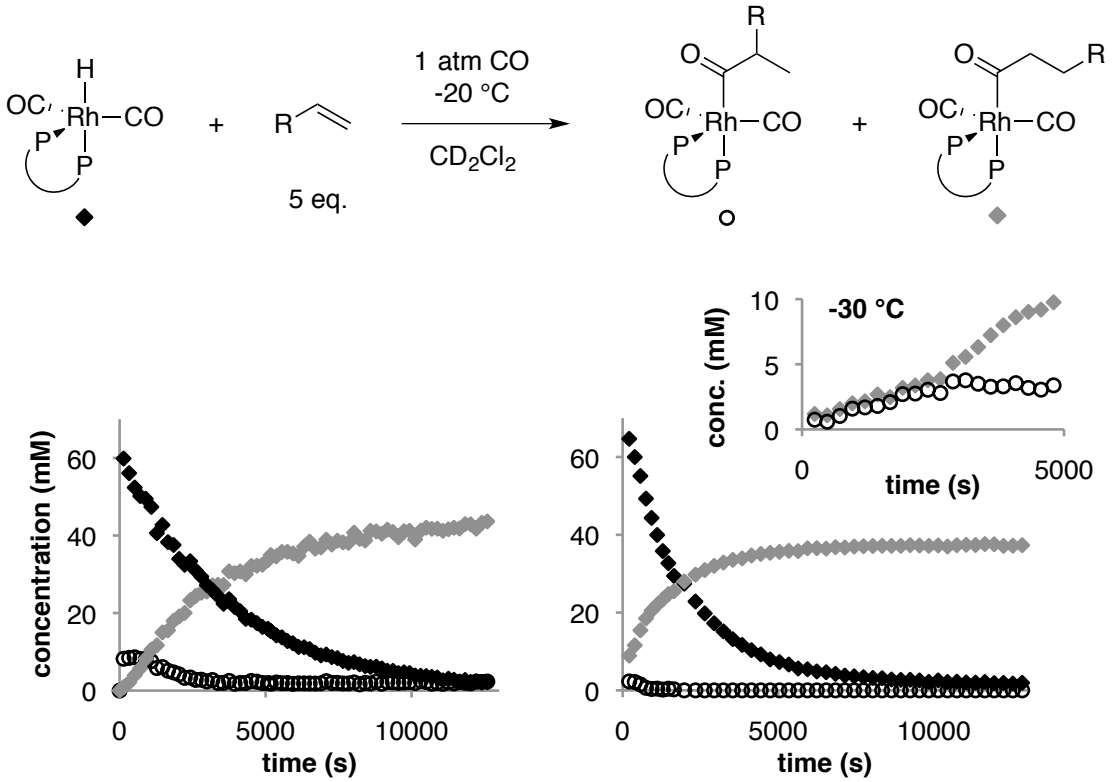

Figure 4.10. Comparison of the reaction of **1** with styrene (left) and **1**-octene (right) at -20 °C. At -30 °C (inset, right), monitoring at short reaction times reveals the absence of kinetic selectivity in the reaction of 1 with 1-octene,

If we assume that the kinetic behavior of the acyl species reflects the kinetic behavior of the alkyl species, and that the relative rates of alkene insertion to give alkyl complexes **4** is the primary factor governing selectivity, the results presented in Figure

4.10 are consistent with the experimental observation of low selectivity in 1-octene hydroformylation by Rh(BDP) catalysts.

4.5 Discussion and Conclusions

For all substrates except vinyl acetate, linear species dominate at the acyl stage. We assume that this is a steric effect, overruled in the case of vinyl acetate by the electron-withdrawing character of the acetate group.

At the alkyl stage, only branched species have been observed for octene and vinyl acetate (and the branched species is preferred for styrene; see Chapter 3). For vinyl acetate, styrene, and other electron-deficient olefins, the presence of an electron-withdrawing group in the α position is thought to stabilize the transition state leading to the branched alkyl species; these experiments, in which the distribution of rhodium species appears to be under thermodynamic control, suggest that (at least for vinyl acetate and styrene) that kinetic preference reflects a thermodynamic preference. However, no such electronic argument exists for 1-octene, an electron-rich olefin. In that case, the preference for the branched alkyl can be explained by the greater strength of a primary C-H vs. C-Rh bond.[6]

Our original motivation in performing these studies was to achieve a greater understanding of catalytic hydroformylation with Rh(BDP) catalysts. However, the majority of the data we have obtained describes five-coordinate acyl complexes **7**, species which are not on the catalytic cycle and whose kinetic and thermodynamic features may or may not have any impact on catalytic selectivity.

The predominance of five-coordinate acyl complexes reflects both a thermodynamic and kinetic preference for binding CO under these conditions (recall that

alkyl complexes only appear late in the reaction, as CO becomes depleted; in no case have we observed the original transition from alkyl to acyl species). CO binding is assumed to be virtually barrierless;[7] however, CO *dissociation* is both energetically uphill by approximately 20 kcal mol^{-1} and has a substantial activation enthalpy[8] (because binding has no barrier, $\Delta H \approx \Delta H^{\ddagger}$). Therefore, we expect a strong temperature dependence. At the low temperatures used in the NMR experiments described in the preceding two chapters, hydrogen cannot compete with CO for the four-coordinate acyl **6**.

At higher temperatures, however, like those typically used for catalytic hydroformylation, CO binding is less favorable and CO dissociation more rapid. In other words, at high temperatures the key selectivity-determining processes are alkene insertion and, in some cases, trapping of the alkyl by CO; at lower temperatures, the competition between CO and H_2 binding to **6** determine selectivity.

On the basis of this analysis, we conclude that the thermodynamic distribution of complexes **7** is not relevant in catalysis. Despite the buildup of acyl dicarbonyls under NMR conditions, the suppression of their isomerization (and therefore formation of **6**, which could undergo hydrogenolysis; see Chapter 3), there is no reason to believe that accumulation of the catalyst in this form would play any role in catalytic hydroformylation. The CO inhibition observed in catalytic reactions stems entirely, we believe, from the necessity of dissociating CO from **1** prior to catalysis.

However, precisely because CO binding is so favorable under NMR conditions, we believe that complexes **7** are reasonable *kinetic* models for catalytically-relevant species: alkyl complexes which form are immediately and stably trapped by CO, so the

kinetic ratio of acyl complexes reflects the kinetic ratio of the alkyl complexes (whose distribution is, of course, relevant in catalytic reactions). This assertion is supported by the observation that, for styrene and 1-octene (the only substrates whose distribution of acyl complexes changed significantly during the reaction), the kinetic ratio of acyl complexes reflects the catalytic selectivity – *i.e.* branched-selective for styrene, unselective for 1-octene. (For vinyl acetate, of course, the thermodynamic and kinetic distributions are virtually identical; for allyl cyanide, we assume that we simply failed to access points early enough on the reaction coordinate to observe the branched acyl **7b$_{ac}$**).

Ultimately, while the narrow scope of this study prevents any broad conclusions about the origin of selectivity in hydroformylation, our investigations into catalyst speciation have provided modest empirical support for our existing kinetic model, where the nature of the insertion step plays a major role in hydroformylation selectivity.

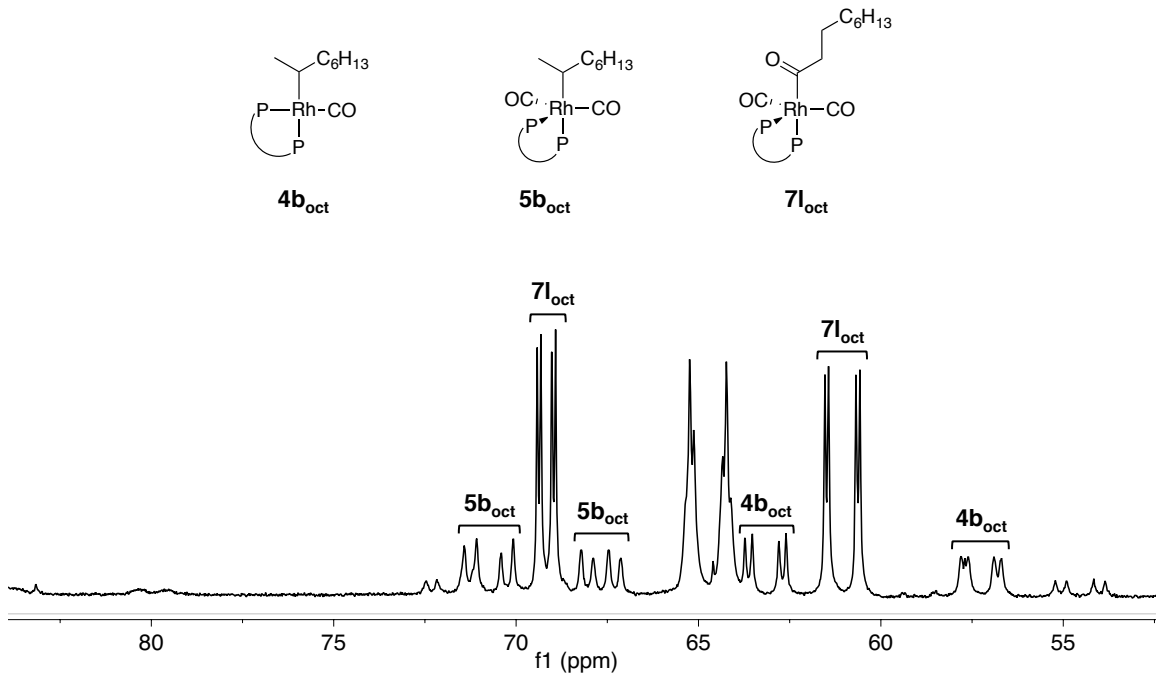

Figure 4.11. $^{31}P\{^{1}H\}$ NMR spectrum taken after the reaction of **1** with 1-octene (202.5 MHz, -20 °C, CH_2Cl_2).

4.6 NMR data

Table 4.2 provides NMR data for alkyl and acyl complexes formed during the reaction of **1** with vinyl acetate, allyl cyanide, and 1-octene. All spectra taken at -10 °C in CH_2Cl_2 or CD_2Cl_2 unless otherwise noted.

Vinyl acetate				
^{13}C		δ (ppm)	J_{CRh} (Hz)	J_{CP} (Hz)
7b	acyl C=O	232.1	90	21.5
	methine	86.2	2.1	33.8

	methyl	14.6	-	-
7b'	acyl C=O	236.2	87.8	21.7
	methine	83.9	2.7	36.7
	methyl	15.7	-	-
7l	acyl C=O	232.5	18.3	79.8
	methylene	60.2	2.1	33.9
	methyl	10	-	-
^{31}P		δ (ppm)	J_{PRh} (Hz)	J_{PP} (Hz)
$7b_{va}$	P_{ax}	69.5	81	19
	P_{eq}	60.4	152	19
$7b'_{va}$	P_{ax}	68.5	80	17
	P_{eq}	57.8	167	17
$7l_{va}$	P_{ax}	70.1	82	21
	P_{eq}	62.4	172	21
$5l_{va}$	P_{ax}	74.8	83	17
	P_{eq}	53.9	160	17
$4b_{va}$	P_{trans}	78.5	107	24
	P_{cis}	54.6	220	24
$4b^*_{va}$	P_{trans}	83.2	254	27
	P_{cis}	67.7	130	27
$4l_{va}$	P_{trans}	82.6	101	28
	P_{cis}	39.2	211	28
^{1}H		δ (ppm)	mult.	J (Hz)
$7b_{va}$	methine	4.14	q	6.5
	methyl	0.77	d	6.5
$7b'_{va}$	methine	4.38	q	6.9
	methyl	0.73	d	6.9
$7l_{va}$	methyl	0.5	t	6.9
	methylene	1.67	dq	18.2, 6.9
		2.61	dq	18.2, 6.9
$5b_{va}$	methine	4.70	-	-
	methyl	1.37	dd	8, 7
$4b_{va}$	methine	4.69	-	-
	methyl	1.58	dd	6.5
$4b^*_{va}$	methine	4.19	m, broad	-
		Allyl cyanide		
^{31}P		δ (ppm)	J_{PRh} (Hz)	J_{PP} (Hz)

7l$_{ac}$	P_{ax}	70.4	82	21
	P_{eq}	63.1	173	21
^{1}H		δ (ppm)	mult.	*J* (Hz)
7l$_{ac}$	γ-methylene	2.74	dt	17.9, 7.3
		1.65	ddd	17.9, 7,7, 5.0
	β-methylene	1.17	m	-
	α-methylene	1.50	m	-
		1-octene		
^{31}P		δ (ppm)	J_{PRh} (Hz)	J_{PP} (Hz)
7l$_{oct}$	P_{ax}	69.1	80	16
	P_{eq}	59.3	171	16
7b$_{oct}$	P_{ax}	68.7	81	15
	P_{eq}	59.5	173	15
5b$_{oct}$	P_{trans}	70.8	203	68
	P_{cis}	67.4	152	68
4b$_{oct}$	P_{trans}	63.2	183	40
	P_{cis}	57.6	181	40
^{1}H		δ (ppm)	mult.	*J* (Hz)
7l$_{oct}$	β-methylene	2.59	m	-
		1.56	m	-
7b$_{oct}$	methyl	0.37	d	6.0
^{13}C		δ (ppm)	J_{CRh} (Hz)	J_{CP} (Hz)
7l$_{oct}$	acyl C=O	232.2	18.7	81.1
	β-methylene	67.3	-	32.4

4.7 Experimental

4.7.1 General considerations

All manipulations were carried out under nitrogen using standard Schlenk, high vacuum, and glovebox techniques. All solvents and liquid reagents were degassed by at least three freeze-pump-thaw cycles unless otherwise noted. Dichloromethane and CD_2Cl_2 were distilled from P_2O_5 and degassed. Tetrahydrofuran was distilled from

sodium benzophenone ketyl and degassed. Vinyl acetate was dried over $CaCl_2$, vacuum-transferred, and degassed. Allyl cyanide (Sigma) was distilled under nitrogen, redistilled under vacuum, and degassed. S-acetoxypropionyl chloride, 2-bromoethylacetate, and 1-octene were degassed. Butyllithium, acetyl chloride, benzoyl chloride, and $^{13}CH_3I$ (all from Sigma), were used as received. ^{13}CO was purchased from Cambridge Isotope Laboratories and used as received. 1:1 $CO:H_2$, CO, and H_2 were purchased from Airgas. $[Rh(acac)(CO)_2]$ was used as received from Dow and stored in the glovebox.

Rh(acac)(BDP) and $[Rh(CO)_2(BDP)]K$ (BDP = tetraphenyl bis(diazaphospholane) were synthesized as described in Chapter 2 and stored in the glovebox. $Rh(H)(CO)_2(BDP)$ was synthesized as needed as described in Chapter 2 and used immediately.

Routine ^1H and ^{31}P NMR spectra were recorded on a Bruker AC-300 MHz spectrometer; ^{13}C, ^{19}F, and all reaction-monitoring and two-dimensional experiments were performed using Varian Inova-500 MHz or Unity-500 MHz spectrometers, or Bruker Avance-500 spectrometers. Proton spectra were referenced to residual protio solvent; an xref macro was used to reference ^{13}C and ^{31}P spectra to accompanying proton spectra.

All pressures given are gauge pressures unless otherwise noted.

4.7.2 Syntheses of rhodium complexes and substrates

$Rh(H)(^{13}CO)_2(BDP)$: In the glovebox, 51 mg (50 μmol) of Rh(acac)(P^P) was dissolved in 0.8 mL CH_2Cl_2 in a 5-mL pressure bottle. The pressure bottle was attached to a reactor head, removed from the glovebox, and connected to the Schlenk line and to a lecture bottle of ^{13}CO. The solution was frozen and the reactor evacuated. The solution

was allowed to warm to room temperature; the valve to the gas tank was opened, and the reactor was pressurized to 20 psi (the maximum delivery pressure of the lecture bottle). The valve to the gas tank was closed and the pressure bottle cooled with liquid nitrogen until the gauge pressure dropped below 10 psi. The valve to the gas tank was opened and quickly closed, and the solution and headspace were allowed to warm to room temperature. This allowed the ^{13}CO pressure in the lecture bottle to reach 40 psi. The reactor was then pressurized with 40 psi H_2 and allowed to stir in a 60 °C oil bath overnight. Conversion: 80% (NMR; other products are the phosphine mono- and dioxides and a complex we believe to be [Rh(acac)(BDP)(CO)]). $^{31}P\{^1H\}$ NMR (204.5 MHz, CH_2Cl_2): δ 82.2 (appears as broad dd, J = 140, 70 Hz). $^{13}C\{^1H\}$ NMR (125.7 MHz, CH_2Cl_2): δ 193.5 (dt; $J_{C\text{-}Rh}$ = 69 Hz, $J_{C\text{-}P}$ = ±14 Hz, terminal *C*=O).

Rh(D)(CO)$_2$(BDP): In the glovebox, 60 mg (59 μmol) Rh(acac)(BDP) was dissolved in 1 mL CH_2Cl_2 in a 15-mL pressure bottle. The pressure bottle was attached to a reactor head, removed from the glovebox, and connected to a CO tank. The reactor was purged with CO for several minutes and then pressurized sequentially with 70 psi CO and 70 psi D_2. The solution was allowed to stir in a 60 °C oil bath for 3 hours (longer reaction times promote H/D exchange). Conversion: 97 % (NMR). $^{31}P\{^1H\}$ NMR (204.5 MHz, CH_2Cl_2): δ 82.6 (d, $J_{P\text{-}Rh}$ = 137 Hz). $^{2}H\{^1H\}$ NMR (76.8 MHz, CH_2Cl_2): δ -9.8 ppm (broad, Rh-*D*).

1-^{13}C-octene: To a Schlenk flask containing 3g (7.4 mmol) $Ph_3P^{13}CH_3I$ and 827 mg KO*t*Bu (7.2 mmol) was added 30 mL dry ether. This created a yellow suspension,

which was stirred for two hours under nitrogen. Heptanal (1 mL, 7.2 mmol) was added via syringe. The suspension immediately became colorless and the solvent refluxed slightly. This mixture was stirred under nitrogen overnight, and then filtered and concentrated under reduced pressure. The product, a colorless oil, was removed from residual $Ph_3P=O$ by distillation. ^1H NMR (400.18 MHz, CD_2Cl_2, 24 °C): δ 5.83 ppm (m, 1H, -C*H*CH_2); δ 4.99 ppm (dddt, J_{HC} = 153.3 Hz, J_{HH} = 16.8, 1.8, 2 x 1.8 Hz, 1H, H_{trans}); δ 4.92 ppm (dddt, J_{HC} = 156.9 Hz, J_{HH} = 10.4, 2.0, 2 x 1.0 Hz, 1H, H_{cis}). For synthesis of $^{13}CH_3PPh_3I$, see Nozaki, K.; Sato, N.; Tonomura, Y.; Yasutomi, M.; Takaya, H.; Hiyama, T.; Matsubara, T.; Koga, N. *J. Am. Chem. Soc.* **1997**, *119*, 12779-12795.

Lithium enolate of acetaldehyde: To 4 mL (48 mmol) dry tetrahydrofuran was added 10.4 mL *n*-butyllithium solution (2.5 M in hexanes; 26 mmol) at -65 °C. Let stir for thirty minutes, then warmed to room temperature. The reaction mixture was stored under N_2 for two weeks; large colorless crystals formed. The crystals were washed four times with hexanes and dissolved in THF. ^1H NMR (500.21 MHz, THF, 24 °C): δ 6.90 ppm (dd, J = 13, 5 Hz, 1H); δ 3.15 ppm (d, J = 5 Hz, 1H); third proton hidden by solvent peak.

Vinyl acetate: To 6 mL (72 mmol) dry tetrahydrofuran was added 2 mL *n*-butyllithium solution (2.5 M in hexanes; 5 mmol) at room temperature. The reaction mixture was allowed to stir for two hours, and then cooled to -60 °C. Degassed acetyl chloride (0.36 mL, 5 mmol) was slowly added via syringe. The reaction mixture was

stirred for three hours, then allowed to sit at room temperature overnight. Following aqueous workup, the organic layer was concentrated under reduced pressure and analyzed by ^{1}H NMR spectroscopy. Yield (NMR): 60%. ^{1}H NMR (400.18 MHz, CD_2Cl_2, 24 °C): δ 7.24 ppm (dd, J = 14.0, 6.4, 1H, -C*H*CH_2); δ 4.86 ppm (dd, J = 14.0, 1.6, 1H, H_{trans}); δ 4.54 ppm (dd, J = 6.4, 1.6, 1H, H_{cis}).

Vinyl benzoate: To 6 mL (72 mmol) dry tetrahydrofuran was added 2 mL *n*-butyllithium solution (2.5 M in hexanes; 5 mmol) at room temperature. The reaction mixture was allowed to stir for two hours, and then cooled to -60 °C. Degassed benzoyl chloride (0.55 mL, 4.7 mmol) was slowly added via syringe. The reaction mixture was stirred for three hours, then allowed to sit at room temperature overnight. After aqueous workup, the organic layer was dried with $MgSO_4$ and concentrated under reduced pressure; the resulting yellow oil was analyzed by ^{1}H NMR spectroscopsy. Yield (NMR): 33%. ^{1}H NMR (400.18 MHz, CD_2Cl_2, 24 °C): δ 5.09 ppm (dd, J = 13.9, 1.7, 1H, H_{trans}); δ 4.72 ppm (dd, J = 6.2, 1.6, 1H, H_{cis}).

Reaction of [Rh(CO)$_2$(BDP)]K with 2-bromoethyl acetate: To an NMR tube containing a solution of [Rh(CO)$_2$(P^P)]K was added 30 μL (0.27 mmol, 5 equivalents) of 2-bromoethyl acetate via a gastight syringe, at room temperature. The tube was inverted several times. ^{31}P{^{1}H} NMR (121 MHz, THF, 24 °C): δ 87.0 (d, $J_{P\text{-}Rh}$ = 207 Hz, 2P).

Reaction of [Rh(CO)$_2$(BDP)]K with *S*-acetoxypropionyl chloride: To a 60 μM solution of [Rh(CO)$_2$(P^P)]K under nitrogen was added 38 μL (0.3 mmol, 5 equivalents) acid chloride via a gastight syringe; a colorless solid precipitated immediately. The reaction mixture was allowed to stir at room temperature overnight, after which the red-brown solution was transferred away from the KCl into an NMR tube via a filter cannula. $^{31}P\{^1H\}$ NMR (121 MHz, THF, 24 °C): δ 90 (dd, $J_{P\text{-}Rh}$ = 175 Hz, $J_{P\text{-}P}$ = 40 Hz, 1P), δ 68 (d, $J_{P\text{-}Rh}$ = 145 Hz, $J_{P\text{-}P}$ = 40 Hz, 1P).

3.8.3 General procedure for NMR experiments

A pressure reactor containing a 60 μM solution of Rh(H)(CO)$_2$(BDP) was depressurized and refilled with 20 psi CO. It was connected via a cannula to an oven-dried septum-capped NMR tube equipped with a vent, and the pressure reactor/NMR tube system was purged with the desired gas (generally CO) for several minutes. The cannula was then used to transfer the solution to the NMR tube, and the tube was sealed with Parafilm. The NMR spectrometer was cooled to the desired temperature (actual temperature determined using a methanol standard), and initial spectra were taken. The sample was ejected from the spectrometer, and the desired alkene was added via a gastight syringe; the tube was inverted three times and quickly returned to the spectrometer. For kinetic experiments, the time elapsed between mixing and taking the first spectrum was recorded (typically less than one minute).

4.8 References

(1) Tolman, C. A.; Faller, J. W. Mechanistic Studies of Catalytic Reactions Using Spectroscopic and Kinetic Techniques. In *Homogeneous Catalysis with Metal Phosphine Complexes*; Pignolet, L. H., Ed.; Plenum Press: New York, 1983; pp 13 – 109.

(2) For selected examples, see (a) Heck, R. F. J. Am. Chem. Soc. 1968. (b) Cheng, J. C.-Y., Daves, G. D., Jr. *Organometallics* **1986**, *5*, 1753-1755. (c) Zhu, G., Lu, X. *Organometallics* **1995**, *14*, 4899-4904. (d) Zhang, Z.; Lu, X.; Xu, Z.; Zhang, Q.; Han, X. *Organometallics* **2001**, *20*, 3724-3728. (e) Williams, B. S.; Leatherman, M. D.; White, P. S.; Brookhart, M. *J. Am. Chem. Soc*. **2005**, *173*, 5132-5146. (f) Yu, J.-Y.; Kuwano, R. *Angew. Chem., Int. Ed*. 2009, 48, 7217-7220. (g) Ogiwara, Y.; Tamura, M.; Kochi, T.; Matsuura, Y.; Chatani, N.; Kakiuchi, F. *Organometallics* **2014**, *33*, 402-420.

(3) (a) Komiya, S.; Yamamoto, A. *J. Chem. Soc., Chem. Commun*. **1974**, 523-524. (b) Komiya, S.; Yamamoto, A. *J. Organomet. Chem*. 1975, 87, 333-339.

(4) Bates, R. B.; Kroposki, L. M.; Potter, D. E. *J. Org. Chem*. **1972**, *4*, 560.

(5) Liu, J.; An, Y.; Wang, Y.-H.; Jiang, H.-Y.; Zhang, Y.-X.; Chen. Z. *Chem. Eur. J.* **2008**, *14*, 9131-1934.

(6) Jiao, Y.; Evans, M. E.; Morris, J.; Brennessel, W. W.; Jones, W. D. *J. Am. Chem. Soc.* **2013**, *135*, 6994−7004.

(7) Rush, L. E.; Pringle, P. E.; Harvey, J. N. *Angew. Chem*.; manuscript in review.

(8) (a) van der Veen, L. A.; Keeven, P. H.; Schoemaker, G. C.; Reek, J. N. H.; Kamer, P. C. J.; van Leeuwen, P. W. N. M.; Lutz, M.; Spek, A. L. *Organometallics* **2000**, *19*, 872 – 883. (b) Sparta, M.; Børve, K. J.; Jensen, V. R. *J. Am. Chem. Soc*. **2007**,

129, 8487 – 8499. (c) Zuidema, E.; Escoriheula, L.; Eichelsheim, T.; Carbó, J. J.; Bo, C.; Kamer, P. C. J.; van Leeuwen, P. W. N. M. *Chem. Eur. J.* **2008**, *14*, 1843 – 1853.

Chapter 5

High-pressure NMR experiments

5.1 Introduction

A major limitation of the experimental setup described in Chapters 3 and 4 is the inability to regulate the gas pressure in the NMR tube, or even to know it with any accuracy. CO pressure has a significant effect on the rate and, in some cases, the selectivity of the reaction, and data provided in Chapter 3 suggest that H_2 pressure may have a previously-unappreciated role in selectivity, also. Therefore, the inability to regulate and measure gas pressure effectively prohibits any detailed kinetic studies. Moreover, while behavior at the limits of high and low pressure is often critical in understanding the mechanisms of reactions involving gases, performing experiments in septum-capped NMR tubes, as in Chapters 3 and 4, limits us to approximately atmospheric pressures.

Since its introduction in the early 1980's[1], high-pressure NMR (HPNMR) has been an invaluable tool for reactions involving gas-solute interactions,[2] including hydroformylation.[3] Broader application of this technique was encouraged by Roe's development of a sapphire high-pressure cell compatible with standard NMR probes,[4] and the subsequent adaptation of this system by Iggo to be used in flow.[5] A flow setup ameliorates the mass-transport problems which typically plague reactions in NMR tubes, where the solvent-gas interface is small and mixing is difficult. In 2001, van Leeuwen and coworkers used this flow cell to monitor the stoichiometric hydroformylation of 1-hexene with their phosphorus diamide ligands.[5] They observed five-coordinate acyl complexes (characterized primarily by ^{13}C NMR spectroscopic data) analogous to those described in Chapters 3-4; however, because they were not able to distinguish linear from

branched regioisomers, they were not able to comment on the role of hydrogenolysis in selectivity.

Since that time, HPNMR flow technology has advanced further. A system developed at LIKAT Rostock[6] achieves both efficient mixing and pressure regulation by adding a finely-perforated gas-delivery capillary to a high-pressure cell designed by Gaemers and coworkers at the University of Amsterdam.[7]

Nicholas Beach, a postdoctoral associate in the Landis group, has built a similar setup in the NMR facility here. Compatible with an existing 10-mM NMR probe, this apparatus can access and regulate pressures up to 80 bar (more than adequate for our purposes), and allows the user to switch gases during the experiment. Dr. Beach has also modified this system to allow injection of materials into the pressure cell while it is installed in the spectrometer. This modification makes it possible to perform experiments of the type described in Chapters 3 and 4, in which a substrate is added to a solution of the hydridodicarbonyl precatalyst **1**.

Adapting this setup for our reaction system will enable us to access a much broader range of pressures – and therefore a potentially broader range of chemical behavior – and to monitor the reaction *in situ* while accurately measuring the rate dependence on CO and H_2 pressures.

3.2 Reaction of acyl complexes 7b,l$_{sty}$ with H_2

5.2.1 Introduction

The first target for investigation by HPNMR was the unexpected hydrogenolysis behavior described in Chapter 3. Despite a higher concentration of the linear acyl,

reaction with hydrogen produced more branched aldehyde than linear aldehyde. This suggested that, at least under stoichiometric conditions, the relative rates of hydrogenolysis of linear and branched acyl complexes substantially influence selectivity. We were surprised by this result because, in catalytic studies of hydroformylation by Rh(BDP) complexes, the hydrogen pressure does not appear to have any effect on either the reaction rate or selectivity (so-called "type 1" hydroformylation kinetics).[8] In general, however, because hydrogenolysis involves the oxidative addition of H_2, it is expected to be slow for complexes of relatively electron-poor phosphorus ligands, so it is not unreasonable that hydrogenolysis might have a significant effect on selectivity for Rh(BDP) catalysts under conditions of low H_2 pressure (like those described in Chapter 3).

HPNMR allows us to investigate this phenomenon qualitatively, and in much greater detail, asking questions such as: how much faster is aldehyde production from the branched versus the linear acyl? At what hydrogen pressure does this turnover become fast, and no longer selectivity-influencing?

Before we can answer those questions, however, it is critical to remember that the conversion of rhodium-acyl complexes **7b,l$_{sty}$** to **1** and aldehydes – heretofore referred to somewhat disingenuously as "hydrogenolysis" – actually involves two distinct processes. Dicarbonyl complexes **7b,l$_{sty}$** must first lose an equivalent of CO to give **6b,l$_{sty}$** (not observed), before the oxidative addition of H_2 and (presumably fast) reductive elimination of aldehyde can occur (see Scheme 5.1). Therefore, faster aldehyde production from the branched isomer could result from either faster CO dissociation ($k_{6\text{-}7,br} > k_{6\text{-}7,lin}$) or faster reaction with hydrogen ($k_{H2,br} > k_{H2,lin}$).

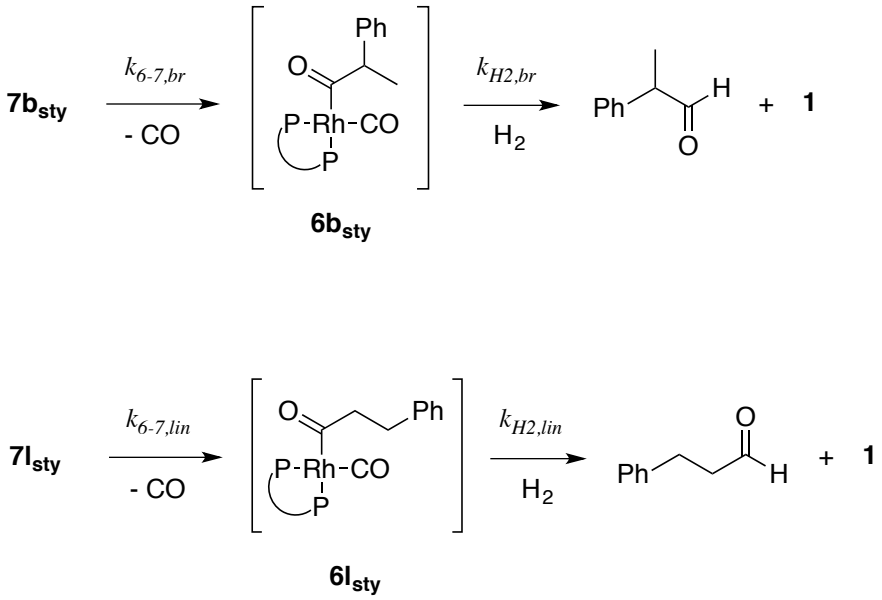

Scheme 5.1. The conversion of complexes **7** to **1** and the corresponding aldehydes requires the dissociation of an equivalent of CO, followed by reaction with hydrogen.

Faster CO dissociation from **7b$_{sty}$** is not implausible; the data in Chapter 3 suggest that CO dissociation is favored for the branched alkyl over the linear alkyl. (The data in Chapter 3 are, of course, taken under equilibrium conditions and therefore speak to thermodynamic parameters; however, as discussed earlier, for $\Delta H = \Delta H^{\ddagger}$ for CO dissociation.) While the reason for this disparity remains unclear, it may be a steric effect, assisted by an interaction of the rhodium center with the phenyl ring as in **4b*$_{sty}$**, or with one of the methyl C-H bonds; these factors may be important at the acyl stage as well.

This complexity must be taken into account when interpreting the results of the experiments described below.

5.2.2 Comfirming faster conversion from ***7b$_{sty}$*** *versus* ***7l$_{sty}$***

An equilibrium mixture of **7b$_{sty}$** and **7l$_{sty}$** can be generated in the HPNMR tube by adding styrene to a solution of **1** under a low (5-10 psig) pressure of CO. Quantitative conversion to the acyl complexes (plus small amounts of the alkyl complexes **4b$_{sty}$**, **4b*$_{sty}$**; see Figure 5.1) typically takes about three hours when [**1**] = [styrene].

Pressurizing this solution with hydrogen and running the gas circulator briefly[§] enables us to monitor the production of aldehydes from of **7b,l$_{sty}$**. After several hours, the acyl complexes have been completely converted to the hydridodicarbonyl precatalyst **1** (see the ^{31}P NMR spectra in Figure **5.1**); ^{1}H NMR spectra show the formation of both linear and branched aldehydes.

[§] At this writing, it was not possible to maintain adequate shims with continuous gas circulation. The absence of H_2 in the ^{1}H NMR spectrum until after complete conversion of **7b,l$_{sty}$** to **1** indicates gas starvation. At this stage, therefore, absolute kinetic parameters are inaccessible.

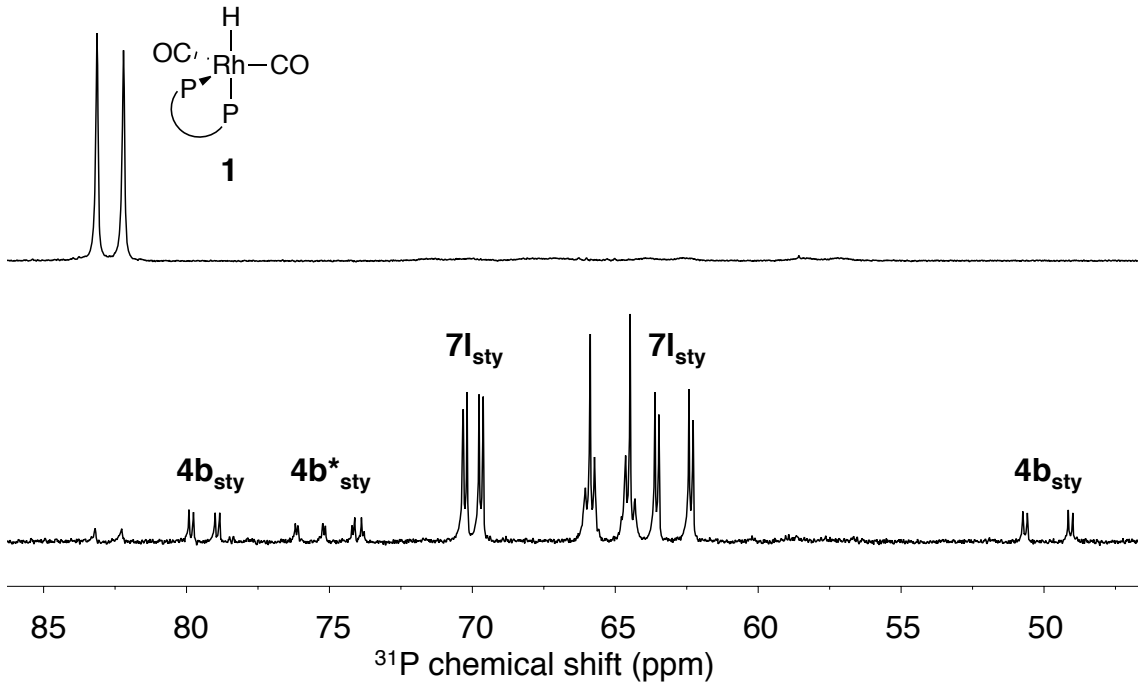

Figure 5.1. $^{31}P\{^{1}H\}$ NMR spectra taken before (bottom) and approximately 10 hours after (top) pressurizing a sample of alkyl and acyl complexes with 100 psig H_2. (-20 °C, CH_2Cl_2)

As reported in Chapter 3, the branched aldehyde is produced at a greater rate than its linear counterpart; in this experiment, the $\mathbf{7b_{sty}}$: $\mathbf{7l_{sty}}$ = 1 : 30, but the ratio of branched to linear aldehydes reaches 1 : 1.7 (see Figure 5.2).

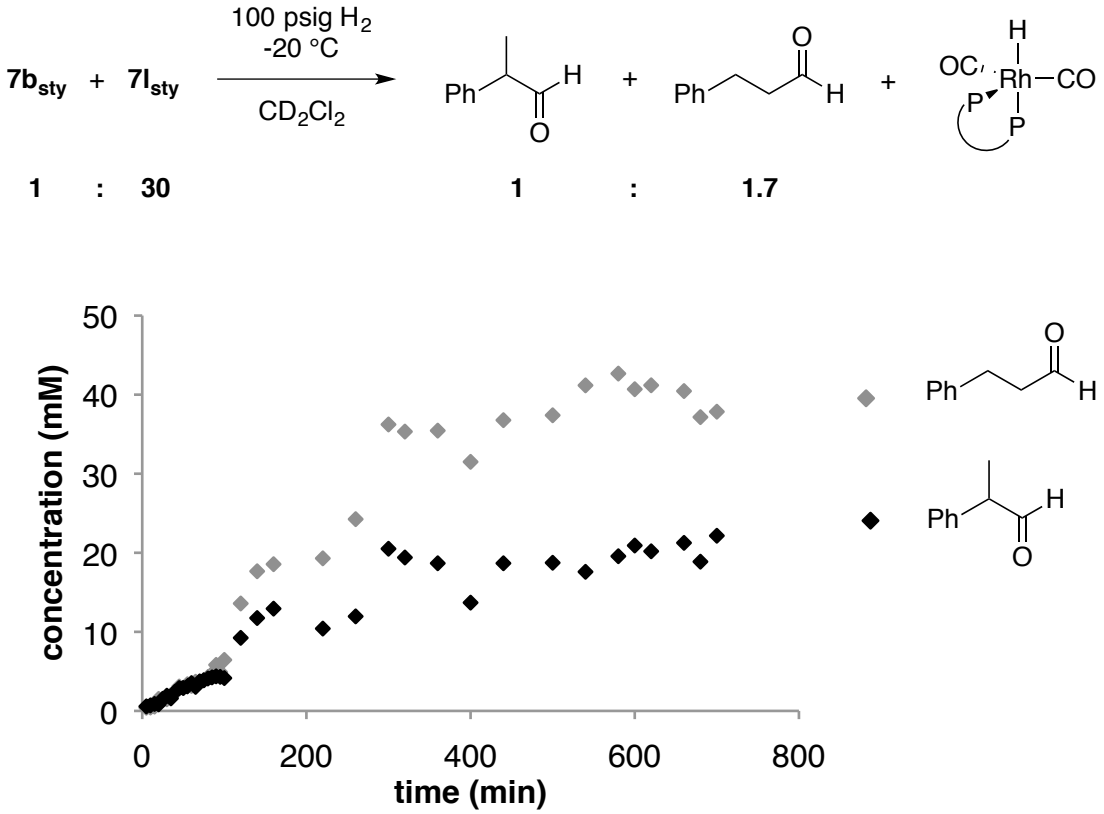

Figure 5.2. Reaction of an equilibrated mixture of complexes **7b,l$_{sty}$** with 100 psig H_2 at -20 °C using the HPNMR apparatus. The b:l ratio of the product aldehydes does not reflect the b:l ratio of the acyl complexes. Aldehyde concentration determined based on $[\mathbf{1}]_0$.

The data presented in Figure 5.2 are not rigorously quantitative. Obtaining adequate shims is problematic using this setup, which makes precise integration difficult. However, while the relative rates of hydrogenolysis are not well-resolved at short time periods (below 100 minutes), it is clear that the final ratio of linear to branched aldehyde (approximately 1.7 : 1) differs substantially from the ratio of linear to branched acyl prior

to hydrogenolysis (approximately 30 : 1). This disparity requires conversion to aldehyde from **7b**$_{sty}$ to be approximately *eighteen times faster* than conversion from **7l**$_{sty}$.

However, the evidence shown in Figure 5.2 cannot distinguish between the effect of CO dissociation and hydrogen oxidative addition on the relative rates of conversion to aldehyde. Manipulating the relative CO and H_2 pressures can provide some insight. We can consider the two extreme cases: first, if CO dissociation is turnover-limiting, and subsequent hydrogenolysis is very fast, changing the hydrogen pressure will have no effect on the rate or selectivity of aldehyde production. However, if hydrogenolysis of **6b,l**$_{sty}$ is slow relative to CO dissociation from **7b,l**$_{sty}$, then increasing the hydrogen pressure should accelerate aldehyde production.

Therefore, we performed the experiment described above at both 50 and 100 psig H_2. The results are shown in Figure 5.3. There does appear to be an increase in the rate of hydrogenolysis at 100 psig vs. 50 psig, by approximately a factor of two, suggesting that hydrogenolysis may be rate-limiting under these conditions. (The regioselectivity is unaffected by H_2 pressure.) However, these experiments need to be repeated, over a broader range of pressures, before any firm conclusions can be reached. At this stage in the development of the apparatus, reproducibility remains a problem.

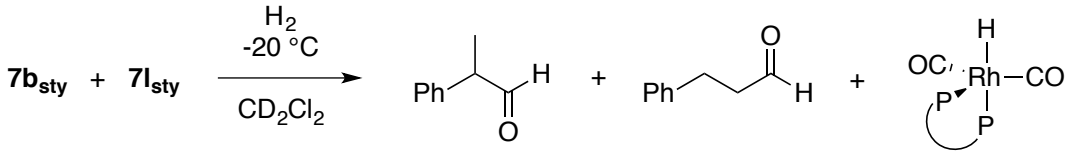

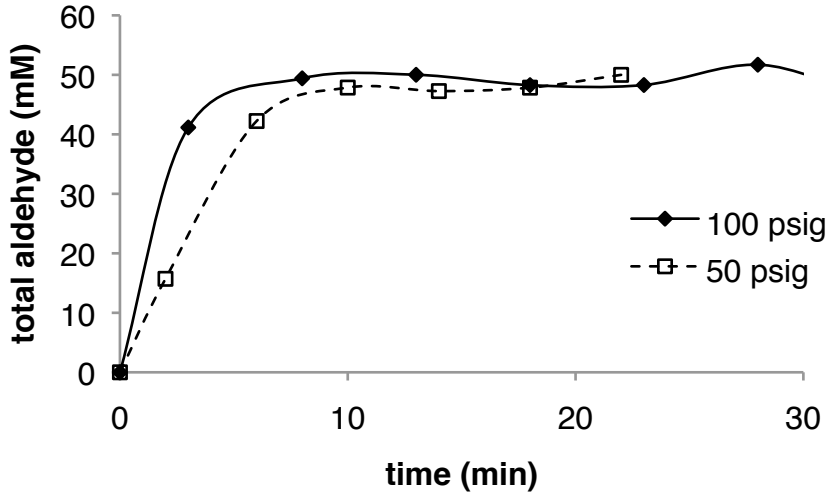

Figure 5.3. Dependence on H_2 pressure of the conversion of **7b,l$_{sty}$** to **1** and aldehydes, measured by integration of the aldehyde peaks over time.

3.3 Conclusions

The experiments described above conclusively demonstrate that production of the branched aldehyde from the branched acyl is faster than the analogous process for the linear isomers. However, whether that disparity originates from a difference in the rates of reaction of the four-coordinate acyl complexes **6$_{sty}$** and **6l$_{sty}$** with hydrogen, or simply a difference in the rates of CO dissociation from **7b$_{sty}$** vs. **7l$_{sty}$** remains unclear, and will be a subject of further study.

5.4 Experimental

5.4.1 General considerations

All manipulations were carried out under nitrogen using standard Schlenk, high vacuum, and glovebox techniques. All solvents and liquid reagents were degassed by at least three freeze-pump-thaw cycles unless otherwise noted. Dichloromethane and CD_2Cl_2 were distilled from P_2O_5 and degassed. Styrene was dried over $MgSO_4$ and degassed. 1:1 $CO:H_2$, CO, and H_2 were purchased from Airgas. [Rh(acac)$(CO)_2$] was used as received from Dow and stored in the glovebox.

[Rh(acac)(BDP)] (BDP = tetraphenyl bis(diazaphospholane) was synthesized as described in Chapter 2 and stored in the glovebox. Rh(H)$(CO)_2$(BDP) (**1**) was synthesized as needed as described in Chapter 2 and used immediately.

All ^1H and ^{31}P NMR spectra were recorded on a Bruker AC-360 MHz spectrometer using the high-pressure apparatus. Proton spectra were referenced to residual protio solvent; an xref macro was used to reference ^{31}P spectra to accompanying proton spectra.

All pressures given are gauge pressures unless otherwise noted.

5.4.2 High-pressure NMR experiments

In the glovebox, 1 mL of a 100-mM solution of **1** in CH_2Cl_2 was transferred from the pressure bottle in which it had been generated to a threaded gastight syringe. Two more threaded gastight syringes were loaded, one with 0.2 mL of a 500-mM solution of styrene in CH_2Cl_2 and one with a 1-mL bolus of CD_2Cl_2. All three syringes were sealed with threaded nuts containing rubber septa, and removed from the glovebox.

The HPNMR apparatus was purged with nitrogen by at least three vent/refill cycles, and the probe was cooled to -20 °C. The rhodium solution was injected into the high-pressure cell, and initial spectra were taken. Then, the styrene solution and plain CD_2Cl_2 (for washing) were injected. The circulator was turned on for 10 seconds at 2 mL/min to ensure that all reagents were well-mixed in the detection region. The HPNMR apparatus was pressurized with approximately 10 psi CO, and the reaction mixture was allowed to sit for several hours to allow the complete conversion of **1** to **7b,l$_{sty}$** (determined by ^{31}P NMR).

The apparatus was pressurized with the desired pressure of H_2 (usually 100 psi). The circulator was run for 30 seconds at 2 mL/min, and then the reaction mixture was allowed to sit under static pressure until complete conversion of **7b,l$_{sty}$** to **1** and aldehydes had been achieved (determined by ^{1}H and ^{31}P NMR). ^{1}H NMR spectra were acquired throughout this reaction period.

5.5 References

(1) (a) Heaton, B. T.; Strona, L.; Jonas, J.; Eguchi, T.; Hoffman, G. A. *J. Chem. Soc., Dalton Trans.* **1982**, 1159 – 1164. (b) Heaton, B. T.; Jonas, J.; Eguchi, T.; Hoffman, G. A. *J. Chem. Soc., Chem. Commun*. **1981**, 331 – 332.

(2) (a) Horvath, I. T.; Miller, J. M. *Chem. Rev.* **1991**, *91*, 1339 – 1351. (b) Laurenczy, G.; Helen, L., High Pressure NMR Cells. In *Mechanisms in Homogeneous Catalysis – A Spectroscopic Approach*; Heaton, B. T., ed.; Wiley-VCH Verlag GmbH & Co. KGaA: Weinheim, 2005; pp. 81 – 106.

(2) For examples involving hydroformylation, see (a) Castellanos-Paez, A.; Castillon, S.; Claver, C.; van der Slot, S. C.; van Leeuwen, P. W. N. M.; de Lange, W. G.

J. *Organometallics* **1998,** *17*, 2543 – 2552. (b) Aghmiz, A.; Orejon, M.; Dieguez, M.; Miquel-Serrano, M. D.; Claver, C.; Masdeu-Bulto, A. M.; Sinou, D.; Lauranczy, G. *J. Mol. Catal. A.* **2003**, *195*, 113-124. (c) Rubio, M.; Suarez, A.; Alvarez, E.; Bianchini, C.; Oberhauser, W.; Peruzzini, M.; Pizzano, A. Organometallics 2007, 26, 6428 – 6436. (d) Torres, A.; Perez. N. M.; Overend, G.; Hodge, N.; Heaton, B. T.; Iggo, J. A.; Satherly, J.; Whyman, R.; Eastham, G. R.; Gobby, D. ACS Catal. 2012, 2, 2281 – 2289.

(3) Roe, D. C. J. *J. Magn. Reson*. **1985**, *63*, 388.

(4) Iggo, J. A.; Shirley, D.; Tong, N. C. *New J. Chem.* **1998**, 1043 – 1045.

(5) van der Slot, S. C.; Kamer, P. C. J.; van Leeuwen, P. W. N. M.; Iggo, J. A.; Heaton, B. T. *Organometallics* **2001**, *20*, 430 – 441.

(6) Selent, D.; Baumann, W.; Boerner, A. Eur. Patent DE10333143, **2005**.

(7) Gaemers. S.; Luyten, H.; Ernsting, J. M.; Elsevier, C. J. *Magn. Reson. Chem*. **1999**, *37*, 25-30.

(8) Watkins, A.; Landis, C. R. *J. Am. Chem. Soc.* **2010**, *132*, 10306 – 10317.

Chapter 6

My research explained to a lay audience

Looking closely at chemical reactions

Why look at chemical reactions?

Chemical reactions are going on all around us, all the time. We're surrounded by (and full of) molecules tumbling around each other and joining together to make new molecules, molecules coming apart into their constituent parts. Some of these reactions, you might pay attention to: drain cleaner foaming up into the sink as the strong bases in it react with water, or sugar caramelizing in a pan of browning onions. But most of them go on invisible, unnoticed.

Except by chemists.

The mystery of turning on thing into another can be as irresistible as alchemy, even if you're not making gold (and let's face it – you're not). Fascinating as they are, though, we also need chemical reactions to be useful: we rely on them to make most of the things we encounter every day. Most of the time, there's more than one way to combine the atoms and molecules in a reaction. Even in a simple made-up case like this one:

Figure 6.1. A simplified representation of what happens in a chemical reaction. Two things combine – and there's usually more than one way to do it.

Now, maybe those two possible products are both okay. But maybe not: maybe they act differently in some context, and you only want one of them. Any time you start

letting atoms interact, you run the risk of getting products you don't want. How can you understand how to tweak the reaction until you only get the product you want? One of the best ways is to look at how the molecules interact.

Why hydroformylation?

My research focused on a reaction called hydroformylation. It's a useful reaction because it takes a molecule that's relatively simple – in some cases, only carbon and hydrogen – and makes it more interesting (and, not incidentally, more valuable) by tacking on an oxygen atom in addition to another carbon and hydrogen (usually with a metal-containing compound thrown in to make the process faster – more on that later). These "value-added" molecules produced by hydroformylation are aldehydes.

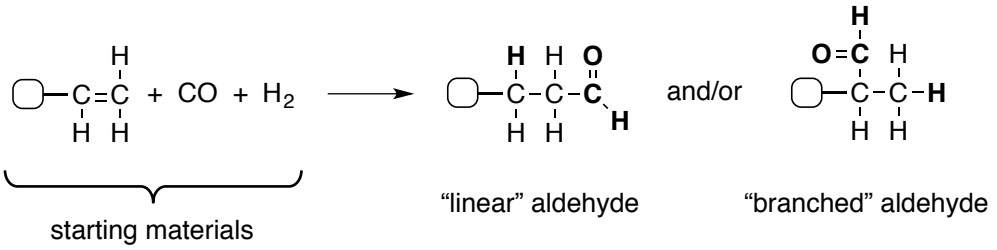

Figure 6.2. Hydroformylation makes aldehydes, molecules with a carbon/hydrogen/oxygen group attached to one of the carbon atoms of the starting material.

You're most familiar with aldehydes – even though you may not know it – as the molecules that produce a lot of common scents. That love-it-or-hate-it soapiness of cilantro? Aldehydes. The aromatic spiciness of cinnamon and vanilla? Aldehydes.

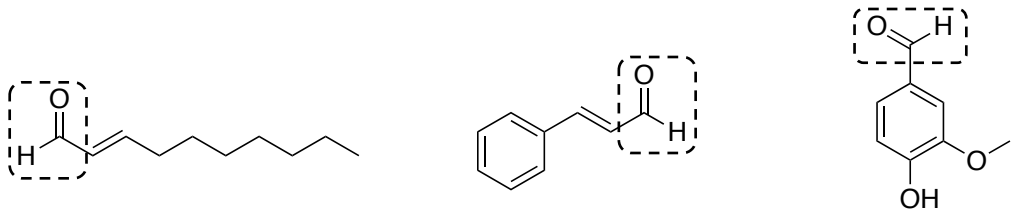

***E*-2-decenal**
cilantro

cinnamaldehyde
cinnamon

vanillin
vanilla

Figure 6.3. Aldehydes you're probably encountered in your kitchen. The C/H/O grouping – in the boxes – is what makes each of these molecules aldehydes.

Most of the aldehydes produced by hydroformylation – about eighteen billion pounds of them – are less exotic. For the most part, they're bulk chemicals, used to make things like detergents that get churned out on huge scales. Practical, but not very interesting.

Selectivity makes all the difference here. During hydroformylation, the carbon/hydrogen/oxygen trio (the aldehyde group) is added to one carbon of the starting material; the other carbon just gets a new hydrogen. Adding the aldehyde to the carbon at the end of the molecule – called the "linear" product because all the carbon atoms in the new molecule are in a single-file line – makes those bulk chemicals.

But the other product, where the new carbon and oxygen are attached to the inner position, is special. This addition makes a branch off the central spine of carbon atoms, and that branch puts these aldehydes in a class of molecules called "chiral." Molecules exist in three dimensions (an easy point to forget, since we're always drawing them in two dimensions), and molecules like these branched aldehydes have four different arms sticking out in different directions.

The key point is that each of these arms is different, like an indecisive four-legged starfish. Each molecule like this has an almost-twin: another molecule, with the same four arms as this one, just in a different three-dimensional arrangement, the first molecule's mirror image. These pairs of fraternal twins are called enantiomers.

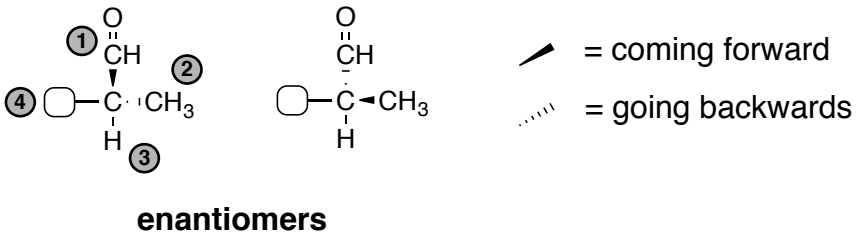

Figure 6.4. The branched aldehydes produced by hydroformylation are chiral: they have four different "arms" that, in three dimensions, can be arranged in one of two ways. In the aldehyde on the left; the aldehyde (CHO) group is pointing out of the page towards you, and the CH_3 group is pointing backwards, away from you. In the aldehyde on the right, their directions are switched. These *enantiomers* look almost the same, but they can react in very different ways.

Enantiomers might look the same, but they don't always *act* the same. Your right and left hands – the most familiar physical enantiomers – look similar, both can open doors and hold spoons and (sort of) write. Good luck, though, getting your right glove to fit on your left hand.

Most reactions that produce chiral molecules make both enantiomers, and they're not always separated. That can have serious consequences in pharmaceutical chemistry, for example, because many drugs are chiral. The best-known, and most tragic, case was

what happened with thalidomide in the late 1950's. The thalidomide given to pregnant women to treat morning sickness wasn't separated into "right-handed" and "left-handed" molecules, and while one enantiomer did ease nausea, the other caused devastating birth defects. Even if one half of a chiral pair isn't actually harmful, some simply work better than others. The popular antidepressant Lexapro is a single enantiomer; its predecessor, Celexa, contained a mixture of the active and inactive enantiomers.

Aldehydes are really useful chemical precursors, because they can easily be turned into other things. The chiral branched aldehydes could be great candidates for use in making pharmaceuticals and other "fine chemicals" – specialized, lucrative molecules that are typically made on a small scale. Because enantiomers function so differently, especially in a biological context, if we want to use hydroformylation to make these valuable chiral molecules, we need it to be selective. We'd also like it to be fast.

That's where that metal compound comes in.

What's rhodium doing in there?

Catalysts make reactions faster by reducing the amount of energy it takes to turn the starting materials into the products. Metals, it turns out, have a special aptitude for this, and rhodium is a particular favorite. A lot of the world's rhodium is busy cleaning exhaust in cars' catalytic converters; some if it finds more aristocratic work in in the jewelry industry, where it's used to give a shiny, protective coating to platinum and white gold. In chemistry labs, though, it's used as a catalyst for a wide range of chemical reactions. In our case, stuck to two phosphorus atoms, with some carbon, hydrogen, oxygen, and nitrogen atoms for decoration, rhodium works hard at hydroformylation. This particular catalyst makes just one enantiomer of the branched aldehyde most of the

time (about four times out of five, on average) and is really fast: it can make more than one aldehyde per second.

What does it mean, though, to reduce the amount of energy a reaction takes?

Imagine you're making a cake. (Food metaphors are ubiquitous in chemistry – both fields involve mixing things together to make other, more desirable, things, and there's so much obvious chemistry in cooking that there's whole subcategory of cookbooks explaining how to use an understanding of chemistry to improve your results in the kitchen.) You're going to have to mix all the ingredients together somehow. You could do it by hand. That requires a lot of energy, though, and in this age of electronic conveniences you're out of practice, so it would probably take you a while.

So you'll probably use an electric mixer. Like a catalyst, it keeps you from having to use as much energy, so the process goes faster – and if you're making cakes on a grand scale, you can bake more than you could if you had to mix every one by hand (obviously a bonus). Other important points about catalysts: the starting and ending points of the process don't change (you start with ingredients and end up with cake batter whether you mixed it with a spoon or an electric mixer) and the catalyst itself isn't used up (once the batter is mixed, the mixer is available for the next round).

In chemical reactions, catalysts can also have a major effect on selectivity. The catalyst interacts with the substrate molecules to join them together. The specifics of that interaction can determine which product you get out. Is it easier to have molecule A upside down or right side up? Does the catalyst prefer to the first carbon atom of A, or the second one? Is it easier to bind B first, and then A, or A first, and then B? Just like mixing the flour and sugar together before you add the butter could be a baking disaster,

the particular way a chemical catalyst interacts with the starting materials can make all the difference in whether you get the product you want – or just a mess.

If we knew exactly how the catalyst was interacting with those molecules, we might be able to figure out why the reaction goes the way it does – and how to make it more selective.

But of course, these molecules are way too tiny for us really look at them directly, the way you might study workers on an assembly line to see how a car gets made. So we have to be creative. Chemists have spent decades devising techniques to squeeze information out of molecules we can't see. Most of these involve bombarding molecules with some type of radiation – visible light, ultraviolet light, x-rays – and seeing what bounces back. One of the most useful of these, called "nuclear magnetic resonance" (NMR), uses radio waves and giant magnets to tell us what molecules look like.

Looking at something too tiny to see

In the early nineteen-forties, the wartime demand for radar technology had physicists spending a lot of time thinking about radio waves. One of the products of these studies was the realization, by two separate scientists, that the nuclei of certain atoms could absorb radio-frequency energy when held in a magnetic field.

An odd number of protons, or neutrons, or both, gives an atomic nucleus a special ability to act like a tiny magnet. Put these miniscule magnets inside the magnetic field of a much bigger one, and they'll line up with it like iron filings arranging themselves in lines around a magnet. But if you hit these nuclei with *just* the right amount of radio-frequency energy, they can be persuaded to flip, and line up the opposite way.

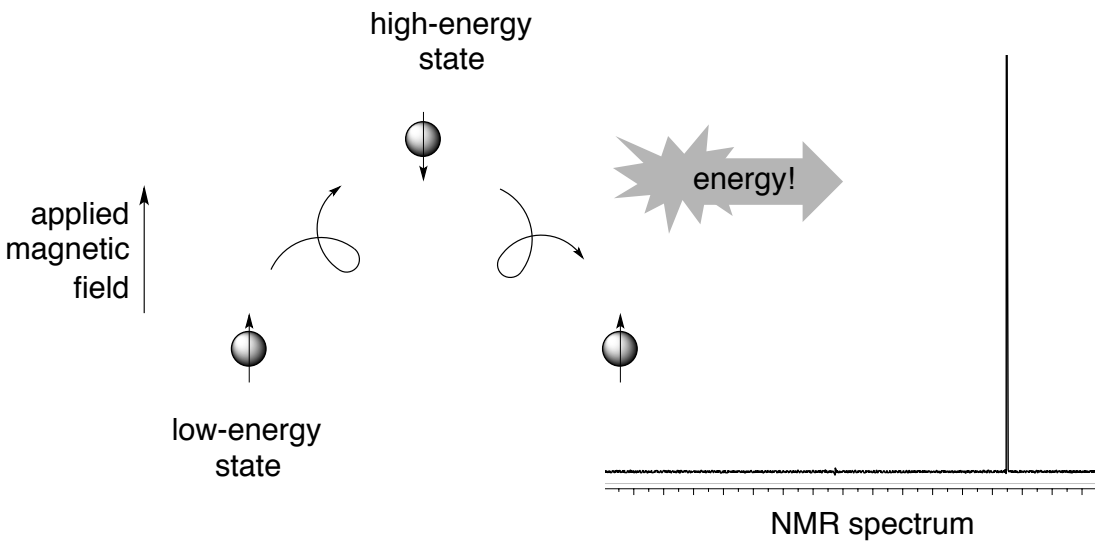

Figure 6.5. When magnetic nuclei drop from a high-energy state (where they're lined up *against* an external magnetic field) to a low-energy state, they release energy that can be translated by an NMR instrument into peaks on a "spectrum" (right); the position and shape of those peaks holds a lot of information about the molecule the nucleus is in.

It takes energy to stay in that state, though, so the nucleus will flip back down like a gymnast at the apex of a vault. On its descent, the nucleus releases a little burst of energy – exactly as much as it absorbed on the way up. An NMR instrument detects that energy, and turns it into a little spike amidst a hum of noise.

Just detecting little packets of energy from gymnastic nuclei wouldn't be all that informative on its own. NMR is so useful because the amount of energy it takes to somersault that nucleus is exquisitely sensitive to what the molecule around it looks like. Every nucleus in a molecule requires a different amount of energy. Blast a sample of molecules with a whole bunch of radio frequencies at once (sort of like tuning your radio

to all the stations at the same time) and one of those frequencies will be just right for a particular nucleus – flip! – and then another – flip! – and then another.

All those blips add up to a kind of magnetic signature. Chemists have been doing this for a long time, correlating the patterns made by these magnetic nuclei with molecular structures. Rhodium and phosphorus both belong to this class of "magnetically-active" molecules, along with protons. So our catalyst, whose business end both rhodium *and* phosphorus, and has plenty of protons, is set up perfectly for analysis by NMR. (The more magnetically-active nuclei are around, the more information you get, because when there are other magnetic nuclei nearby, they interact with their neighbors, doubling their peaks or giving them little satellites.) This means that we have direct access to a lot of information about our catalyst.

My job was to find out more about how hydroformylation happened. Why were the branched aldehydes formed so much faster than the linear ones? All I had to do was to add the starting materials to the catalyst – at low enough temperatures that everything slowed down a little – and use NMR to catch them in the act of joining together, seeing what combinations form.

It's a complicated reaction. The molecular dance that rhodium does to turn the starting materials into aldehydes has seven separate steps, with subtle variations for each possible product. The work in this thesis opens only a very small window into this process. It's not enough to tell us why our particular catalyst is so effective. Progress in science is incremental – it takes years to piece together a robust understanding of a chemical process, let alone use that understanding to design an even better one. But in the meantime, it's just fun to try to figure out how things work.

Acknowledgements

Clark Landis, did me a great favor by entrusting this project to me, and a greater one by teaching me how to think about it. Luke Nelsen and Zheng Huang taught me how to do all the chemistry I know how to do. Charlie Fry lost hours of his life showing me NMR techniques and answering my questions – many of them more than once. The work in this thesis would have been impossible without them.

Preston and Norman Leake showed me the pleasure of learning how things work. I hope that they would be pleased.

Appendix:

Supporting Information

Chapter 2

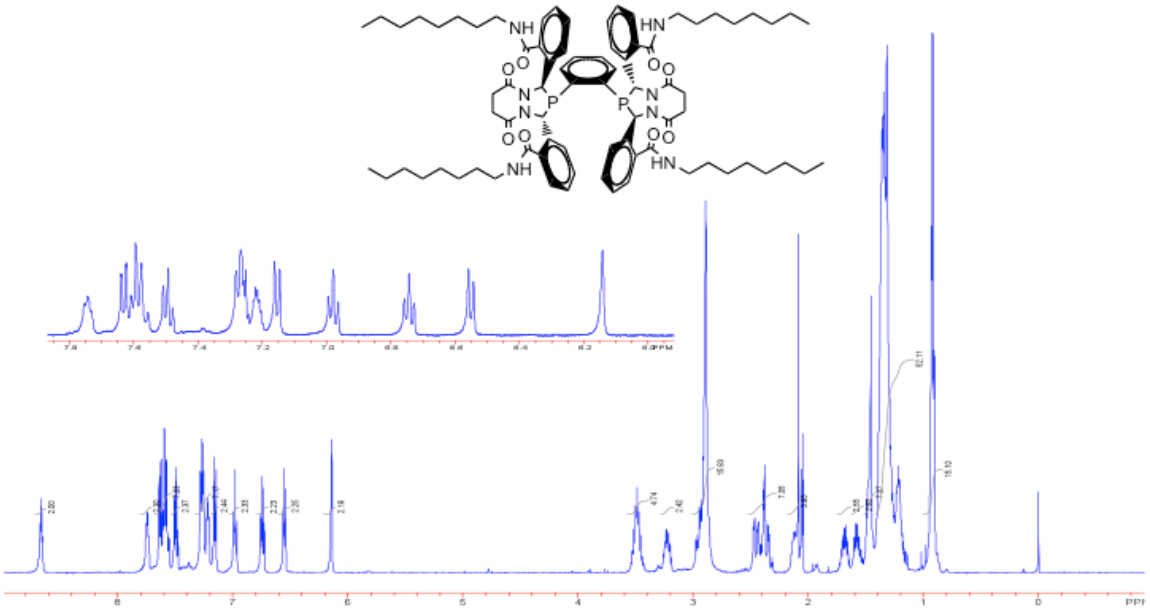

Figure S1. ^{1}H NMR spectrum (300 MHz) of octylamide bis(diazaphospholane). 24 °C, acetone-d_6.

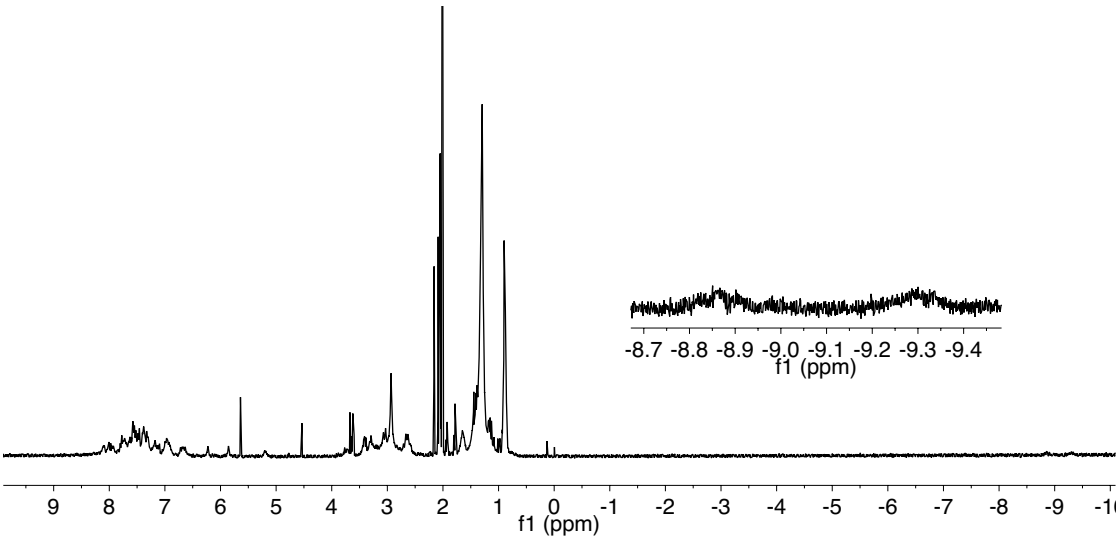

Figure S2. ^{1}H NMR spectrum of [Rh(H)(CO)$_2$(P^P)]; (P^P) = octylamide bis(diazaphospholane); hydride peak (inset) is a broad doublet, with a large (130-Hz) coupling to the *trans* phosphorus atom (300 MHz, 24 °C, 1 atm CO, acetone-d_6).

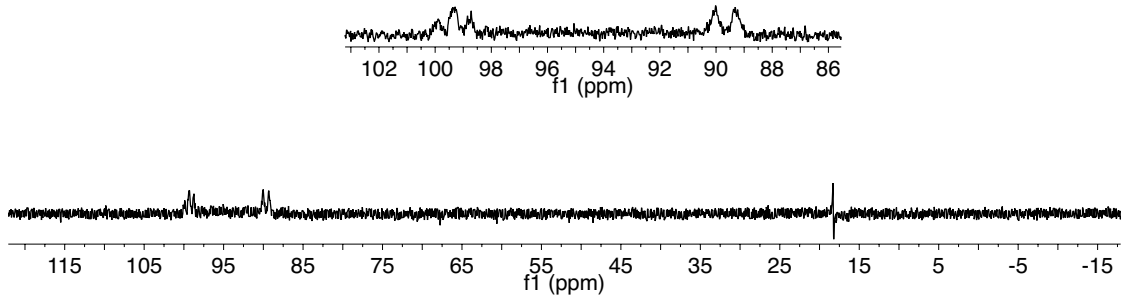

Figure S3. $^{31}P\{^{1}H\}$ NMR spectrum (121.4 MHz) of [Rh(H)$(CO)_2$(P^P)]; (P^P) = octylamide bis(diazaphospholane). The two phosphorus atoms are inequivalent, and the axial phosphine (inset, downfield signal) shows a 130-Hz coupling to the hydride (121.4 MHz, 24 °C, 1 atm CO, acetone-d_6).

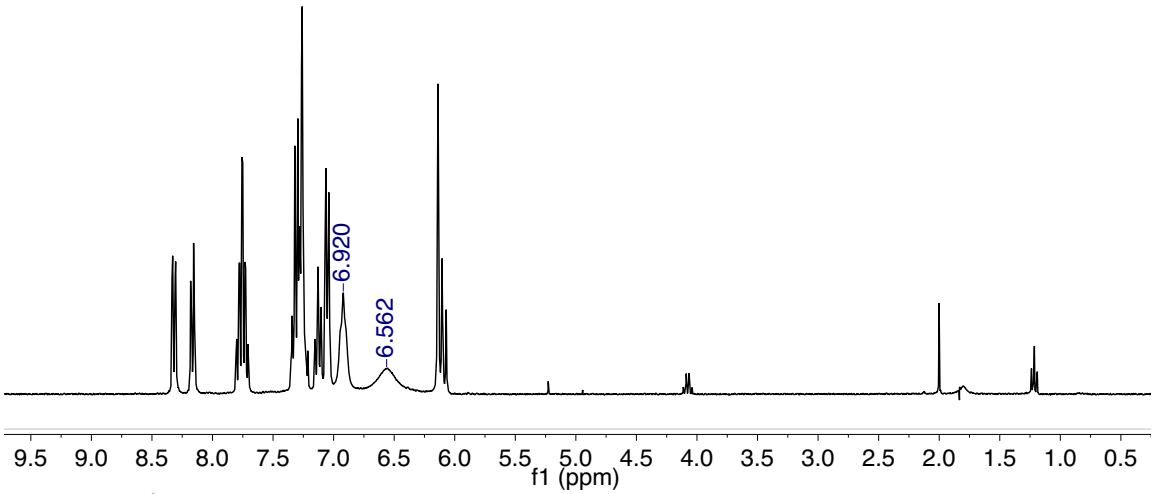

Figure S4. ^{1}H NMR spectrum (300 MHz) of tetraphenyl bis(diazaphospholane); methine protons indicated. 24 °C, $CDCl_3$.

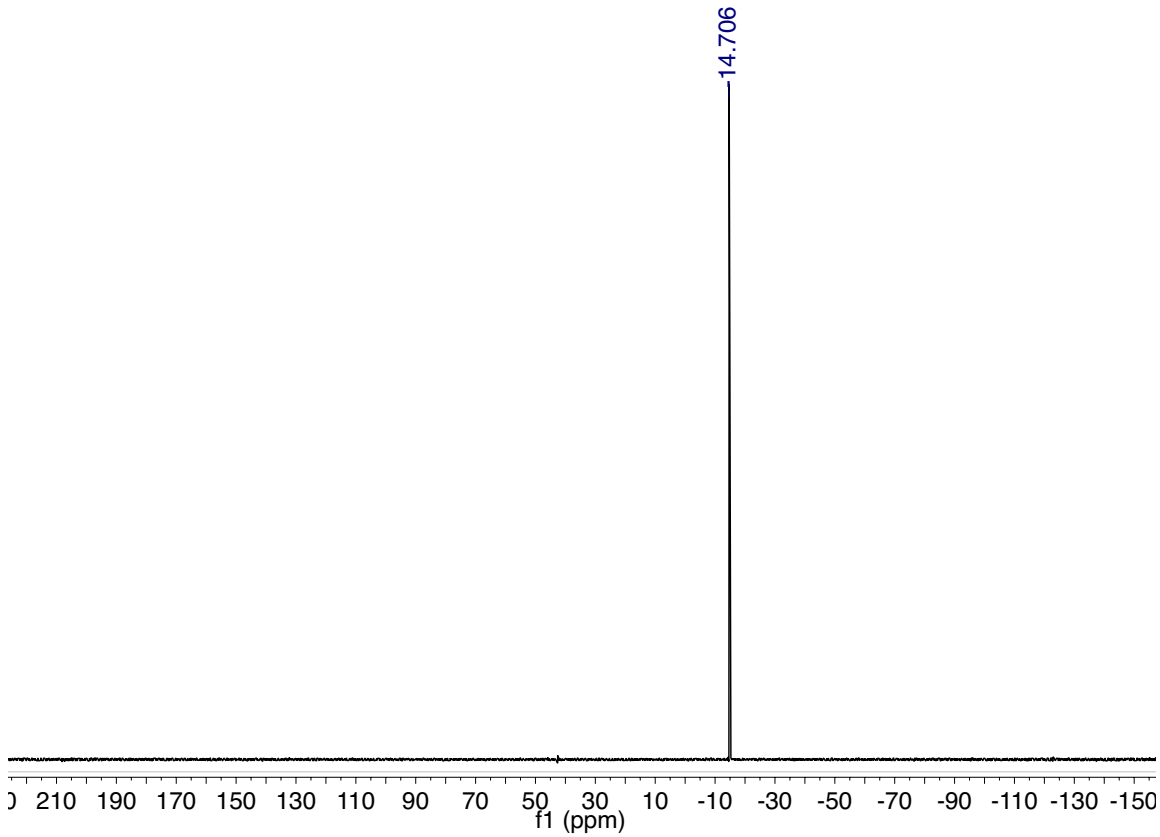

Figure S5. $^{31}P\{^{1}H\}$ NMR spectrum (121.4 MHz) of tetraphenyl bis(diazaphospholane). 24 °C, $CDCl_3$.

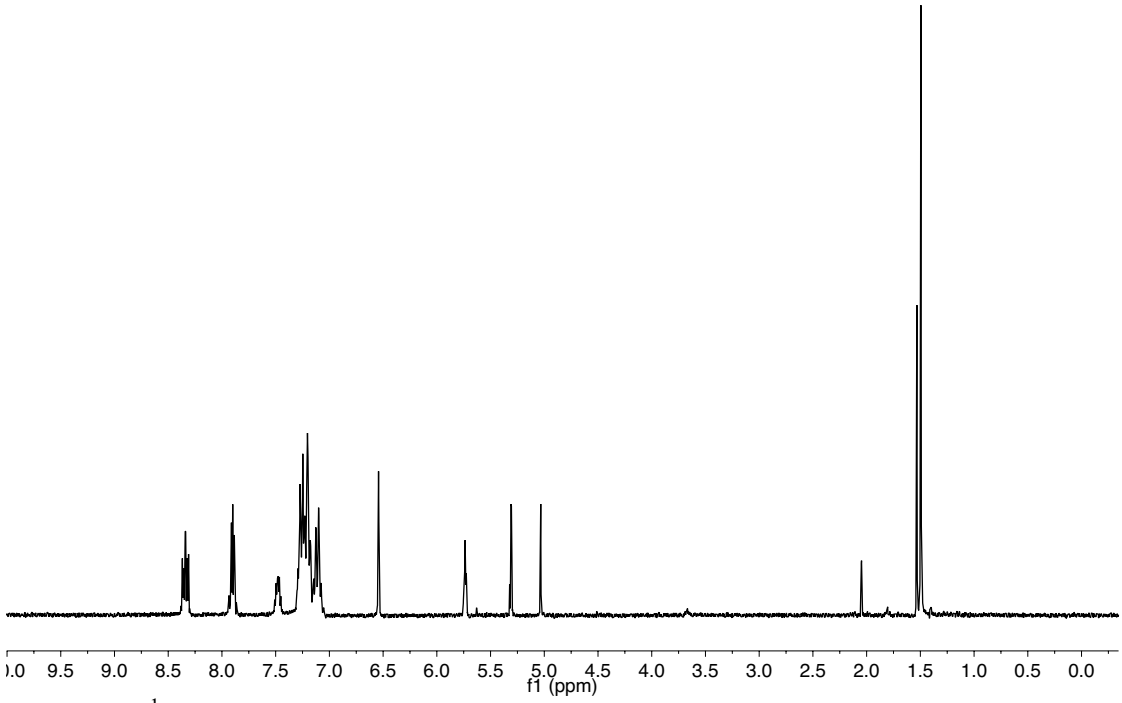

Figure S6. ^{1}H NMR spectrum of [Rh(acac)(BDP)] (300 MHz, $CDCl_3$, 24 °C).

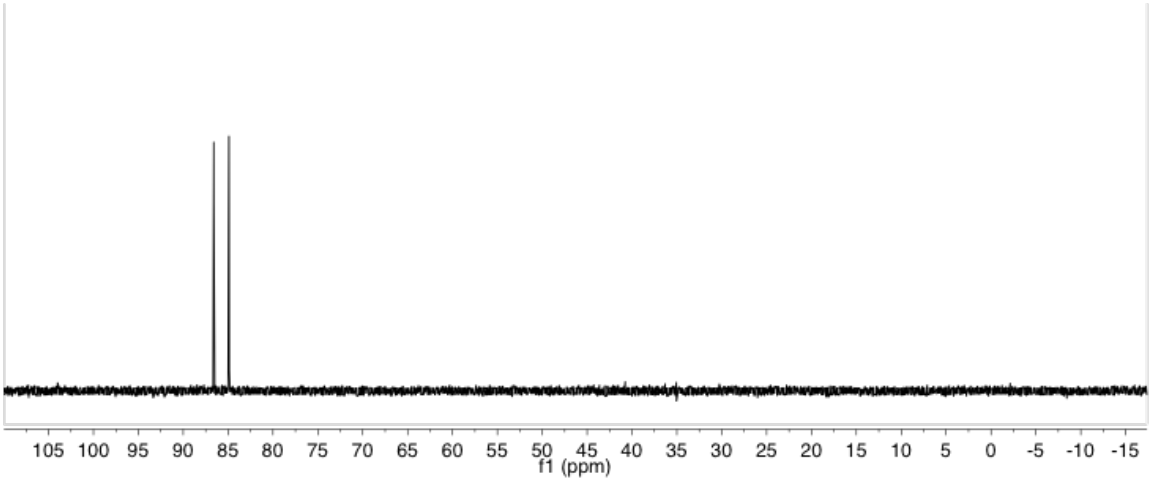

Figure S7. $^{31}P\{^{1}H\}$ NMR spectrum of [Rh(acac)(BDP)] (121.5 MHz, $CDCl_3$, 24 ° C).

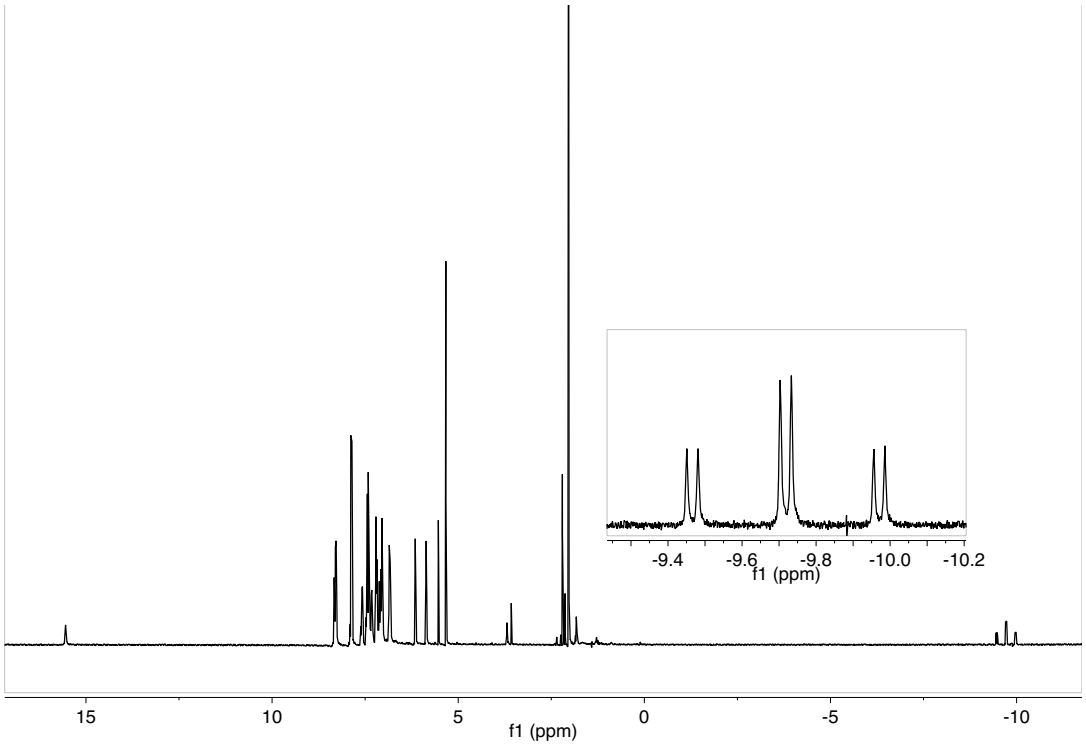

Figure S8. ^{1}H NMR spectrum of [Rh(H)(CO)$_2$(BDP)] (**1**) (500 MHz, CD_2Cl_2, 24 °C).

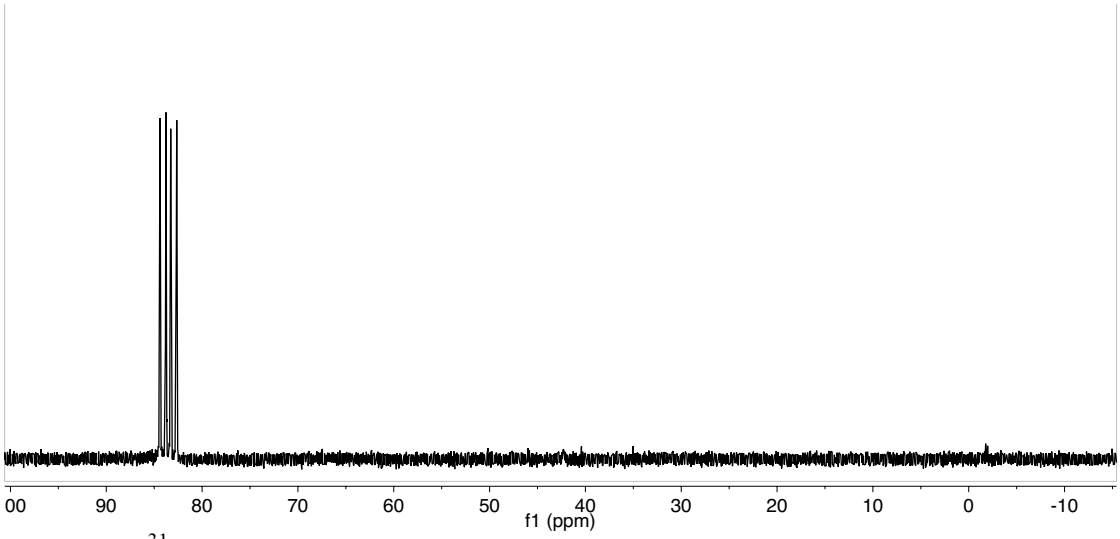

Figure S9. ^{31}P NMR spectrum of **1** (121.5 MHz, CD_2Cl_2, 24 °C).

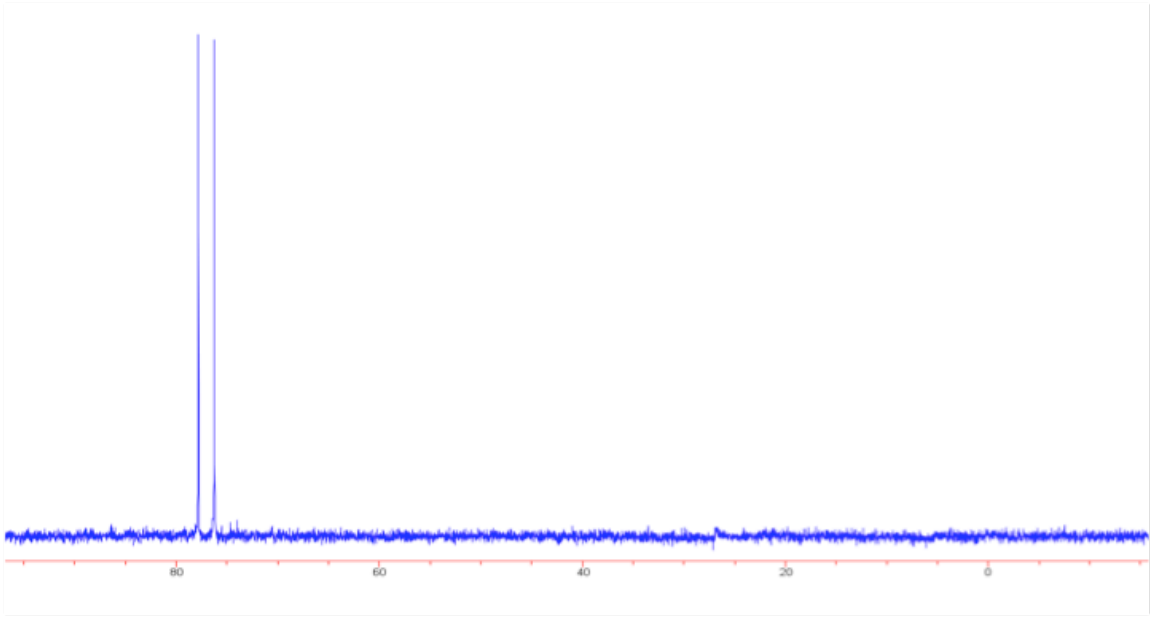

Figure S10. $^{31}P\{^{1}H\}$ NMR spectrum of $[Rh(CO)_2(BDP)]K$. (121.4 MHz, 24 °C, 1 atm CO, tetrahydrofuran).

Chapter 3

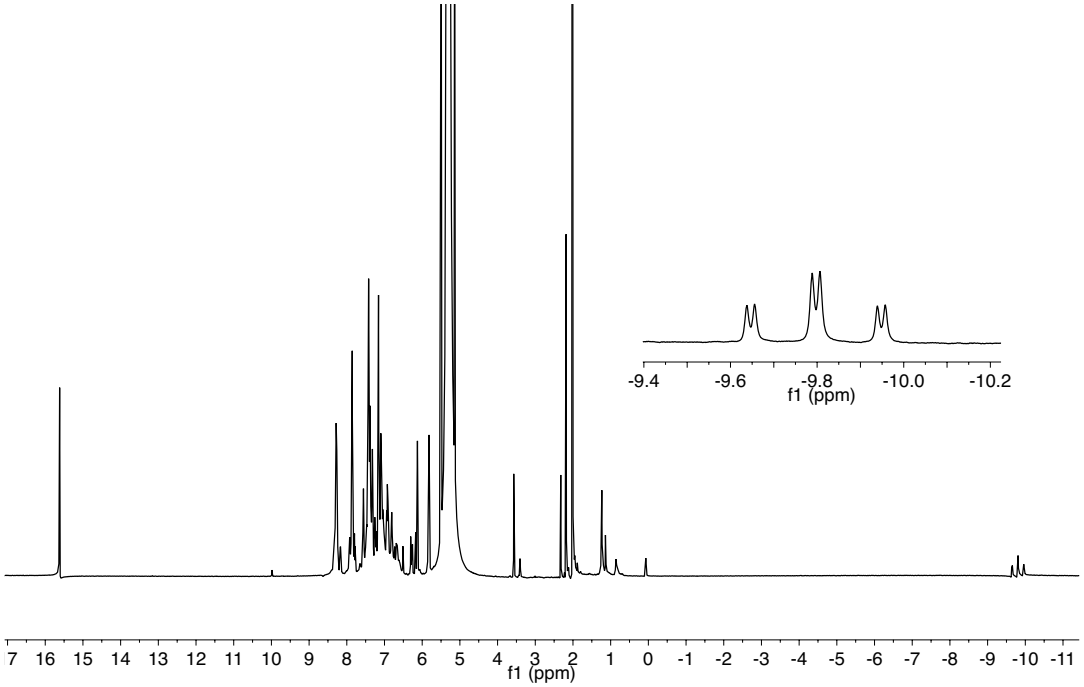

Figure S11. ^{1}H NMR spectrum of $[Rh(H)(^{13}CO)_2(BDP)]$ (500 MHz, CH_2Cl_2, -20 °C).

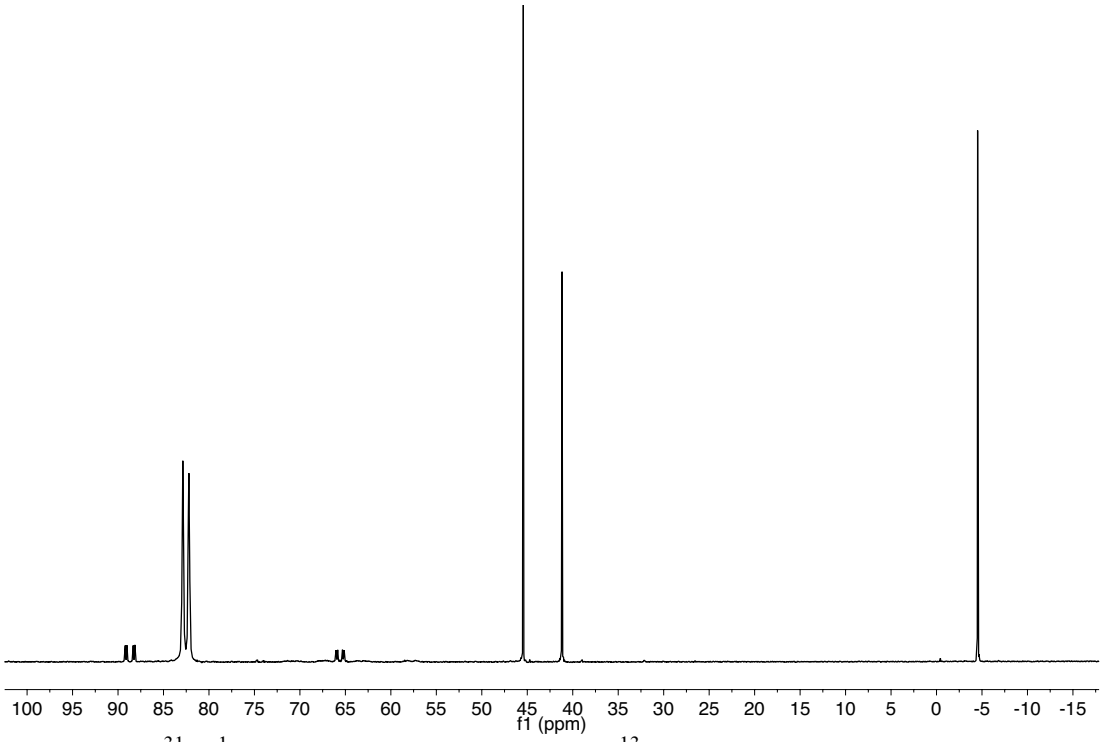

Figure S12. $^{31}P\{^{1}H\}$ NMR spectrum of [Rh(H)($^{13}CO)_2$(BDP)] (202.5 MHz, CH_2Cl_2, -20 °C).

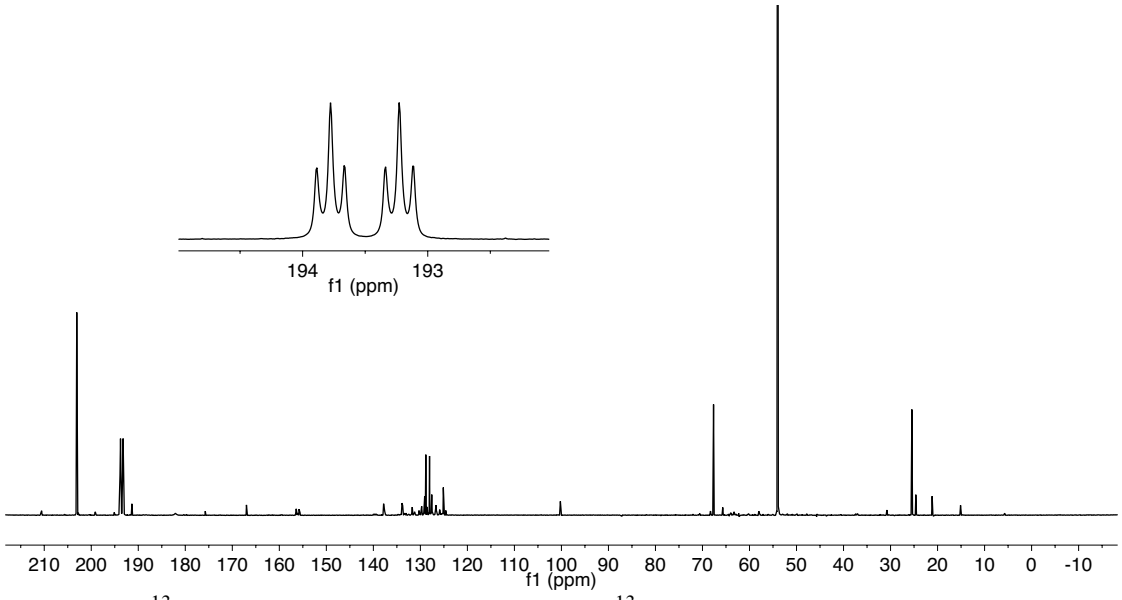

Figure S13. $^{13}C\{1H\}$ NMR spectrum of [Rh(H)($^{13}CO)_2$(BDP)] (125.8 MHz, CH_2Cl_2, -20 °C). Inset shows terminal carbonyl resonances; $^{2}J_{CP} = \pm$ 14Hz.

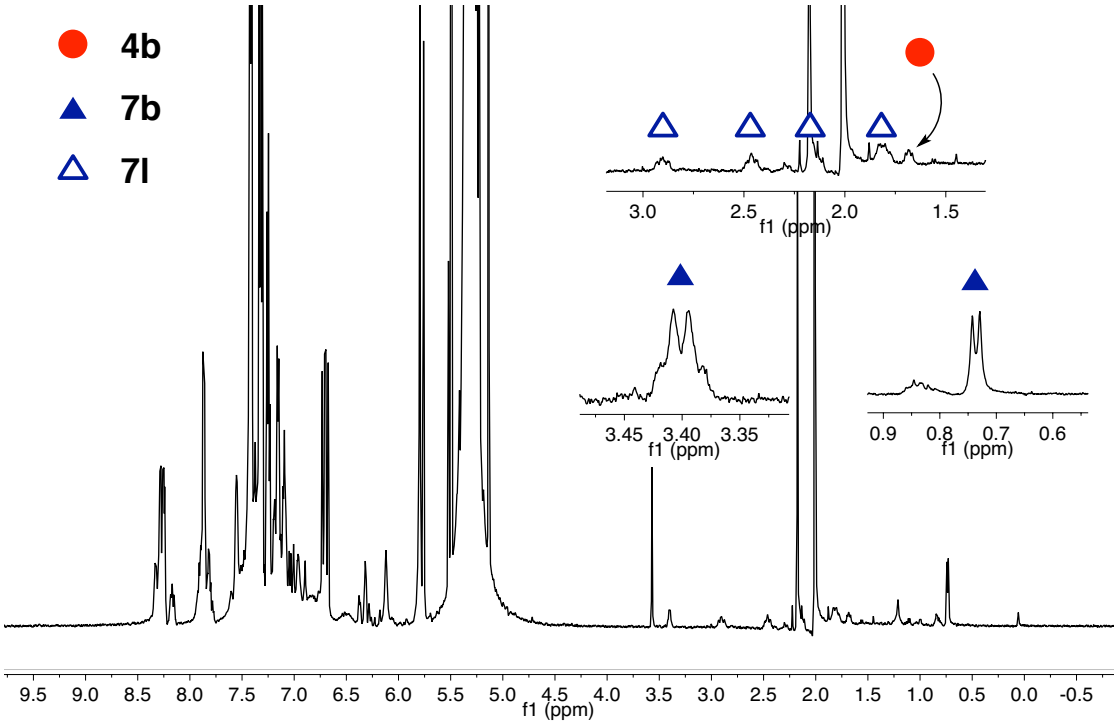

Figure S14. ^{1}H spectrum during the reaction of **1** with styrene (1 atm CO, 500 MHz, CH_2Cl_2, -40 ° C).

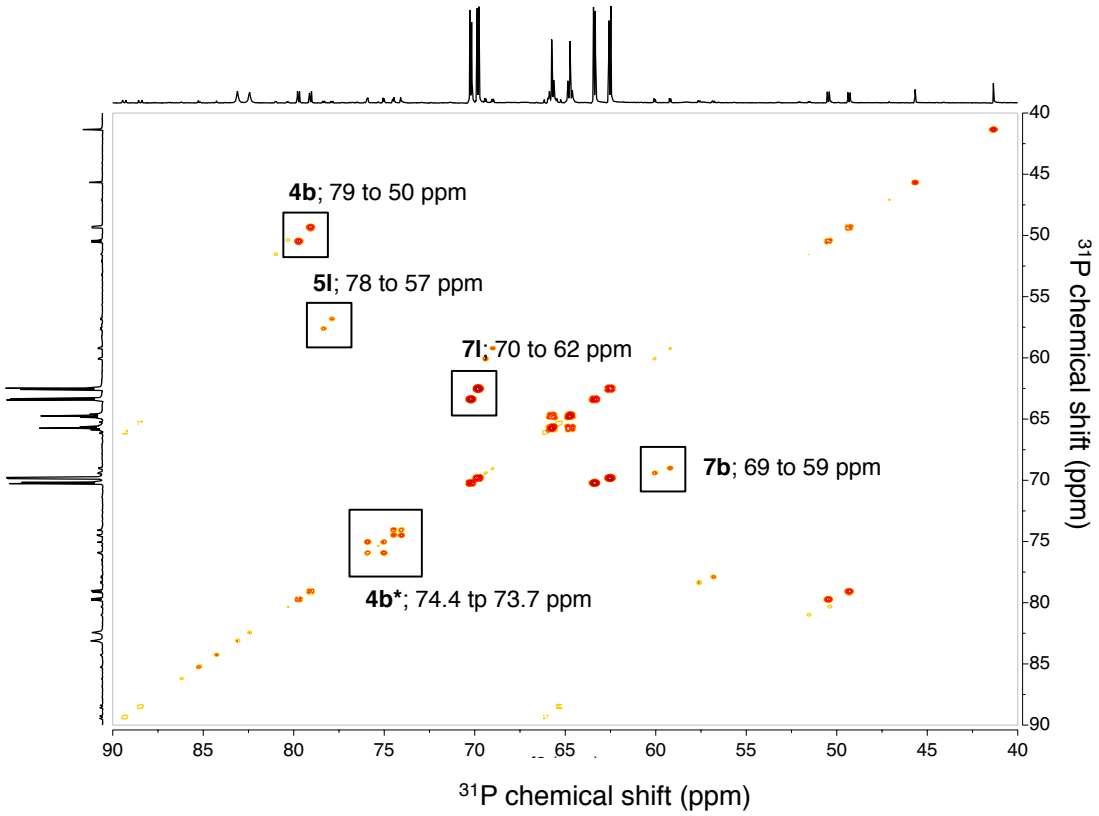

Figure S15. ^{31}P-^{31}P gCOSY during the reaction of **1** with styrene (1 atm CO, 202.5 202.5 MHz, CO atmosphere, -20 °C; nt = 2, ni = 1024, D1 = 2.0 sec).

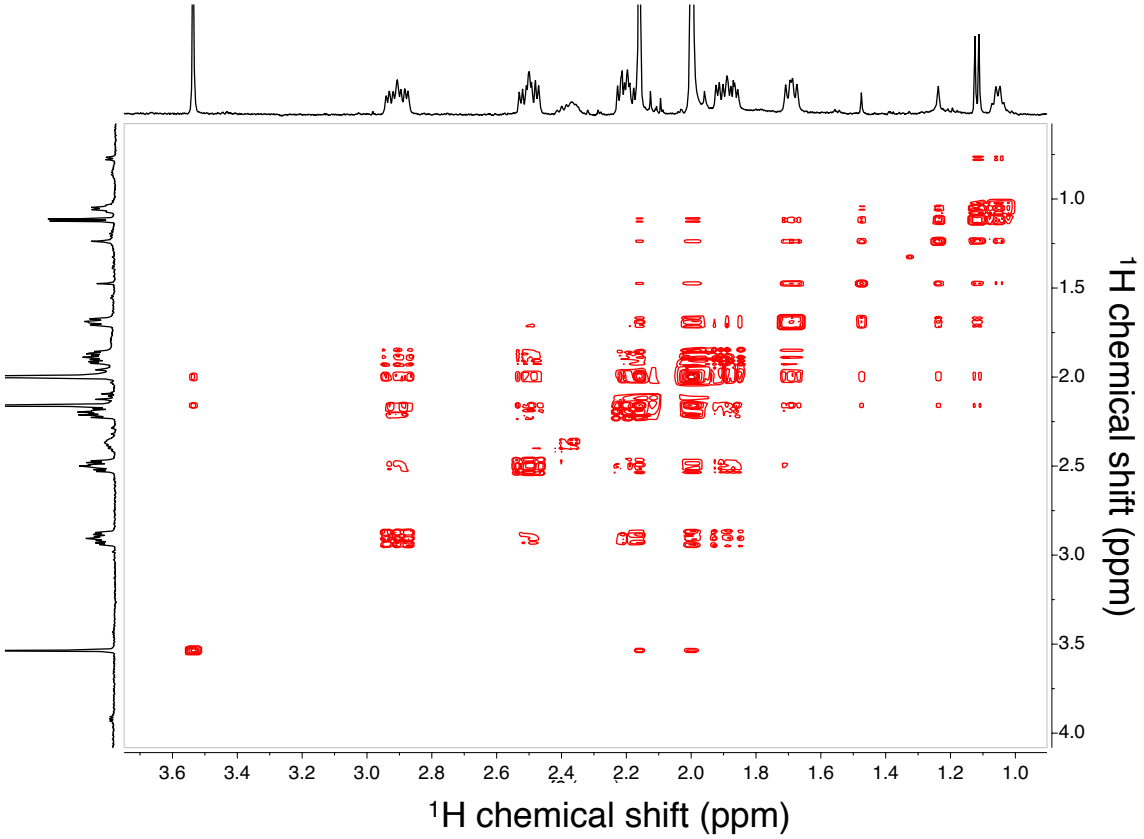

Figure S16. ^{1}H-^{1}H gCOSY taken after the reaction of **1** with styrene; crosspeaks show correlations between the four diastereotopic methylene protons of **7l**. (500 MHz, CH_2Cl_2, -15 °C; nt = 8, ni = 256).

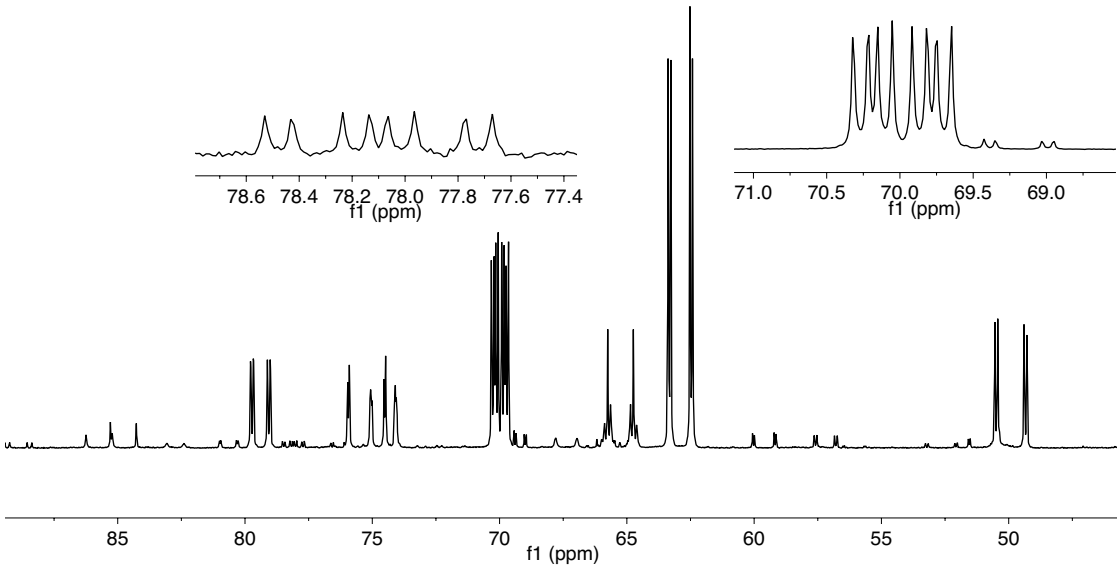

Figure S17. $^{13}P\{^{1}H\}$ NMR spectrum taken after the reaction of **1** with β-^{13}C-styrene. Insets show ^{13}C-^{31}P coupling in $\mathbf{5l_{sty}}$ (left) and $\mathbf{7l_{sty}}$ (right), demonstrating that these are the linear regioisomers (1 atm N_2, 202.5 MHz, CH_2Cl_2, -20 °C).

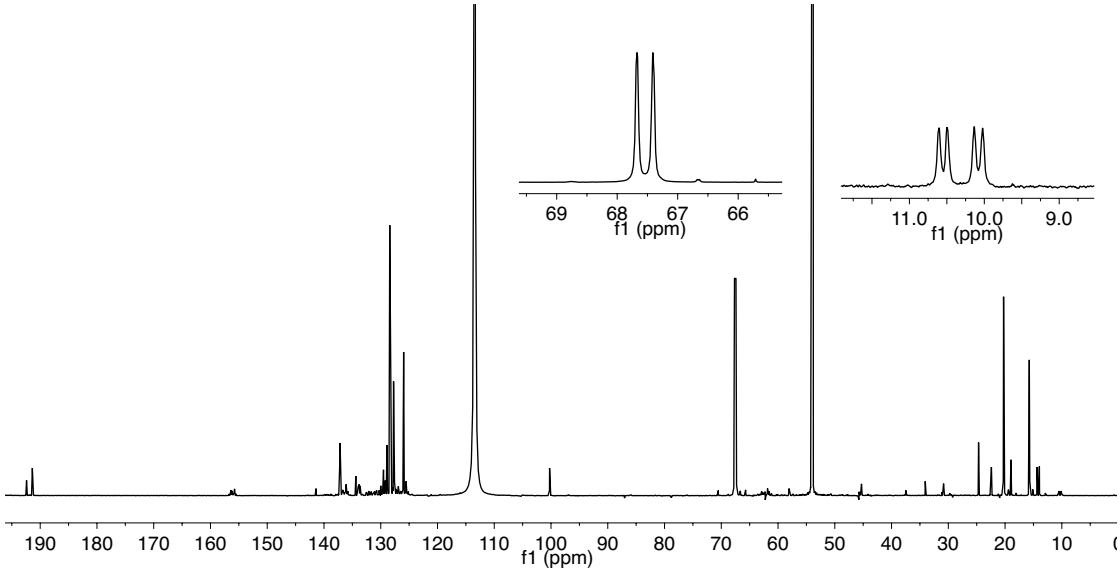

Figure S18. $^{31}C\{^{1}H\}$ NMR spectrum taken after the reaction of 1 with β-^{13}C-styrene. Insets show β-methylene signals of $\mathbf{7l_{sty}}$ (left) and $\mathbf{5l_{sty}}$ (right); ^{13}C-^{103}Rh splitting in $\mathbf{5l_{sty}}$ confirms that it is an alkyl species (125.8 MHz, CH_2Cl_2, -20 °C).

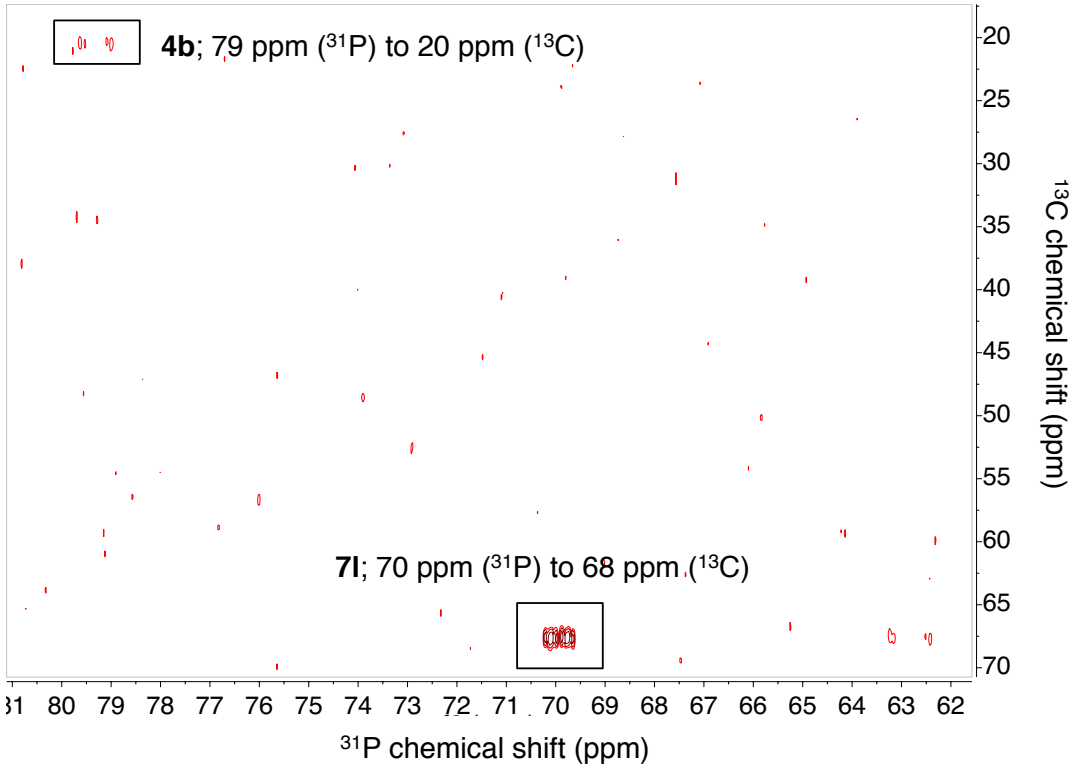

Figure S19. ^{31}P-^{13}C gHMBC taken during the reaction of **1** with β-^{13}C-styrene, to identify the methyl carbon of $\mathbf{4b_{sty}}$ (box, upper left). ((f2, f1) = (243, 151MHz), N_2 atmosphere, CH_2Cl_2, -20 °C; jnxh = 20 Hz).

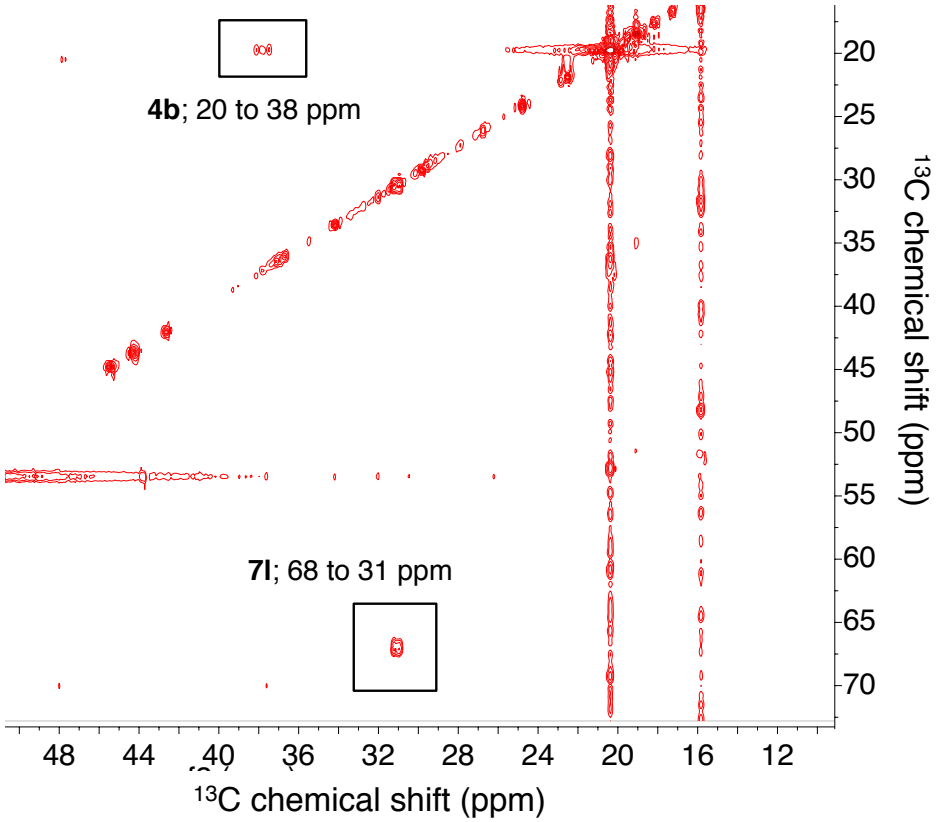

Figure S20. ^{13}C-^{13}C gCOSY taken after the reaction of **1** with β-^{13}C-styrene, to identify the methine carbon of **4b$_{sty}$** (box, upper left) and the α-methylene carbon of **7l$_{sty}$** (box, lower right). (125.8 MHz, 1 atm N_2, CH_2Cl_2, -20 °C; ns = 8, ni = 256).

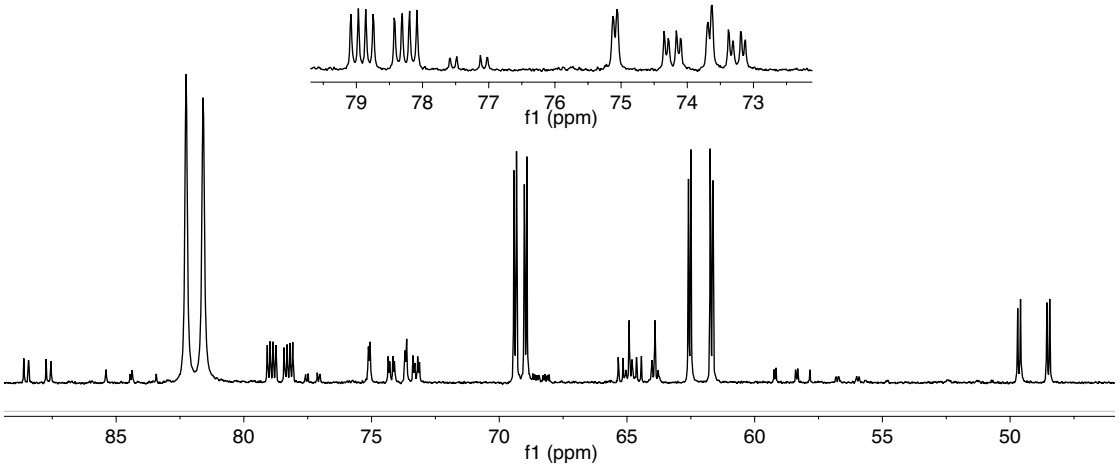

Figure S21. $^{31}P\{^1H\}$ NMR spectrum taken during the reaction of **1** with α-13C-styrene. Inset shows strong ^{13}C-^{31}P coupling for **4b$_{sty}$** (left) and **4b*$_{sty}$** (right), demonstrating that these are branched alkyl species (1 atm N_2, 202.5 MHz, CH_2Cl_2, -20 ° C).

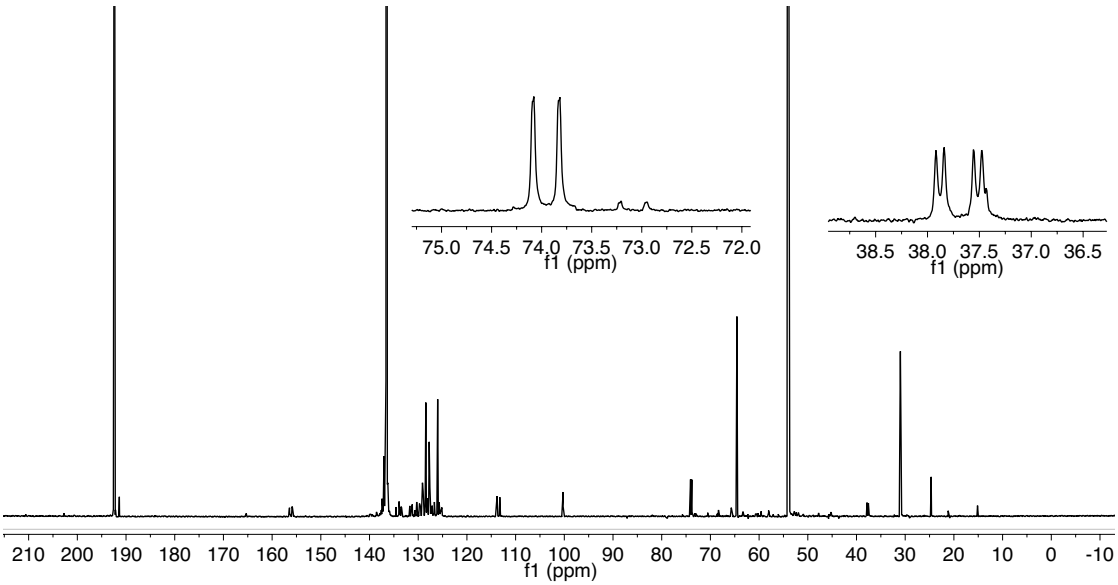

Figure S22. $^{13}C\{^{1}H\}$ NMR spectrum taken during the reaction of **1** with α-13C-styrene. Insets show methine carbons of **7b** (left) and **4b** (right); ^{13}C-^{103}Rh coupling for **4b** confirms that it is a Rh-alkyl species (1 atm N_2, 125.8 MHz, CH_2Cl_2, -20 ° C).

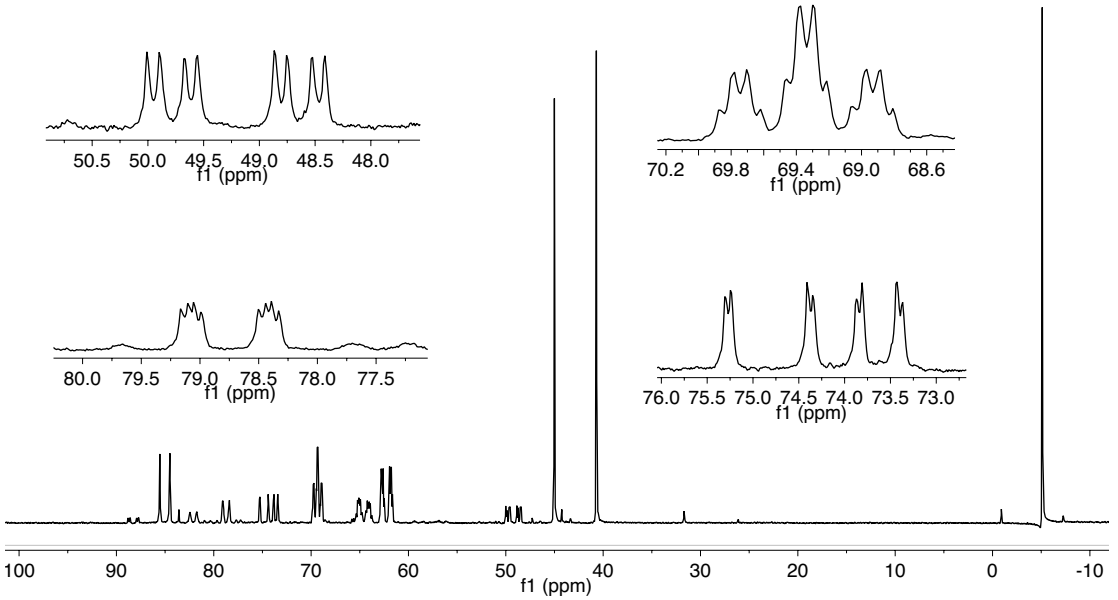

Figure S23. $^{31}P\{^{1}H\}$ NMR spectrum taken after the reaction of $[Rh(H)(^{13}CO)_2(BDP)]$ with styrene. Insets show one additional ^{31}P-^{13}C coupling for the phosphorus signals of $\mathbf{4b_{sty}}$ (upper and lower left), two for the downfield signal of $\mathbf{7l_{sty}}$ (upper right), and none for $\mathbf{4b^*_{sty}}$ (lower right), indicating that these species have one, two, and zero terminal CO ligands, respectively (1 atm H_2, 202.5 MHz, CH_2Cl_2, -20 °C).

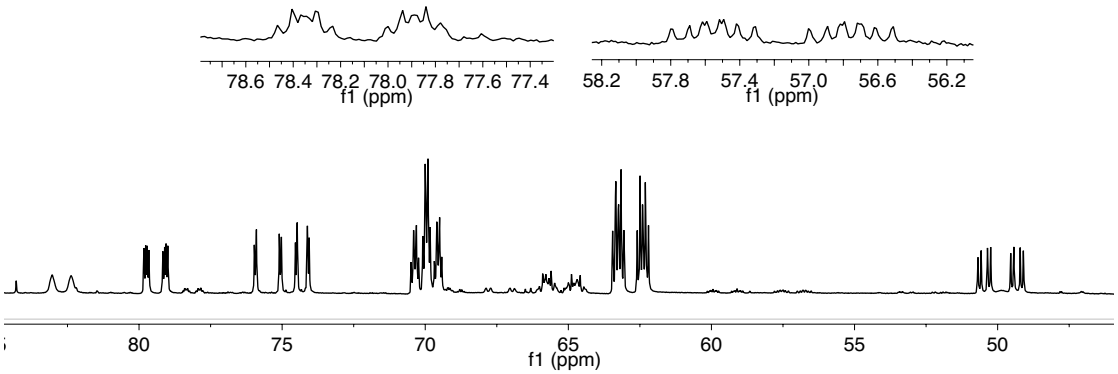

Figure S24. $^{31}P\{^{1}H\}$ NMR spectrum taken after the reaction of [Rh(H)($^{13}CO)_2$(BDP)] with styrene. Insets show two additional ^{31}P-^{13}C coupling for the phosphorus signals of **5l$_{sty}$**, indicating that this species has terminal CO ligands (1 atm H_2, 202.5 MHz, CH_2Cl_2, -20 °C).

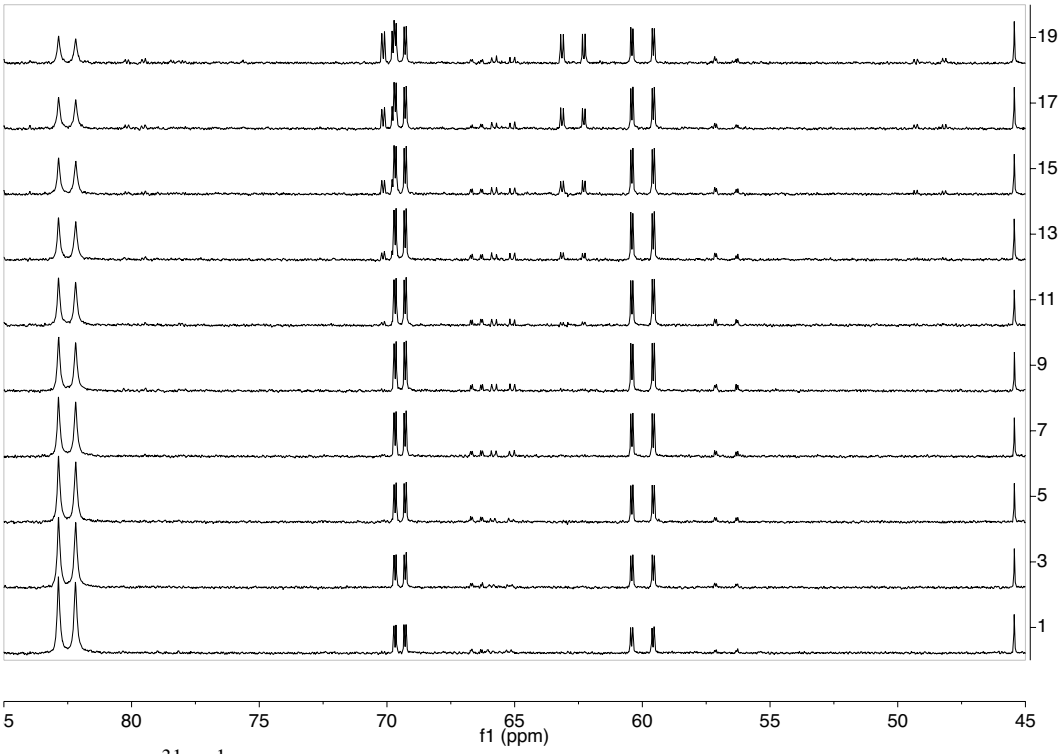

Figure S25. $^{31}P\{^{1}H\}$ spectra following the reaction of **1** with *p*-CF_3-styrene; one spectrum every three minutes (1 atm CO, 202.5 MHz, CH_2Cl_2, -20 °C).

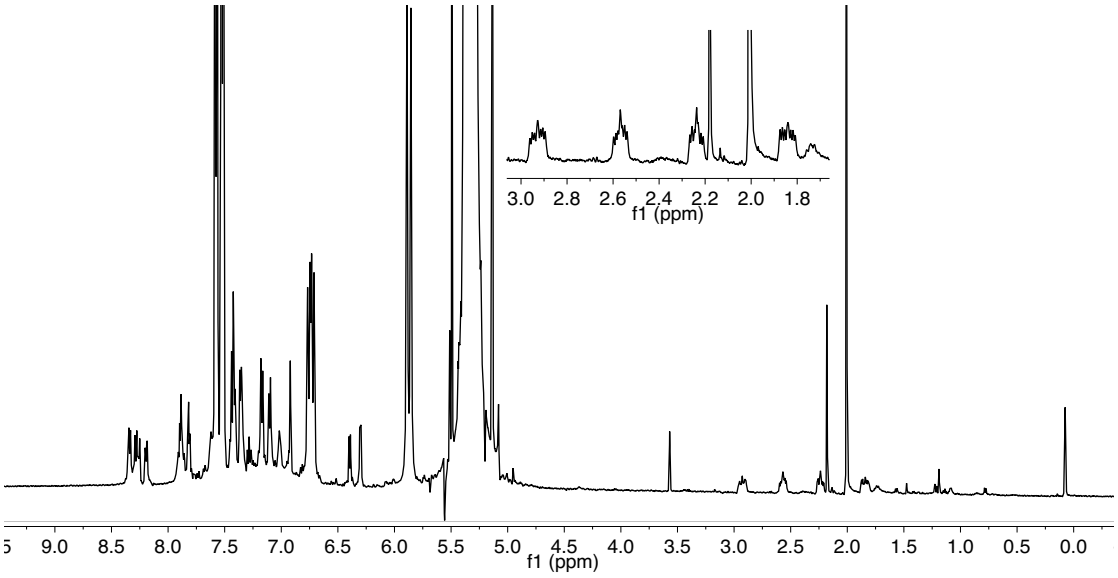

Figure S26. ^{1}H spectrum taken after the reaction of **1** with *p*-CF_3-styrene; methylene protons (inset) show that the major acyl species is linear (1 atm CO, 500 MHz, CH_2Cl_2, -20 °C).

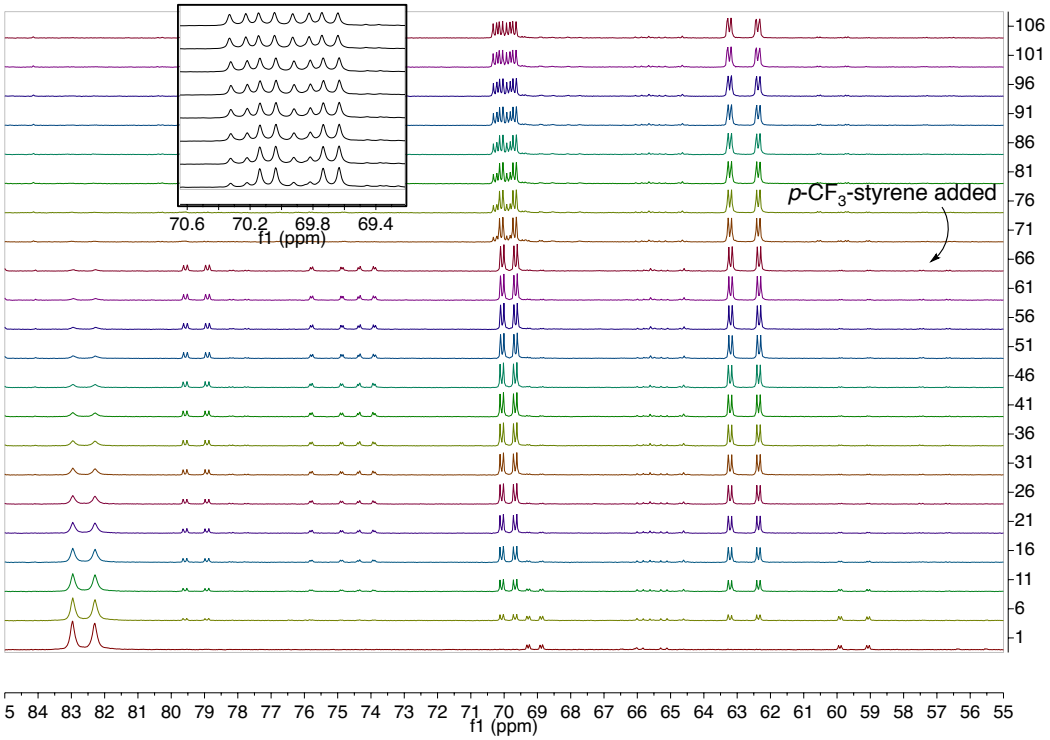

Figure S27. $^{31}P\{^{1}H\}$ spectra following the reaction of **1** with styrene, then of equilibrated **7b$_{sty}$**, **7l$_{sty}$** with *p*-CF_3-styrene; one spectrum every three minutes. Inset shows downfield peaks for **7l$_{sty}$** and the analogous linear fluoro species, which were used to calculate the concentration of each over time. (1 atm CO, 202.5 MHz, CH_2Cl_2, -20 °C).

Table S1. Catalytic hydroformylation of styrene. Conditions: 0.3 M styrene, 0.5 mol % [Rh(acac)((*S*,*S*)-BDP)], 24 hours (48 hours for reactions at -10 °C). Conversion measured by NMR vs. Ph_2CH_2 internal standard; b : l and *R* : *S* measured by GC. Average of two runs.

***T* (°C)**	**b : l**		***R* : *S***	
	140 psig	40 psig	140 psig	40 psig
20	19.6	20.8	4.0	4.2
10	25.2	21.4	3.6	4.8
0	30.4	23.9	4.7	4.5
-10	25.5	11.1	3.7	3.3
	% conversion		**tof (h^{-1})**	
20	65	100	5.4	8.3
10	26	27	2.1	2.2
0	12	14	1.0	1.2
-10	13	7	0.5	0.3

Chapter 4

Vinyl acetate

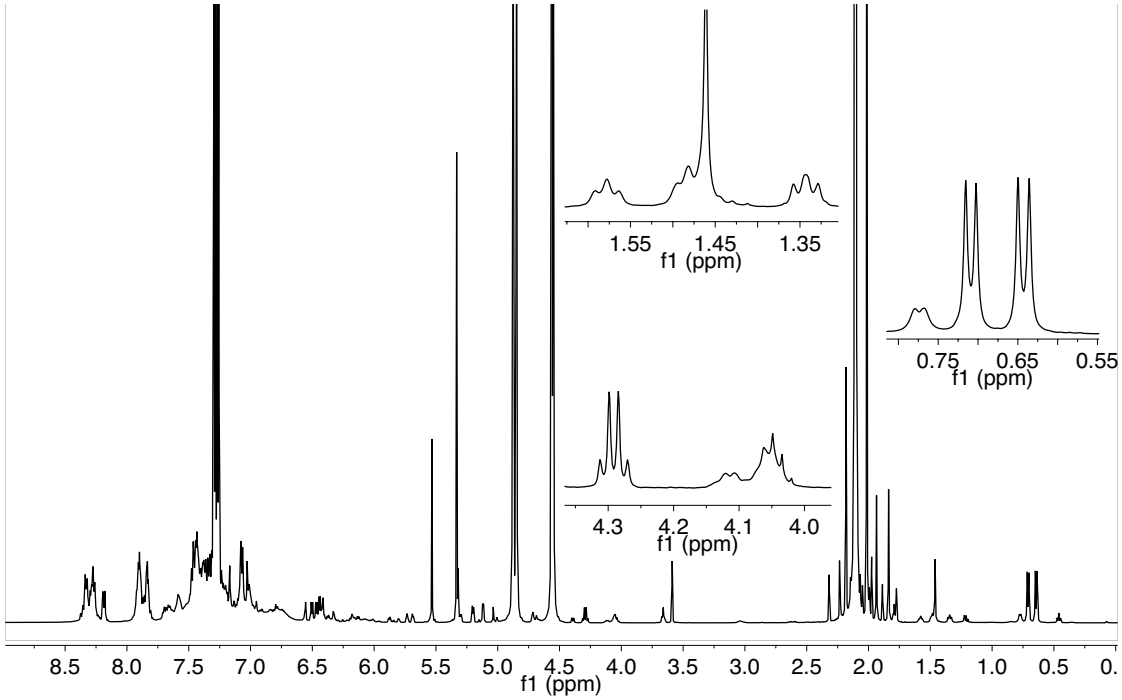

Figure S28. ^{1}H NMR spectrum taken after the reaction of **1** with vinyl acetate. Insets show the methyl (right) and methine (center, lower) resonances of **7b,b'$_{va}$** and methyl resonances (center, upper) of **4b$_{va}$**, **5b$_{va}$** (500.22 MHz, -40 °C, CD_2Cl_2).

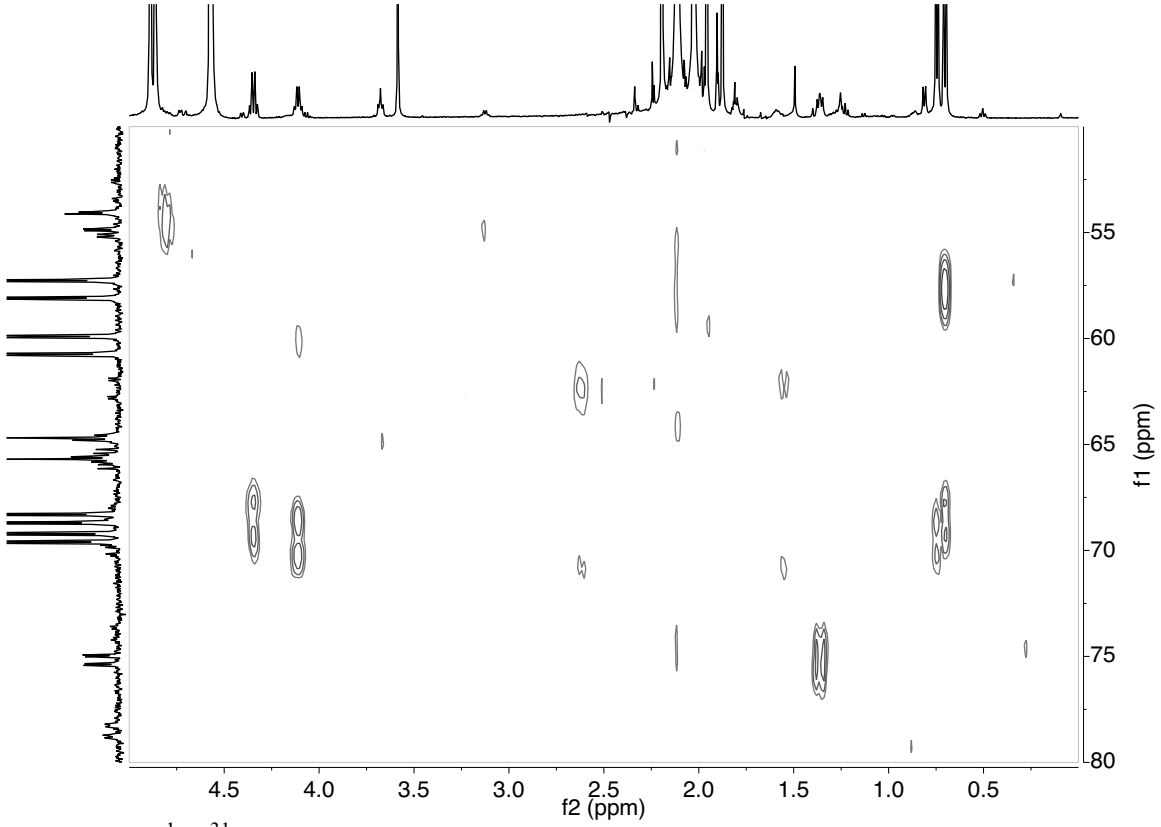

Figure S29. ^{1}H-^{31}P gHMBC during the reaction of **1** with vinyl acetate (1 atm CO, 202.5 MHz, CO atmosphere, -10 °C; nt = 8, ni = 128, jnxh = 3.0 Hz, D1 = 3.0 sec).

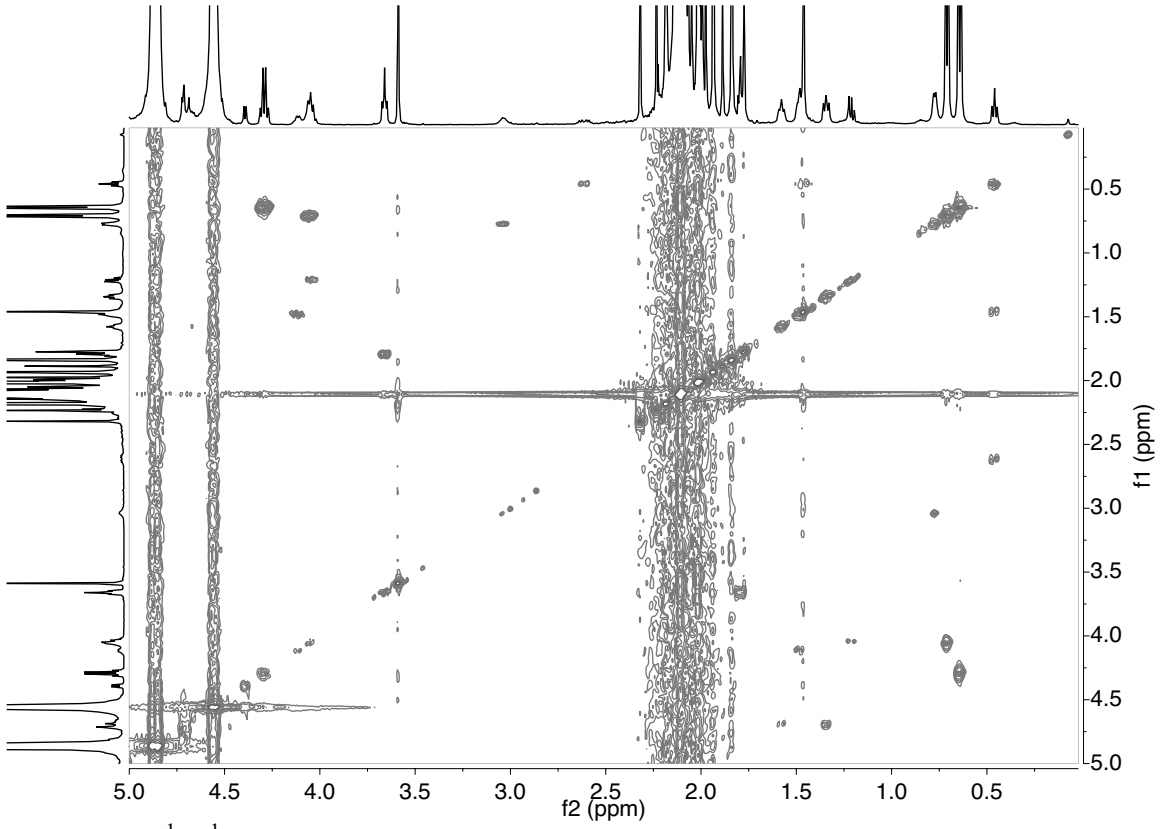

Figure S30. ^{1}H-^{1}H gCOSY taken after the reaction of **1** with vinyl acetate. (500.2 MHz, CH_2Cl_2, -40 °C; nt = 2, ni = 256).

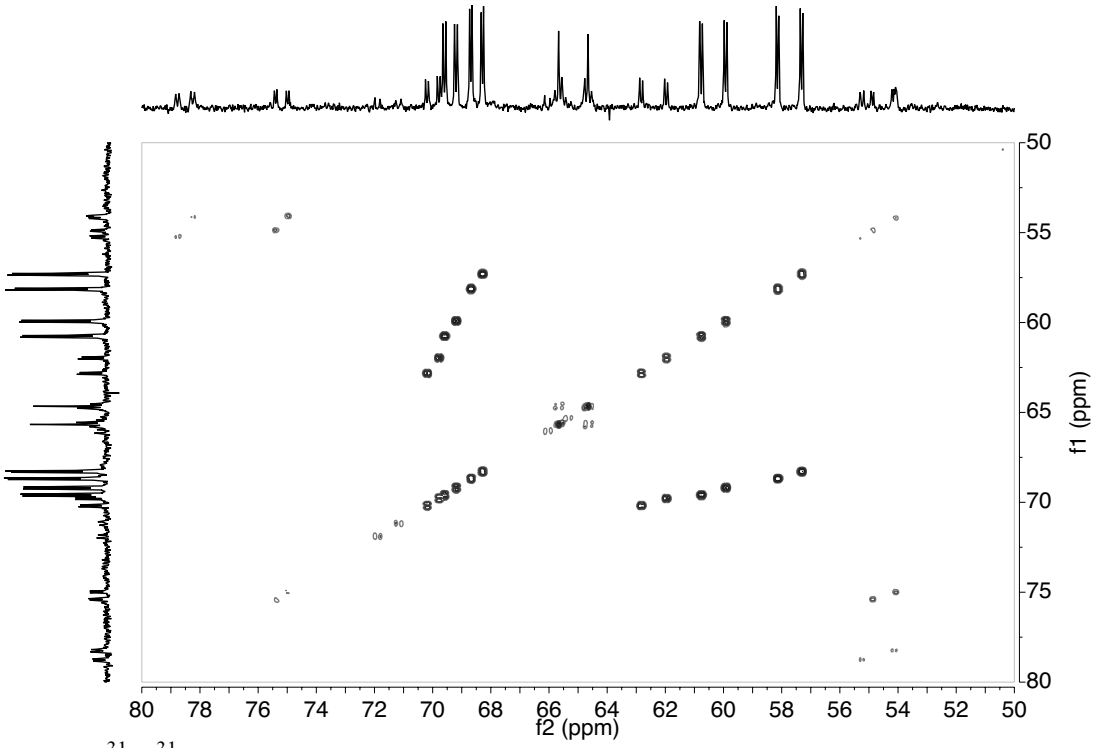

Figure S31. ^{31}P-^{31}P gCOSY taken after the reaction of **1** with vinyl acetate (1 atm CO, 202.5 MHz, CH_2Cl_2, -10 °C; nt = 8, ni = 512).

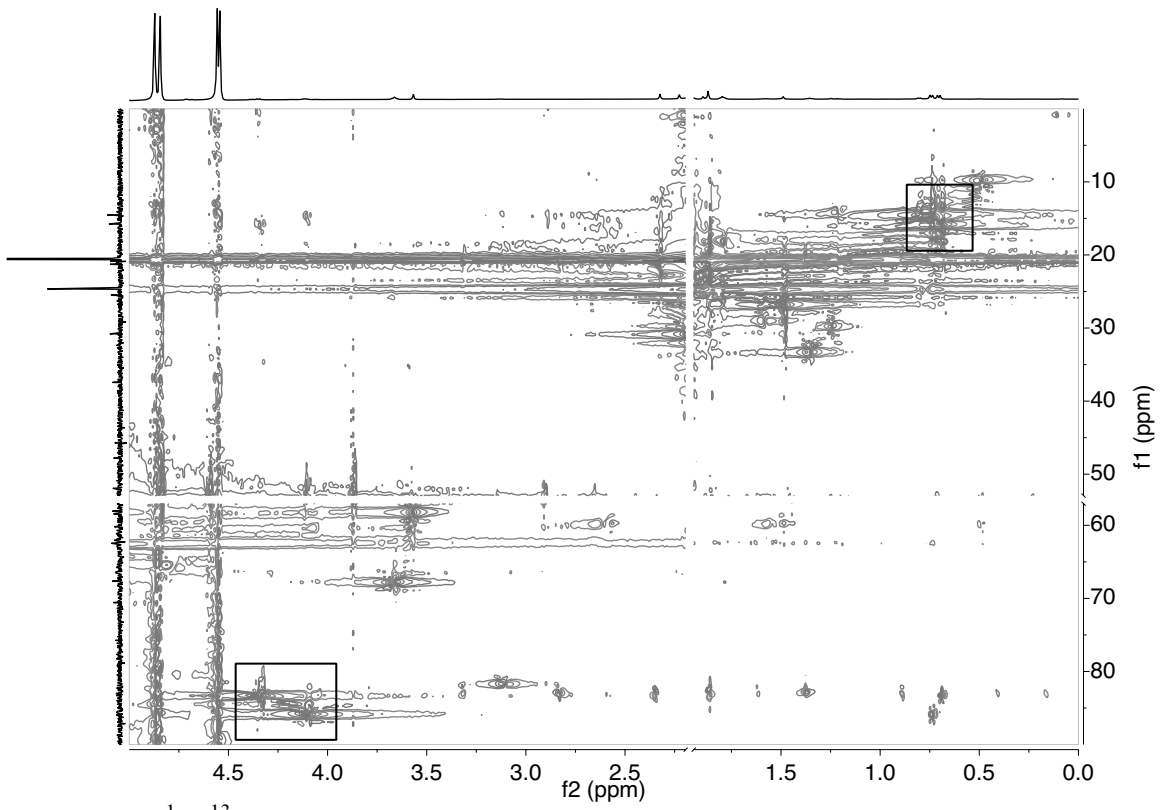

Figure S32. ^{1}H-^{13}C HSQC taken following the reaction of **1** with vinyl acetate. Correlations for the methyl (upper right) and methine (lower left) groups indicated. ((f2, f1) = (500.22, 125.79 MHz), 1 atm CO, CH_2Cl_2, -20 °C).

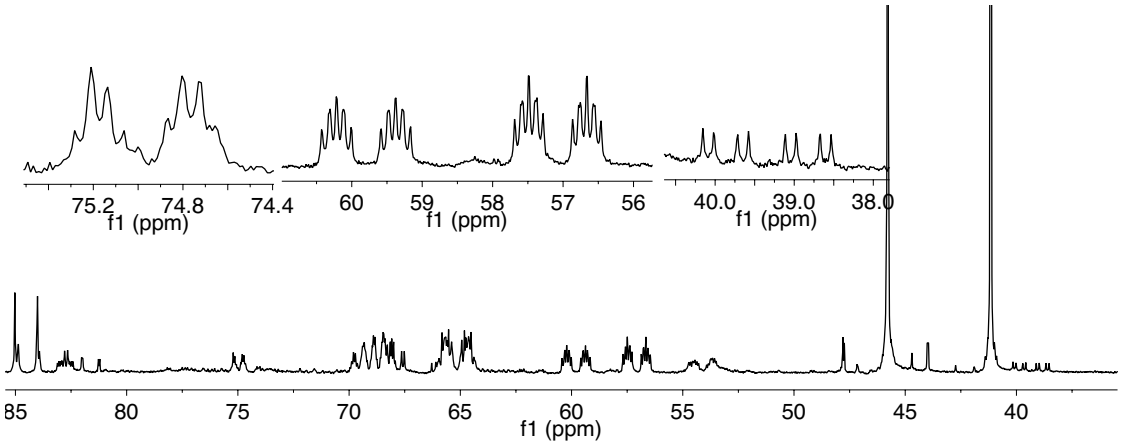

Figure S33. ^{31}P{^{1}H} NMR spectrum taken following the reaction of [Rh(H)(^{13}CO)$_2$(BDP)] with vinyl acetate. Insets show two new $^{2}J_{PC}$ for 5bva (left), three each for $\mathbf{7b_{va}}$ and $\mathbf{7b'_{va}}$ (center), and one for $\mathbf{4b_{va}}$ (right) (202.5 MHz, -40 °C, CD_2Cl_2).

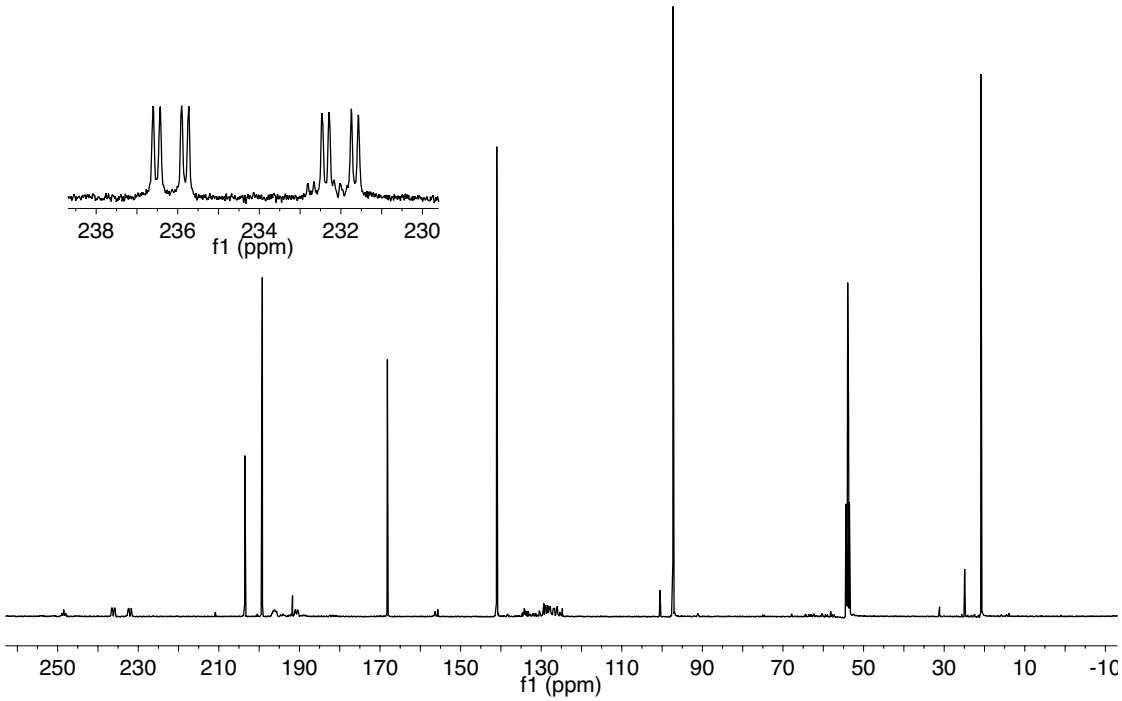

Figure S34. $^{13}C\{^{1}H\}$ NMR spectrum taken following the reaction of [Rh(H)($^{13}CO)_2$(BDP)] with vinyl acetate. Inset shows acyl carbonyl resonances of (left to right) **7b'$_{va}$**, **7l$_{va}$**, **7b$_{va}$** (125.79 MHz, -40 °C, CD_2Cl_2).

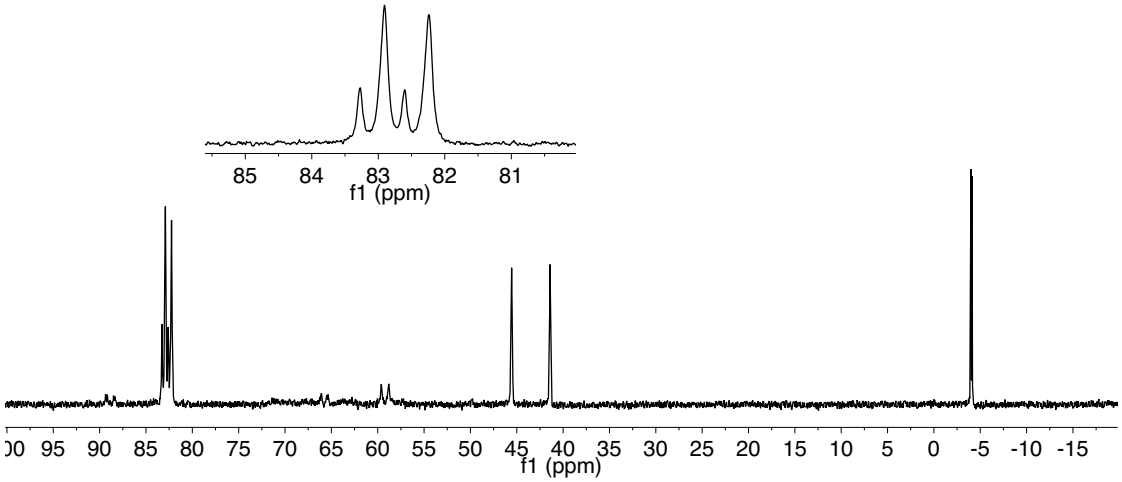

Figure S35. $^{31}P\{^{1}H\}$ NMR spectrum of [Rh(D)$(CO)_2$(BDP)]. Inset shows that both the deuteride (upfield doublet) and hydride (downfield doublet) are present (202.5 MHz, -10 °C, CH_2Cl_2).

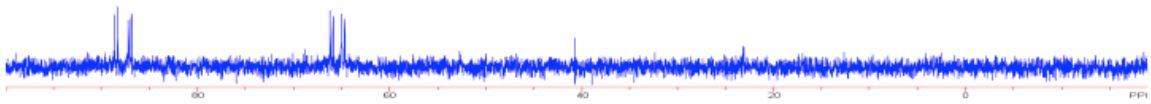

Figure S36. $^{31}P\{^{1}H\}$ NMR spectrum (121.4 MHz) of the product of the reaction of $[Rh(CO)_2(BDP)]K$ with *S*-acetoxyproionyl chloride.

Allyl cyanide

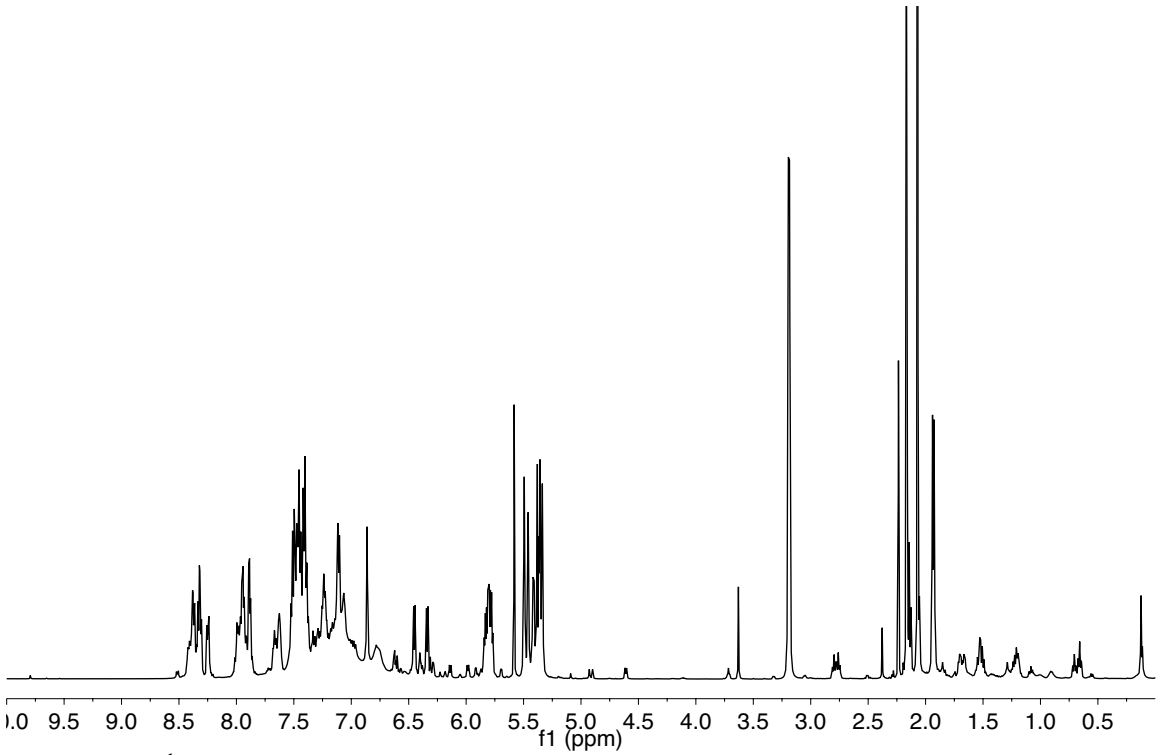

Figure S37. ^{1}H NMR spectrum taken following the reaction of **1** with allyl cyanide (500.22 MHz, -20 °C, CD_2Cl_2).

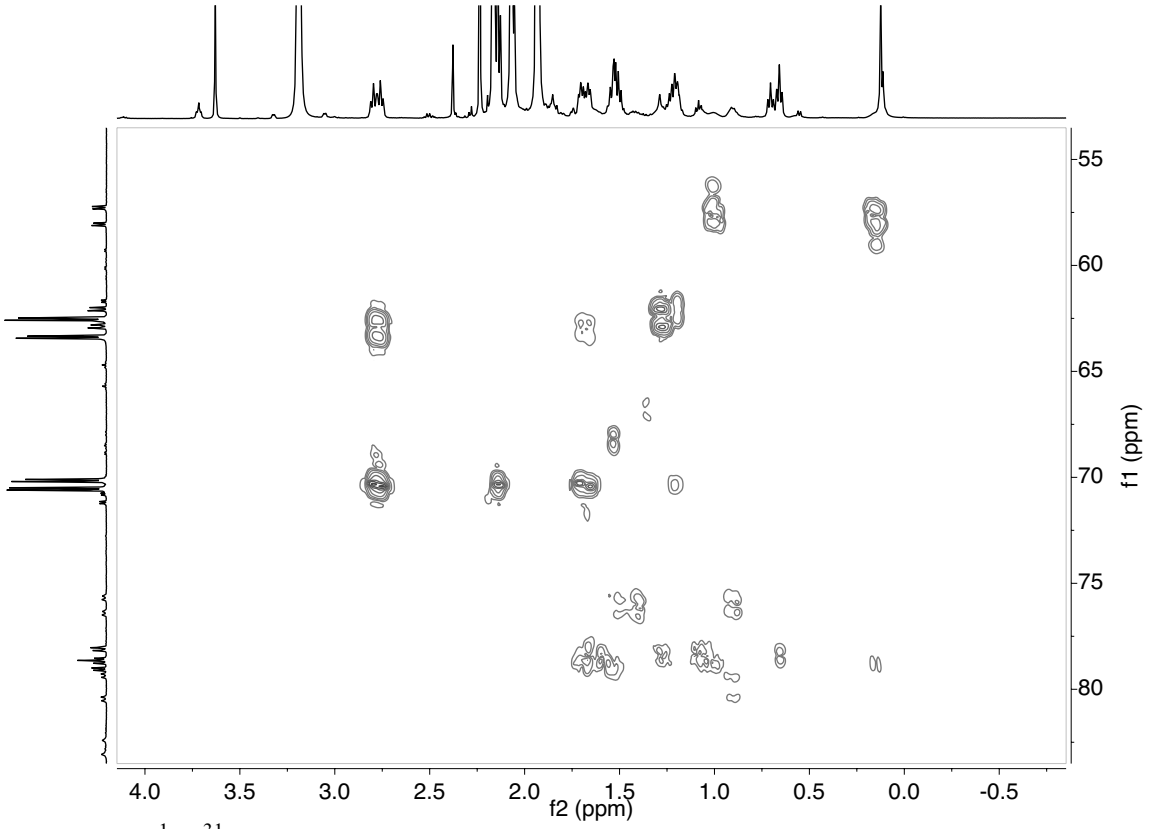

Figure S38. ^{1}H-^{31}P gHMBC during the reaction of **1** with allyl cyanide (1 atm CO, (f2,f1) = 500.22, 202.5 MHz, -20 °C; nt = 8, ni = 256, jnxh = 3.0 Hz).

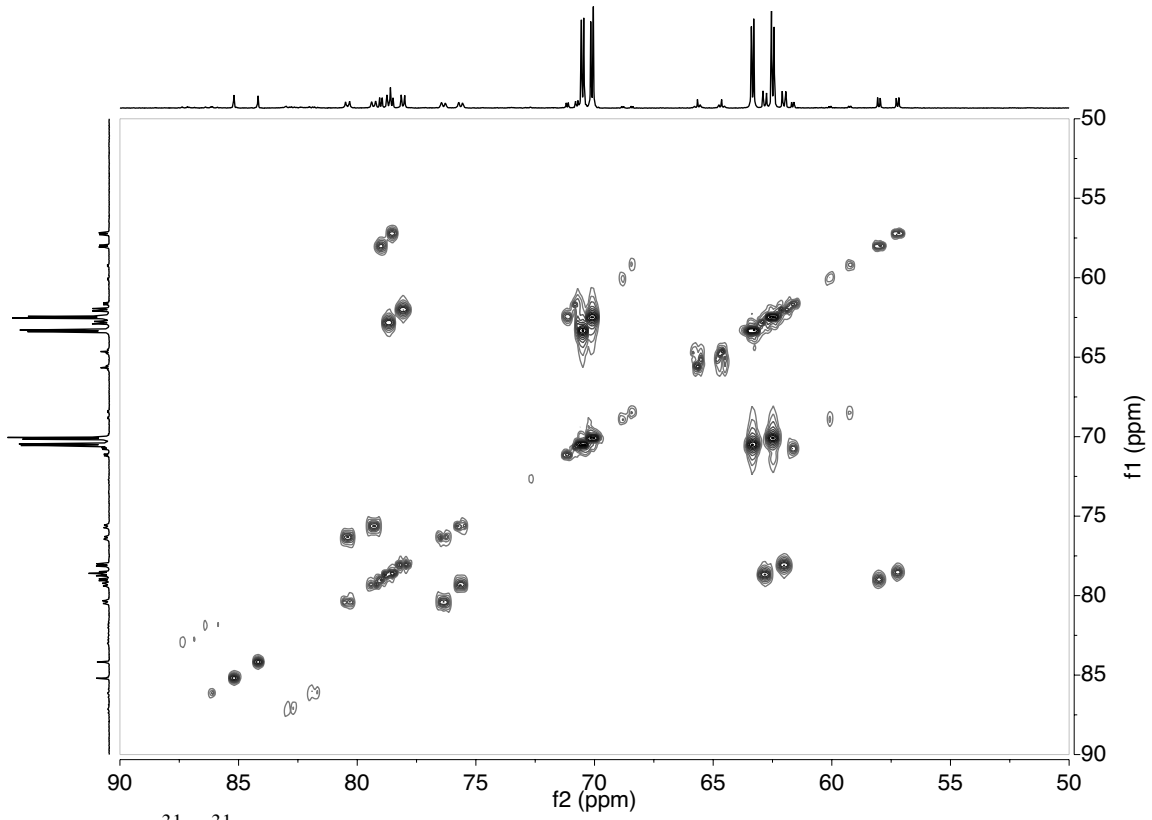

Figure S39. ^{31}P-^{31}P gCOSY taken after the reaction of **1** with allyl cyanide (1 atm CO, 202.5 MHz, CH_2Cl_2, -20 °C; nt = 8, ni = 256).

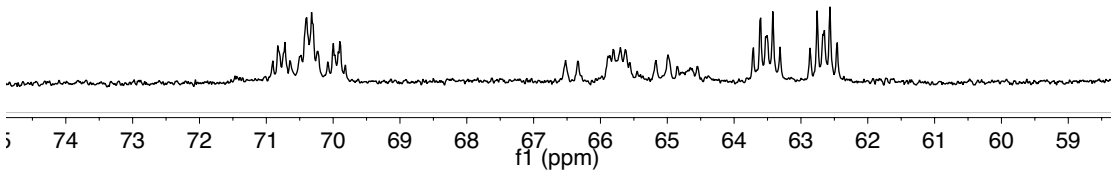

Figure S40. $^{31}P\{^1H\}$ NMR spectrum taken following the reaction of [Rh(H)($^{13}CO)_2$(BDP)] with allyl cyanide. The axial (downfield) peak of **7l$_{ac}$** shows three new $^2J_{PC}$, indicating that **7l$_{ac}$** is an acyl dicarbonyl species (1 atm H_2, 202.5 MHz, -10 ° C, CD_2Cl_2).

1-octene

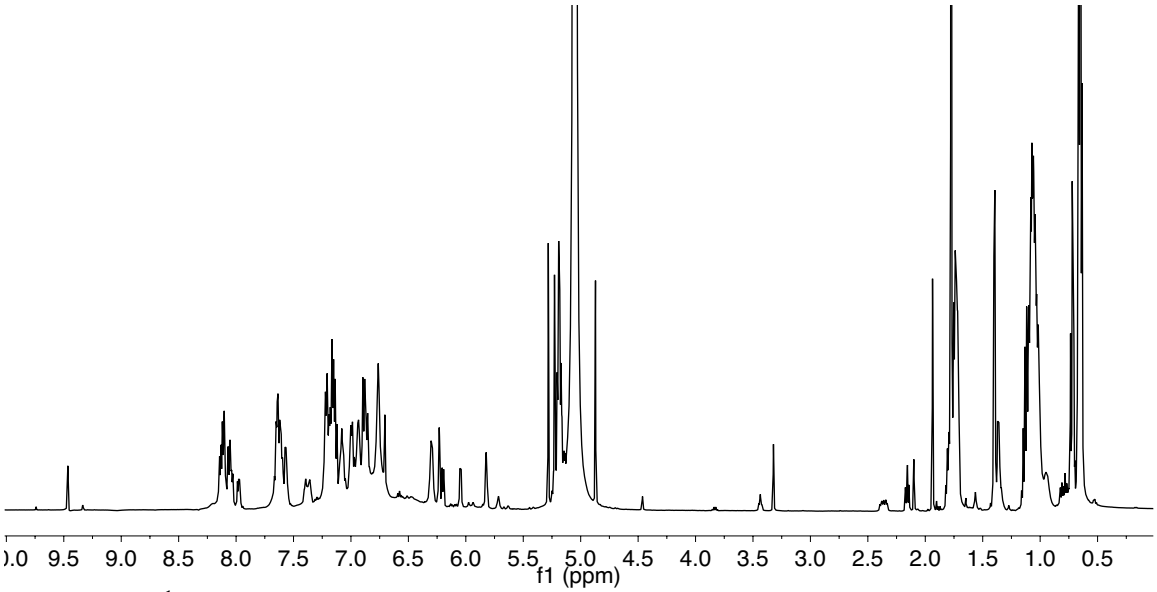

Figure S41. ^{1}H NMR spectrum following the reaction of **1** with 1-octene (1 atm CO, 500.22 MHz, -10 °C, CH_2Cl_2).

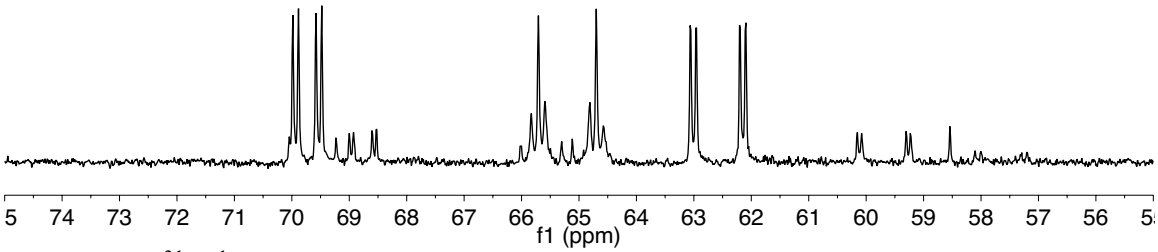

Figure S42. $^{31}P\{^{1}H\}$ NMR spectrum taken during the reaction of **1** with allyl cyanide at -30 °C. The larger eight-line pattern is $\mathbf{7l_{ac}}$; the smaller is $\mathbf{7b_{ac}}$ (1 atm CO, 202.5 MHz, -30 °C, CD_2Cl_2).

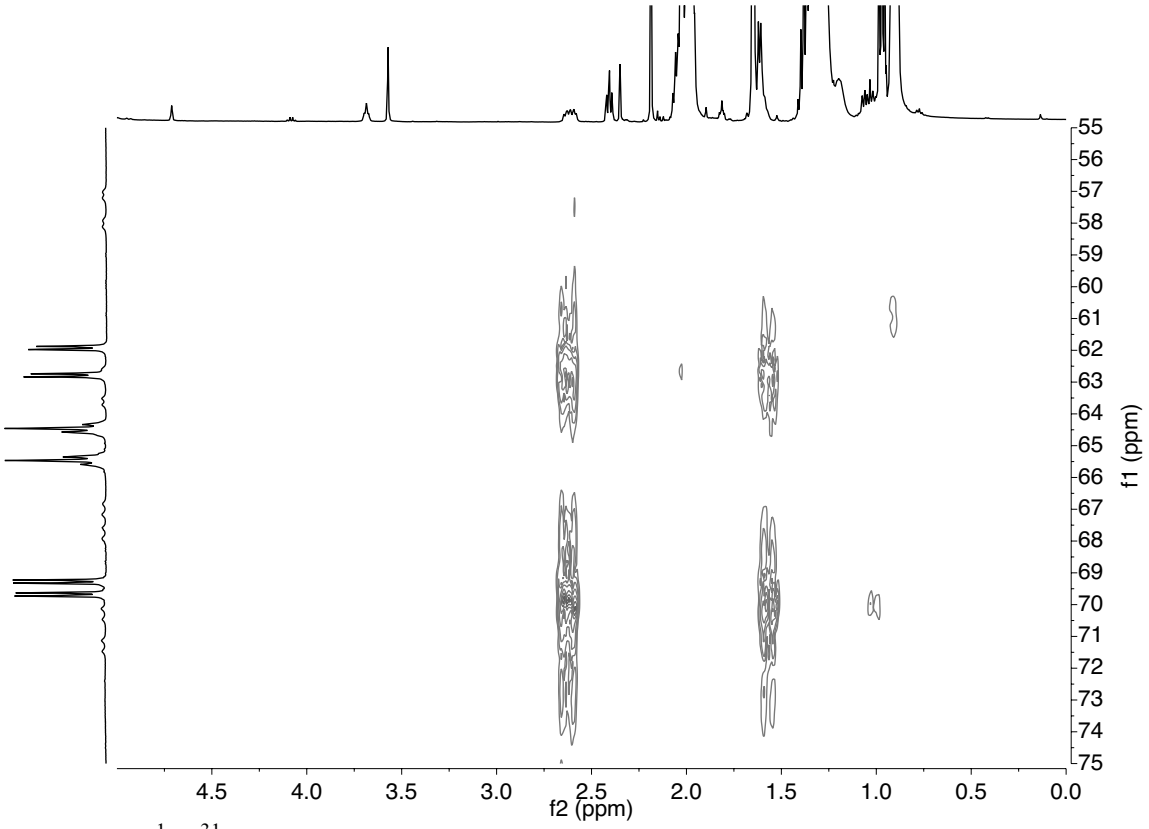

Figure S43. ^{1}H-^{31}P gHMBC following the reaction of **1** with 1-octene (1 atm CO, (f2,f1) = 500.22, 202.5 MHz; -30 °C; nt = 16, ni = 256, jnxh = 3.0 Hz).

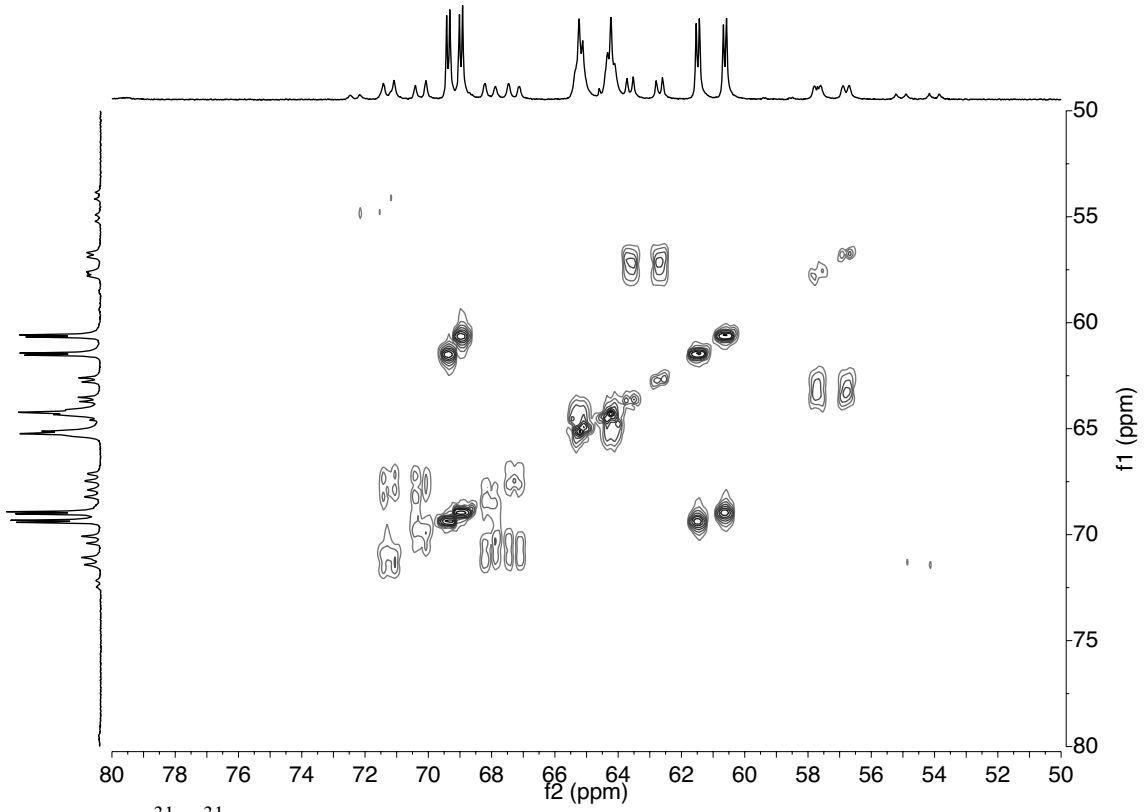

Figure S44. ^{31}P-^{31}P gCOSY taken after the reaction of **1** with 1-octene (1 atm CO, 202.5 MHz, CH_2Cl_2, -80 °C; nt = 4, ni = 256).

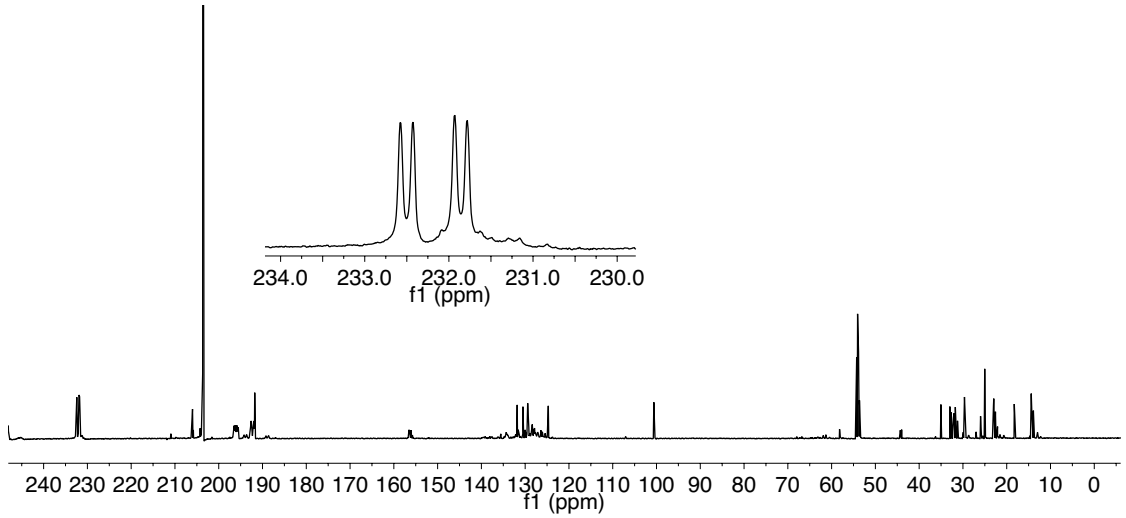

Figure S45. $^{13}C\{^1H\}$ NMR spectrum taken after the reaction of $[Rh(H)(^{13}CO)_2(BDP)]$ with 1-octene; inset shows acyl carbonyl resonance of $\mathbf{7l_{oct}}$ (1 atm H_2, 125.79 MHz, -40 °C, CD_2Cl_2).

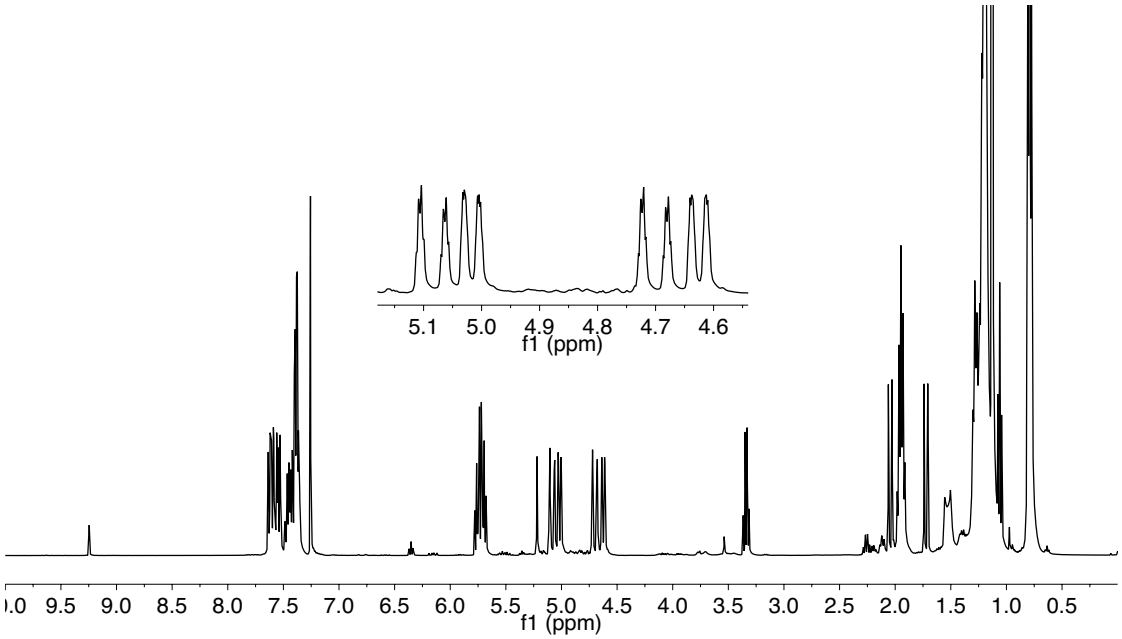

Figure S46. ^{1}H NMR spectrum of 1-^{13}C-octene; inset shows overlapping *dddt* for terminal alkene protons (400 MHz, 24 °C, $CDCl_3$).

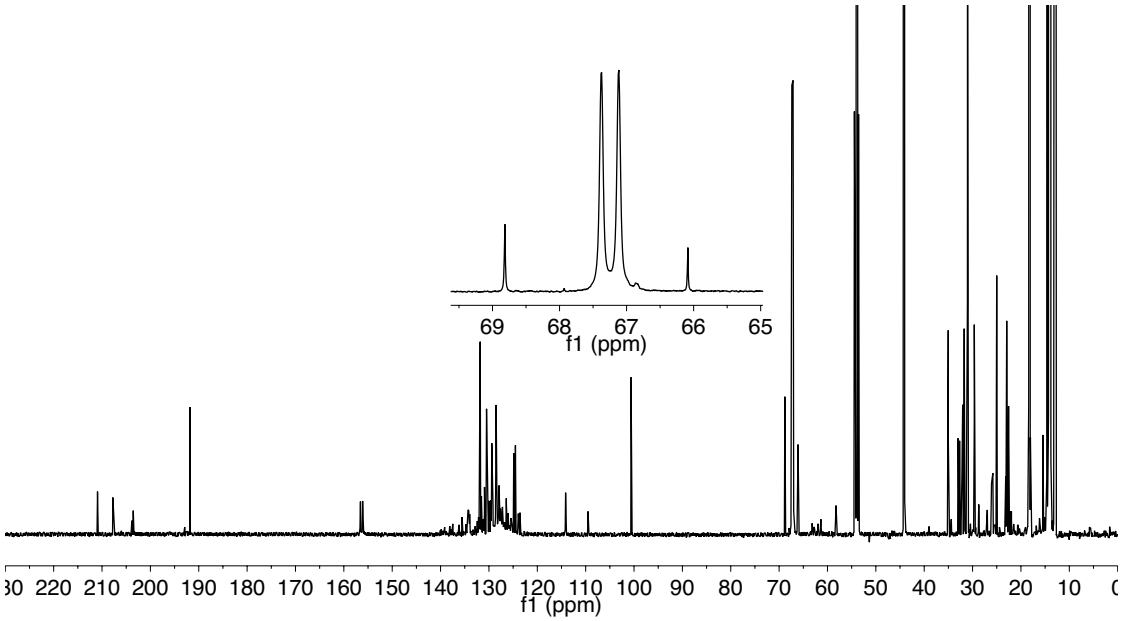

Figure S47. ^{13}C NMR spectrum taken following the reaction of **1** with 1-13C-octene. Inset shows labeled methylene carbon of **7loct** (1 atm CO, 125.79 MHz, -40 °C, CD_2Cl_2).

Chapter 5

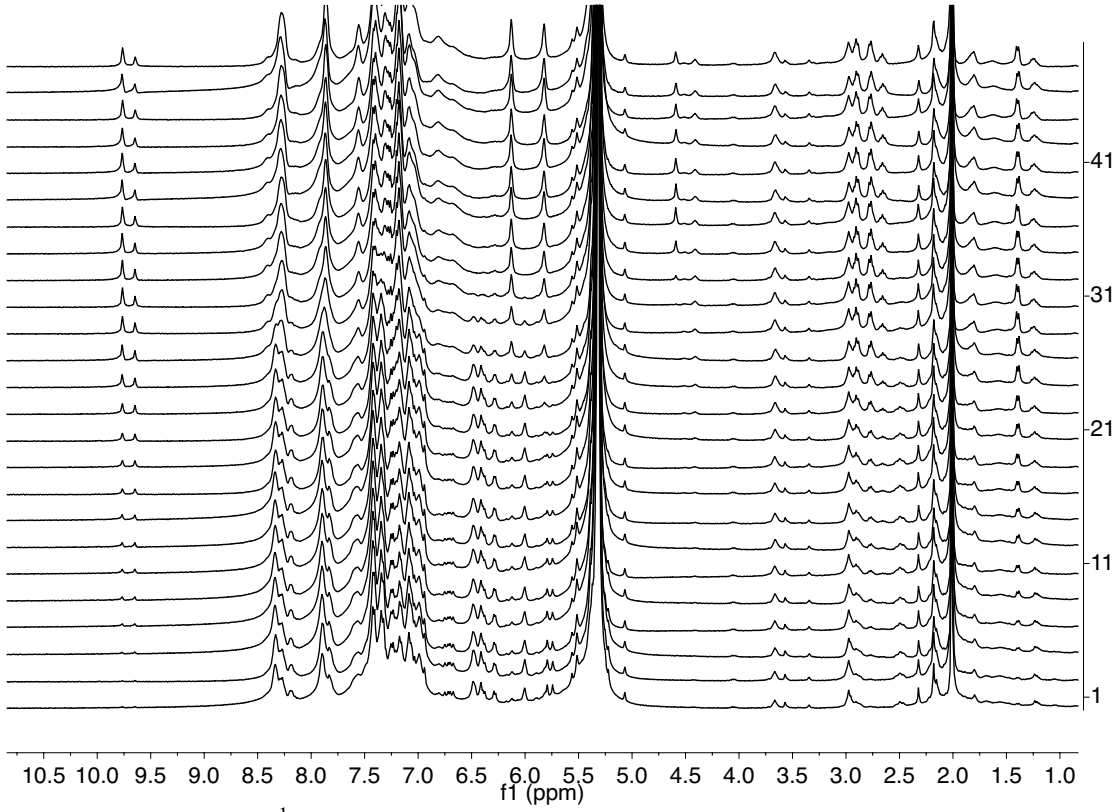

Figure S48. Arrayed ^{1}H NMR spectra (one every five minutes) taken during the reaction of **7b,l$_{sty}$** with 100 psig H_2 using the HPNMR apparatus. Aldehyde peaks grow in between δ 9.5 and 10 ppm; the absence of H_2 (δ 4.6 ppm) prior to 85 minutes indicates gas starvation (100 psig H_2, 360.13 MHz, -20 °C, CH_2Cl_2).

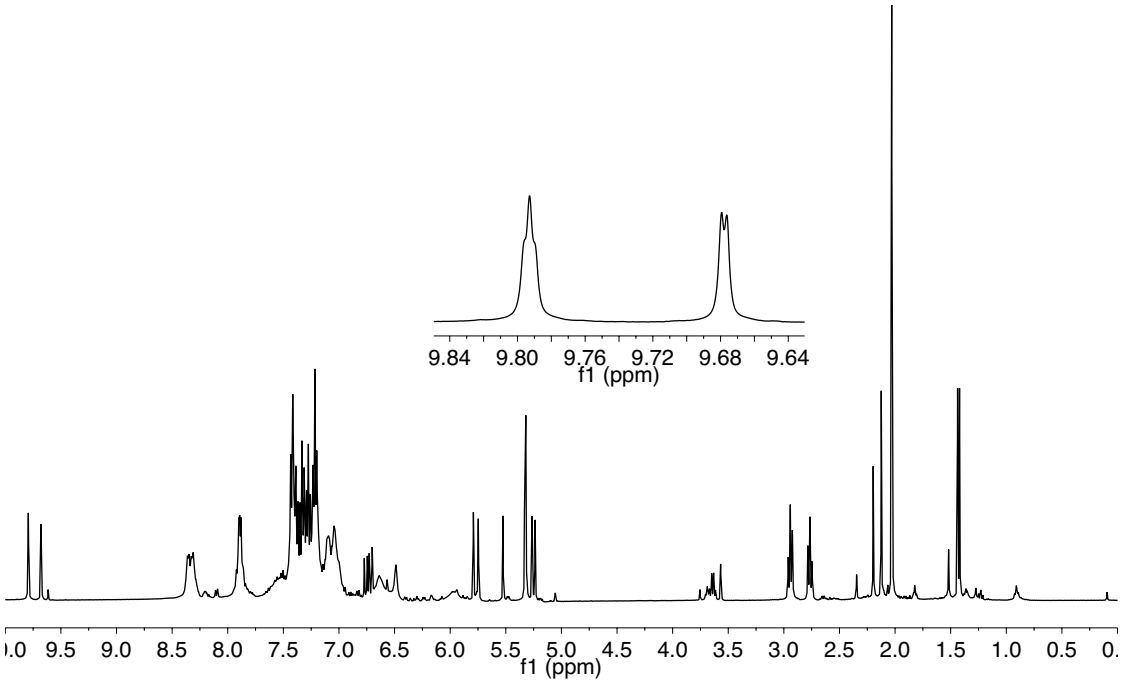

Figure S49. ^{1}H NMR spectrum taken following the reaction of **7b,l$_{sty}$** with 100 psig H_2 using the HPNMR apparatus. Inset shows linear (left) and branched (right) aldehyde resonances (400 MHz, 24 °C, CD_2Cl_2).